FRACTURE TOUGHNESS IMPROVEMENT OF LOWER BAINITE IN ULTRA HIGH STRENGTH LOW ALLOY STEELS

Lu Fang

B.E. Beijing Institute of Technology, Beijing, China, 1982

A dissertation submitted to the faculty of the
Oregon Graduate Institute of Science & Technology
in partial fulfillment of the
requirements for the degree
Doctor of Philosophy
in
Materials Science

January, 1994

The dissertation "Fracture Toughness Improvement of Lower Bainite in Ultra High Strength Low Alloy Steels" by Lu Fang has been examined and approved by the following Examination Committee:

William E. Wood, Thesis Adviser
Professor

David G. Atteridge
Associate Professor

Jack H. Devletian
Professor

Khalid H. Khan
Associate Professor
Multnomah School of Engineering
University of Portland

DEDICATION

This work is dedicated to

my parents

ACKNOWLEDGEMENT

I thank Prof. W. E. Wood for his guidance and support through this work. I also thank Prof. J. H. Devletian, Drs. D. G. Atteridge, and K. H. Khan for agreeing to examine my dissertation. I am indebted to Drs. M. S. Kumosa, J. T. Stanley, and M. E. Ziomek-Moroz for sharing their professional opinion regarding various crucial aspects involved in this study with me. I deeply appreciate the many invaluable discussions I had with my fellow students R. Devanathan, R. Parthasarathy, V. Dikshit, R. Dighde, J. Ding, S. Ding, N. Jin, and M. Li. Special thanks are due to Mr. R. Turpin and Mr. K. Burns for their assistance in adjusting various machines to the appropriate running conditions for this work. I wish to thank Dr. Vaught-Alexander for her advises on concise writing. Special thanks are due to my wife, Jie Wang, for her understanding, patience, and support.

TABLE OF CONTENTS

CONTENT PAGE

CONTENT PAGE

CONTENT PAGE

CONTENT PAGE

LIST OF TABLES

LIST OF FIGURES

ABSTRACT

FRACTURE TOUGHNESS IMPROVEMENT OF LOWER BAINITE IN ULTRA HIGH STRENGTH LOW ALLOY STEELS

LU FANG

Oregon Graduate Institute of Science and Technology
1994

Supervising Professor: William E. Wood

This study investigated the toughening mechanisms of lower bainite and established a relationship between microstructure and fracture toughness in an ultra high strength low alloy steel. A two-step approach was employed. Firstly, toughness was studied as a function of heat treatment parameters. It was then related to the microstructural parameters that controlled fracture toughness of the steel.

In the first step, attention was focused on the effect of bainite transformation and austenitizing temperatures on fracture toughness. With low transformation temperatures, the steel showed a strong intergranular fracture tendency in room temperature tests. As the transformation temperature was increased from 220 to 320°C, quasi-cleavage became the dominating fracture mode. Correspondingly, fracture toughness increased by over 100%.

Increasing austenitizing temperature and bainite transformation temperature simultaneously imposed a stronger effect on fracture toughness. With austenitizing temperatures above 900°C, an additional 20% increase in toughness, without reduction in strength, could be obtained through low temperature tempering.

Microstructural analysis showed that toughness increased with prior austenite grain diameter until grain growth temperature was reached. Toughness improvement from the increase of bainite transformation temperature, on the other hand, arose from the reduction of carbon supersaturation in bainitic ferrite due to the increase in carbide volume fraction.

A fracture mechanics model was developed to account for the effect of prior austenite grain size and bainite lath width on toughness. The energy needed to cleave a bainite lath and to tear a bainite lath boundary as well as the energy required to rupture an austenite grain boundary were also embraced. Due to the absence of energy data in the literature, this model could only be used in a qualitative sense.

For a comprehensive understanding of the relationship among phase transformation, microstructure, and fracture toughness, this work also studied overall bainite transformation kinetics. It applied a modified Johnson-Mehl-Avrami equation to the collected isothermal transformation data and revealed a relationship between the curve shape constant and the transformation temperature. Using this relationship, the temperature ranges for lower bainite, upper bainite, and pearlite transformations were determined. The validity and accuracy of the determinations were subsequently confirmed by microscopic analysis. The simplicity and efficiency of this technique over the conventional, tedious metallographic method of microstructure identification made it an attractive alternative for microstructure characterization.

The coupling of the microstructure characterization and the fracture toughness comparisons rationalized the toughness ranking of the microstructures. Lower bainite had higher toughness than tempered martensite. Duplex martensite/bainite structures with bainite matrix were inferior to bainite, while those with martensite matrix were less tough than quenched and tempered martensite, especially when the bainite was transformed at temperatures below 280°C.

The major contributions of this investigation to phase transformation and structure-property relationship studies include the discovery of the correlation between the curve shape constant and transformation temperature, and the development of a fracture mechanics model.

INTRODUCTION

Ultrahigh strength low alloy steels (<5% total alloy content) are usually used in place of the more expensive alloys for applications that require about 1400 MPa (200 ksi) yield strength. At such high strength levels, toughness becomes the critical property that guarantees high performance and long product service life. A favorable combination of high strength and toughness makes bainite the preferred candidate over martensite and pearlite in these steels.

The microstructure and the mechanical properties of bainite vary with heat treatments. However, current knowledge of structure-property relationships of bainite limits the ability to predict the transformation characteristics, the effective toughening mechanisms, and the optimum heat treating conditions for a given application. This study has been directed towards developing and understanding the structure-property relationships to optimize toughness and strength of a 0.69%C low alloy steel.

This investigation employed a fractional factorial analysis to evaluate the influence of austenitizing temperature, bainite transformation temperature, and bainite transformation time on fracture toughness. The results showed that toughness increased with austenitizing and bainite transformation temperatures but remained the same as bainite transformation time was extended from 10 to 50 minutes. The effect of austenitizing temperature and bainite transformation temperature on fracture toughness was further studied in a systematic manner. The results demonstrated again that fracture toughness increased with austenitizing temperature to the austenite grain growth temperature and with bainite transformation temperature into the upper/lower bainite transition range. The bainite reaction temperature was found to be a stronger factor on fracture toughness of the steel than the austenitizing temperature.

The effect of tempering treatment on toughness was also studied; tempering increased fracture toughness by about 20%, if austenitizing temperature was above 900°C but had no effect when the austenitizing temperature was at or below 900°C.

To advance the observed trends between fracture toughness and heat treatment parameters to a microstructure-toughness relationship, this work evoked a phase transformation study. It applied a modified Johnson-Mehl-Avrami equation to isothermal bainite transformation kinetic date and, for the first time, revealed a relationship between the curve shape constant and transformation temperature. Further analysis of this relationship led to a correlation between transformation mode and temperature, and a new method that could accurately and efficiently determine the transformation temperature range for each product. This development not only extended the application of the Avrami equation from transformation data representation to transformation mode and product volume fraction predictions but also provided a foundation for fair mechanical property comparison of the same microstructure in different steels.

A rational for microstructure ranking in terms of fracture toughness was reached through microstructure characterization and fracture toughness comparison. Lower bainite had higher toughness than martensite. Duplex martensite in bainite matrix structures were inferior to bainite, while bainite in martensite structures were less tough than quenched and tempered martensite.

For a better understanding of toughness development in lower bainite in ultra high strength low alloy steels, this investigation developed a fracture mechanics model to describe the effect of different microstructural features on fracture toughness in the form

$$K_{IC} = 16.7\sqrt{\frac{2E\left(\frac{r^*}{d}\gamma_d + \frac{r^*}{w}\gamma_l\right)}{a}}$$

where K_{IC} is the critical plain strain stress intensity factor, E is Young's modulus, r^* is characteristic distance, d and w are prior austenite grain size and bainite lath width, respectively, γ_d is the energy needed to rupture prior austenite grain boundary, γ_l is the energy spent in cleaving a bainite lath and tearing a lath boundary, and a is the initial crack length. This equation qualitatively predicted the trend of toughness with the change of the microstructural parameters. However, a quantitative evaluation of fracture toughness based on this model was difficult at present due to the difficulty in the assessment of the energy terms.

The procedures employed in this work are applicable to the study of other steels. The established relationships, however, should be used with caution since fracture toughness depends on the microstructure which in turn depends on the composition and heat treatment. Not only the primary microstructure but also all other structural constituents affect the property of a component. To make the matter more complex, different toughening mechanisms may prevail in different steels. An appropriate analysis should characterize the microstructure, especially the main toughness controlling microstructural feature, identify the toughening mechanism, and evaluate the effect of heat treatment parameters on these features. Attention should also be paid to the non-bainitic structures such as martensite and retained austenite which have been shown many times to strongly affect toughness of components.

CHAPTER 1

LITERATURE SURVEY

This work developed relationships among austempering heat treatment parameters, bainite microstructure, and mechanical properties of bainite in a high carbon low alloy steel and optimized fracture toughness and strength of the steel.

This literature survey on bainite and its mechanical properties was conducted to assist the experimental design and analysis of results. Recognizing the similarities between martensite and bainite in their structures and properties as well as in strengthening and toughening mechanisms, references to both martensite and bainite were made. However, the focus remained on bainite. The mechanical behavior of bainite in different steels was very different; it was not necessary to cover the fracture mechanics of bainite in other alloys. Only the immediately relevant fracture mechanics topics were included in the discussion chapter (Chapter 5). Other relevant issues were briefly summarized in the following sections.

1.1. Bainite

In the steels of greatest interest, the carbon content exceeds the solubility of carbon in ferrite. Under these conditions bainite comprises non-lamellar aggregates of ferrite and carbide[1] formed by a non-cooperative mode decomposition of austenite.[2] It may also contain residual phases consisting of untransformed austenite or of martensite and carbide which form subsequent to bainite transformation.[3] The microstructure is named after Bain,[4] who first discovered it in the late 1920's during his pioneering studies on the isothermal transformation of austenite.

Bainite has its own transformation curve (C curve) in a time-temperature-transformation (TTT) diagram.[5] The upper temperature above which austenite does not transform by the bainitic mode is designated as B_s. Below this temperature, bainite forms relatively rapidly[5] by nucleation and coherent growth,[6] and stops before all of the austenite has been transformed.[7] The amount of bainite increases as the reaction temperature is lowered. For alloy steels, the bainite C curve may separate from the pearlite C curve and martensite C curve (M_s temperature), but for plain carbon and low alloy steels the C curves usually overlap.

Four variants of bainite are often observed: upper bainite, lower bainite, carbide free bainite, and granular bainite. The first two are the classical bainite, originally distinguished from each other by Mehl[8]. The other two are the non-classical bainite. In hypoeutectoid and eutectoid steels, bainite assumes the classical forms; while in ultra-low carbon and silicon containing steels, especially during continuously cooling, bainite tends to have the non-classical variants. This literature review is restricted to the classical bainite forms relevant to this study.

1.1.1. Upper Bainite

Upper bainite consists of sheaves[9] of parallel ferrite laths. Each lath is a sub-unit of a sheaf. The laths in a sheaf tend to have the same crystallographic orientation with a small misorientation across the boundaries. The macroscopic habit plane is close to $\{111\}_\gamma$[10] and the longest dimension of a lath is near the close packed direction of the ferrite which is also nearly parallel to a corresponding close packed direction of the parent austenite.[11] The relative orientation relationship between ferrite and austenite is close to the classical Kurdjumov-Sachs (KS)[12] and Nishiyama-Wassermann (NW)[13] relationships but is never exactly KS or NW. The KS and NW relationships are expressed as

KS:

$$(011)_\alpha \parallel (111)_\gamma$$

$$(11\bar{1})_\alpha \parallel (10\bar{1})_\gamma$$

$$(\bar{2}1\bar{1})_\alpha \parallel (\bar{1}2\bar{1})_\gamma$$

NW:

$$(001)_\alpha \parallel (0\bar{1}1)_\gamma$$

$$(\bar{1}10)_\alpha \parallel (\bar{1}11)_\gamma$$

$$(110)_\alpha \parallel (211)_\gamma$$

The carbide, which is almost always cementite, precipitates from carbon enriched residual austenite between and parallel to the upper bainite laths. The orientation relationship between cementite and retained austenite follows that described by Pitsch:[14]

$$\{001\}_\theta \parallel \{\bar{2}25\}_\gamma$$
$$<100>_\theta \text{ within } 2.6° \text{ of } <\bar{5}5\bar{4}>_\gamma$$
$$<010>_\theta \text{ within } 2.6° \text{ of } <\bar{1}10>_\gamma$$

where θ represents cementite. Direct and indirect measurements[15,16] of the relative orientation between ferrite and cementite have resulted in variants of the Bagaryatski relationship[17] which can be expressed as:

$$(100)_\theta \parallel (0\bar{1}1)_\alpha$$

$$(010)_\theta \parallel (1\bar{1}\bar{1})_\alpha$$

$$(001)_\theta \parallel (211)_\alpha$$

In alloy steels, other carbides also exist.[18-20]

1.1.2. Lower Bainite

Lower bainite contains ferrite laths or plates and intralath carbides. The orientation relationship between the bainitic ferrite and the parent austenite is also close to KS and NW relationships. The habit plane of bainite is irrational[21] and is close to $\{254\}_\gamma$.[22,23]

The frequently observed carbides in lower bainite are ϵ-carbide[24-32] and cementite.[33-35] In many cases, ϵ-carbide occurs only as a transient phase in the precipitation sequence;[25] it transforms to cementite subsequently. Therefore, some investigators consider cementite to be the common carbide associated with lower bainite.

The hexagonal close packed ϵ-carbide has a crystallographic orientation relationship with respect to ferrite as that reported by Jack[36]:

$$(0001)_\epsilon \parallel (011)_\alpha$$

$$(10\bar{1}1)_\epsilon \parallel (101)_\alpha$$

Kalish and Cohen[37] have shown that carbon atoms tend to remain segregated at dislocations rather than precipitate as ϵ-carbides. If dislocation density is high, dislocations would absorb sufficient carbon atoms and reduce ϵ-carbide precipitation tendency. They have estimated that a dislocation density of 2×10^{12} cm^{-2} would prevent ϵ-carbide precipitation in steels containing up to 0.2 wt% carbon.

Cementite precipitates within ferrite plates at an angle of about 55 to 60° from the longitudinal direction of the plate axis.[16,21,28,31,33,38,39] The habit plane of the carbide is close to $\{112\}_\alpha$[40] and the commonly observed orientation relationship between the carbide and the ferrite is Bagaryatski relationship.[35] Similar to the martensitic carbides, cementite in the lower bainite grows in the $<111>_\alpha$ directions but different from the martensitic carbides which grow in four equivalent $<111>_\alpha$ directions, the bainitic carbides grow primarily in only one of the $<111>_\alpha$ directions in a bainite plate. In medium and high carbon steels, carbide also precipitates between bainitic ferrite plates.[25,31]

1.2. Bainite Transformation Mechanism

The formation of bainite constitutes a complex problem in competitive reaction kinetics involving the allotropic transformation of γ to α, partition of carbon between these phases, precipitation of cementite or other carbides from ferrite and/or austenite as well as accommodation and relaxation of transformation strain.[5,29] This complexity of the problem has made it difficult to study the reaction mechanism and the reaction rate controlling processes. The similarities between bainite and martensite on one hand and between bainite and Widmanstatten ferrite on the other hand have resulted in several divergent views of bainite reaction mechanism,[5] which can be categorized into two main schools of thought.

One school consists of those who believe that bainite forms by a martensitic type mechanism; while the other school contains those who believe that bainite transformation is diffusional in nature, similar to that of Widmanstatten ferrite formation.[41] In the literature, each school presents some evidence to support its theory whereas the other group questions the validity of the results or the interpretations, and counters with contrasting evidence.

The diffusional school of thought maintains that the ferritic component of bainite develops over the whole bainitic temperature range by a diffusional ledge mechanism analogous to the proposals made to account for the formation of Widmanstatten proeutectoid ferrite.[5] The carbon content of this ferrite is considered to be between the $\alpha/\alpha+Fe_3C$ and the extrapolated $\alpha/\alpha+\gamma$ phase boundaries, and the bainitic carbides are considered to form primarily on the austenitic side of the austenite/ferrite interface.[5] Detailed electron diffraction studies of the carbide precipitation reactions have been interpreted to support this hypothesis.[31] A solute drag model is invoked to explain the bay in the TTT curve at the B_s temperature.[42] The incomplete reaction characteristic of the bainite transformation is claimed not to be a general phenomenon.[5]

The opposing school of thought considers the bainite reaction to be a displacive transformation controlled essentially by the rate at which composition change is accomplished by carbon removal to the surrounding austenite or by some other rate controlling process such as strain energy relaxation.[28,29,43] Hence, the austenite/ferrite interface is expected to exhibit the same characteristics as in the martensitic transformation. The ferritic component of bainite is thus thought to form with a carbon supersaturation,[28,29] which in lower bainite is relieved by carbide precipitation within the ferrite. This reaction is thus analogous to autotempered martensite. The existence of a metastable eutectoid reaction controlling the carbide precipitation event has been postulated.[42] This concept is also extended to support the idea of a discontinuous change from upper to lower bainite at a temperature of 350°C virtually independent of steel composition. The B_s temperature is considered to be due to the intersection of two separate C-curves for reactions occurring by fundamentally different mechanisms.[5,44]

Bainite transforms in the intermediate temperature range. In this range, especially in the lower bainite formation temperature range, iron atoms and substitutional atoms diffuse very slowly but bainite transforms at relatively high rate. Therefore, bainite transformation is considered to take place through a martensitic type mechanism. However, the application of martensitic mechanism requires the bainite transformation to possess the most important crystallographic or geometric features of the martensitic transformations which according to Lieberman[45] are

(1) a shape deformation which results in upheavals on a polished reference surface of the parent, indicating that, from a macroscopic point of view, the transformation consists of shear on an undistorted plane, the habit plane, and a possible volume change perpendicular thereto,

(2) the habit plane separating the parent and product is generally irrational; the set of direction cosines of its normal is characteristic of the specific transformation,

(3) a rather precise orientation relationship between principal directions and planes in the two phases on either side of the interface, as revealed by x-ray analysis,

(4) evidence of a fine inhomogeneous structure in the product phase, and

(5) the atoms move less than an interatomic distance, nearest neighbors are maintained, and any degree of order in the parent persists in the product during the transformation.

Surface relief associated with bainite reaction, which was similar to that obtained during the formation of martensite, was originally observed by Ko and Cottrell[6] and was considered as evidence of coherent growth of the product phase. These investigators proposed that the term "coherent transformation" be used for describing the processes by which both martensite and bainite were formed. At low temperatures at which transformation was diffusionless, the product was martensite. At high temperatures at which the process of coherent growth was controlled by diffusion, the product was bainite.

Surface relief signifies a systematic shape change which necessarily implies a lattice correspondence between the parent and the product phases.[46] This correspondence is maintained if there is a coordinated movement of lattice and substitutional atoms from the parent to the product phase,[47] which is only likely through shear transformation.

To make the Ko-Cottrell definition more rigorous, the subsequently developed phenomenological theory of martensite[48,49] was applied. It followed that the ferritic component of bainite must be a plate in three dimensions, not a needle, and the relief effect must be an invariant plane strain.[50,51] Upper bainite, however, often appeared as needles[52,53] and Widmanstatten ferrite sometimes yielded an invariant plane strain relief[51]. Dahmen[54] showed that both martensitic and diffusion-controlled transformations could exhibit an invariant plane strain surface relief and suggested that surface relief not be used as a martensitic reaction criterion.

Aaronson and Kinsman, who support the diffusional bainite transformation theory, showed that the formation and growth of bainite were through repeated formation and movement of ledges (subunits).[5] Using thermionic emission microscopy, which was believed[55] to have the necessary resolution, they demonstrated that the lengthening and thickening rates of upper bainitic subunits were controlled by the volume diffusion of carbon in austenite and ruled out a variety of shear-based growth mechanisms.[5] Bhadeshia,[56] however, in supporting shear transformation mechanism, determined the growth rate of a bainite plate in a Fe-Mn-Si-C alloy to be orders of magnitude greater than that expected from carbon diffusion-controlled growth, using hot stage photoemission electron microscopy. Hehemann,[5] from the displacive thought of school,[57] stated that the results on lengthening rates were consistent with either a ledge or a shear mechanism. To date, the transformation mechanism of bainite is still not clear after over 60 years of study from different angles.

1.3. Mechanical Properties of Bainite

The mechanical properties of a steel depend on its microstructure which in turn depends on the composition and the applied thermomechanical process.[58] Bainite can be obtained by either isothermal transformation or continuous cooling with the latter being preferred since isothermal processes have been considered impractical for sizeable samples of steels.[3] However, continuous cooling produces mixed microstructures, which presented the early researchers with tremendous difficulties in microstructure and mechanical property control. Mixed microstructures of allotriomorphic ferrite and bainite are formed in lightly alloyed steels, whereas bainite, untempered martensite, and/or retained austenite are typical in heavily alloyed steels;[3] neither class of steels offers good mechanical properties in as-transformed conditions.

The dilemma was partially solved by the addition of boron and molybdenum to low alloy, low carbon steels.[59] Boron effectively retards proeutectoid ferrite formation but does not strongly affect bainite reaction. This allows more uniform bainite microstructures to be obtained over a wide range of cooling rates and permits the characterization of the mechanical properties of bainite in isolation.

Uniform microstructure is the key to property characterization and, therefore, lends substantial advantages to structure-property studies of isothermally transformed bainite over continuous cooling microstructures. This study focuses on isothermal bainite-property relationships; the conclusions may not apply to continuous cooling situations.

1.3.1. Tensile Strength

Many mechanisms contribute to the strength of bainite. Some may be operative most of the time; others are not. In a particular steel, one mechanism may dominate but usually more than one mechanism is at work. An understanding of each mechanism is instructive even though at present the theories do not adequately predict the strength of bainite in steels.

1.3.1.1. Bainite Grain and Lath Strengthening

Plates of bainitic ferrite are typically 10 μm in length and about 0.5 μm in width.[60] These small dimensions limit the mean free path for dislocation glide, especially since the probability of the slip plane lying parallel to the plate is rather small,[59] and thus strongly contribute to the strength of bainite.

Many attempts have been directed at an analysis of the grain size effect on the strength of bainite, most of them being based on the Hall-Petch relationship which predicts a linear relationship between the strength and the reciprocal of the square root of grain size. Although some data on bainite and martensite can be fitted to the Hall-Petch relationship,[61-65] the results are difficult to interpret because the platelet size cannot be altered without influencing other variables such as dislocation density and carbide particle density.

The Hall-Petch relationship relies on a description of macroscopic yielding in which a dislocation pile-up generates a large enough stress concentration to stimulate a dislocation source in an adjacent grain, thereby transmitting deformation across grains. If the grain size is large, then the number of dislocations that can participate in the pile-up increases, and the larger stress field of the pile-up makes it easier to stimulate distant sources. Hence, the yield strength decreases. This description does not apply to the fine grained structures.

Langford and Cohen[66] studied the behavior of iron wire during cold drawing and found a linear relationship between the strength of the specimens and the reciprocal of elongated grain diameter *d*

$$\sigma = \sigma_0 + k_y d^{-1} \tag{1.1}$$

where σ_0 is the friction stress required to move free dislocations along the slip planes in ferrite and k_y is a material constant. They reasoned that in very fine grained samples the slip plane dimensions were too small to allow the existence of pile-ups, and yielding was determined by the stress necessary to expand a dislocation loop across a slip plane. The change over from the Hall-Petch to the Langford-Cohen relationship was found to occur when the slip plane dimensions became about 1 μm. The Langford-Cohen relationship was satisfactorily applied by several investigators.[60,66-71] Using this relationship, Smith and Hehemann[60] estimated the strength contributions from bainite and martensite laths to be about 45 and 65 MPa, respectively.

Considering that not only the lath width but also the lath length, to a certain degree, determines the slip plane length, Naylor[69] derived a composite term M to express the effect of both the lath width and length on the strength

$$M=\frac{2}{\pi}\{d\ln[\tan(\frac{arcos\frac{d}{D}}{2}+\frac{\pi}{4})]+\frac{\pi}{2}D-Darcos(\frac{d}{D})\} \qquad (1.2)$$

where D is the lath length which is about the same as bainite or martensite packet size. Therefore, expression (1.2) accounts for the effects of both lath size and packet size of bainite on its strength.

1.3.1.2. Solid Solution Strengthening

Solid solution strengthening can arise from both substitutional and interstitial atoms. The effect of substitutional elements on the strength comes mainly from their effects on transformation behavior of an alloy, or the change of reaction product at a temperature or through a heat treating route due to alloy additions. The solid solution strengthening is due to the symmetrical lattice distortion the atoms cause. This effect is not very significant.[72]

Interstitial solutes (mainly carbon and nitrogen), on the other hand, produce a strengthening effect 10-100 times that of the substitutional atoms[72] even though the concentration of these elements in bainite is very low. The effect comes from the asymmetrical lattice distortion associated with the atoms and, more importantly from the interaction between the atoms and dislocations.[72] Brozzo *et al* [71] have suggested the following empirical relationship in low carbon steels:

$$\sigma = \sigma_0 + \sigma_{INT} + k_y d^{-1} \tag{1.3}$$

where σ_{INT}, evaluated as $1900(C\%+N\%)^{1/2}$ MPa, is due to interstitial carbon and nitrogen solid solution strengthening.

Due to the high carbon diffusion rate at bainite reaction temperatures, any supersaturation of carbon atoms in bainitic ferrite is expected to disappear in a few milliseconds[73], therefore, it seems reasonable to assume that interstitial strengthening is not significant. However, early studies by Vasudevan *et al*[74] using internal friction techniques indicated a supersaturation of carbon in the ferrite. Bhadeshia and Waugh,[7] using atom-probe field-ion microscope techniques, also demonstrated a supersaturation of carbon in bainitic ferrite. The observed higher than equilibrium carbon concentration and non-uniform distribution imply bonding of carbon atoms to dislocations. This arrangement was estimated to contribute roughly 150 to 200 MPa to the strength of bainite.[75]

1.3.1.3. Carbide Dispersion Strengthening

The coarse cementite particles formed between lath boundaries in upper bainite do not appear to affect the strength of the microstructure via dispersion strengthening. They may, however, hinder dislocation motion across lath boundaries, thereby confining slip within the laths and raising the lath size contribution to flow stress.

The fine carbides in lower bainite contribute to the strength by the dispersion strengthening mechanism. With decreasing reaction temperature, the carbides in the bainitic structure for a given carbon content tend to become finer, more numerous, and more evenly dispersed[62]. This change is expected to increase the carbide strengthening effect. More detailed analysis[76] has indicated that the strengthening can be described by an Ashby-Orowan relationship as

$$\sigma_\theta = A n_\theta \ln\left(\frac{B}{n_\theta}\right) \tag{1.4}$$

where n_θ is the number of effective carbides per unit area, and A and B are material constants.

1.3.1.4. Dislocation Strengthening

Dislocation strengthening is a very important source of strength for martensitic and bainitic microstructures. The effect of dislocations comes from their contribution to the shear flow stress

$$\sigma_f = \alpha \mu b \sqrt{\rho} \tag{1.5}$$

and dislocation-carbide interactions,[77]

$$\sigma_d = \frac{k \mu b}{\lambda} \tag{1.6}$$

where μ is shear modulus, b is Burger's vector, ρ is dislocation density, λ is the spacing of a random array of impenetrable point obstacles, and α and k are constants. Hence, the strength increases with dislocation density, fine carbide volume fraction, and the reciprocal of carbide spacing.

Dislocations are generated in a material through many mechanisms, including deformation, transformation, and local stress/strain due to the differences in thermal expansion coefficients between particles and matrix. In bainitic structures, the main source of dislocations is phase transformation. Yang[78] has determined the dislocation density of bainite in a 0.03C steel to be of the order of 10^{14} which is lower than that in martensite but higher than that in proeutectoid ferrite. He has estimated that this dislocation density would raise the strength by about 145 MPa.

Considering all the above factors, the strength of bainite can be expressed as

$$\sigma = \sigma_0 + \Sigma_i \sigma_{SS}^i + \sigma_\theta + k_y d^{-1} + K_p \lambda^{-1} + k_d \sqrt{\rho} \tag{1.7}$$

Although conveying the bainite strengthening concepts in a compact form, equation (1.7) is impractical since the constants and the parameters change with chemistry and heat treatment. A more practical way of predicting the strength of bainite is by using the empirical relationship suggested by Pickering[62]

$$\begin{aligned}\sigma(MPa) &= 246 + 1900\%C + 230(\%Mn + \%Cr) + 185\%Mo \\ &\quad + 90\%W + 125\%Ni + 65\%Cu + 385(\%V + \%Ti)\end{aligned} \tag{1.8}$$

1.3.2. Toughness

The fracture resistance of a high strength material can be measured in two ways: impact toughness and fracture toughness. The former test measures the amount of plastic deformation and the absorbed energy during fracture, whereas the latter determines the critical value of the plane strain stress intensity factor at the onset of unstable crack growth ahead of an atomically sharp crack.

The impact toughness test, such as the Charpy V-notch test, involves the use of small specimens and impact loading. The tests are quick, convenient and inexpensive to perform. Through the years, a large amount of impact toughness data on many steels have been collected; these data show not only the amount of energy absorbed by a material during fracture but also the relationship between impact energy and test temperature. The 50% fracture appearance transition temperature (FATT) or impact transition temperature (ITT), a critical temperature range at which the behavior of a steel changes from ductile to brittle, can be determined from this test and is used in design against catastrophic failure of engineering structures. However, the absorbed energy from this test cannot be directly related to structural design parameters. Furthermore, the tests are conducted on small specimens (10 mm square rectangular bars) at extremely high strain rates (typically 10^1 - 10^2 s^{-1}) and involve fracture ahead of shallow, blunt notches (root radius about 0.25 mm) where the energy absorbed in crack initiation and crack propagation cannot be readily distinguished.[79]

An alternative approach to materials toughness evaluation has been provided by the use of linear elastic fracture mechanics. Here toughness is characterized by the critical value of the plane strain stress intensity factor, or the fracture toughness K_{IC}, and can be utilized in design applications since stress intensity is related quantitatively to nominal stress and flaw size. This approach applies to high strength and ultra high strength steels in martensitic and bainitic conditions.

Many workers have studied the relationships between the bainite structure and its toughness. The microstructural features that contribute to toughness are prior austenite grain size,[80] bainite packet size,[63,81] bainite lath size,[82,83] retained austenite volume fraction, retained austenite morphology,[83,84] carbide size,[85-87] and carbide distribution.[85] Alloying elements also affect fracture toughness. Rarely, if ever, is only a single toughening mechanism operative; in most instances two or more mechanisms influence the toughness and it is very difficult to experimentally alter the contribution of one factor without simultaneously affecting that of the others. Nonetheless, it is instructive to consider these factors separately.

1.3.2.1. Prior Austenite Grain Toughening

Similar to the considerations held for the martensitic and pearlitic structures, fine prior austenite grain size is also regarded as a contributor to the toughening of the bainitic structure.[88] Among all the strengthening mechanisms, only grain refinement improves strength and impact toughness simultaneously; the others increase strength at the expense of toughness.[89] Many investigators have studied the effect of prior austenite grain size on the impact transition temperature of martensite and bainite.[90-93] They all show a decrease in ITT with decreasing prior austenite grain size. This can be explained as neither martensite nor bainite transformation destroys prior austenite grain boundaries, which remain as barriers to crack propagation. The finer the grains, the denser the boundaries, therefore, the greater the resistance of a material to fracture. An exception to this rule was the observation made by Yokota and Lai[94] who reported an increased impact toughness with an increasing prior austenite grain size for both lath and plate martensite in a Fe-Ni alloy system.

If the effect of austenite grain size on fracture toughness is considered, the situation will be very different. Numerous investigations attempting to correlate fracture toughness with prior austenite grain size have arrived at the conclusion that toughness of steels increases with increasing austenitizing temperature and, therefore, increasing austenite grain size.[79,80,95-105] One of the proposed toughening mechanisms attributes the effect to the reduction or elimination of undesired microstructure due to the increase of hardenability associated with austenite grain growth.[104]

Ritchie[79] has rationalized the opposite effects of prior austenite grain size on the impact toughness and fracture toughness in terms of a differing response of the microstructure to the influence of notch root radius. He proposed that the maximum tensile stress σ_{yy}^{max} must exceed a fracture stress σ_f over a characteristic distance (or process zone) at a crack tip for fracture to occur. In front of a blunt notch, σ_{yy} increases slowly and reaches the maximum value at the elastic-plastic interface[106] which is located at a distance greater than the characteristic distance from the crack tip. Therefore, the distance requirement is fulfilled; fracture occurs as soon as σ_f is reached. Since higher austenitizing temperature reduces σ_f, it decreases the impact toughness.

The tensile stress σ_{yy} increases abruptly, on the other hand, to a maximum value in front of a sharp crack and then drops to the nominal stress at a distance away from the crack tip. Here, the characteristic distance, which is proportional to the grain size or carbide interspacing, controls the fracture process. In structures with big grains, or large characteristic distance, the fracture criterion is hard to meet; therefore, fracture toughness is high.

Other workers, however, have found correlations between the increase in fracture toughness and microstructural changes. These changes are more closely related to the effect of high austenitizing temperature than austenite grain size and will be considered in a later section.

1.3.2.2. Bainite Grain and Lath Toughening

Packet boundaries in martensitic and bainitic structures are also high angle boundaries similar to prior austenite grain boundaries. Therefore, refining packet size is expected to affect both the strength and toughness of martensite and bainite. Experimentally this mechanism was observed to operate in martensite[65], upper bainite[107], lower bainite[71], and mixed martensite and lower bainite microstructures.[81,108,109] Matsuda *et al*[110] demonstrated that the toughness of bainite was primarily controlled by the co-variant bainite packet size and was only modestly modified by the prior austenite grain size. They showed a continuous decrease in bainite packet size and improvement in toughness with decreasing transformation temperature. A similar trend was also observed in high carbon low alloy steels by Sandvik and Nevalainen.[82]

Naylor and Blondeau[111] and Naylor[69] demonstrated that not only packet size but also martensite/bainite lath size affected impact toughness. Toughness improved with decreasing packet size and lath width as described by the following equation:[107]

$$\theta_{50/50} = \frac{1}{\alpha} \ln C - \frac{1}{2\alpha} \ln\gamma_1 - \frac{1}{\alpha} \ln (d_p * \epsilon_1)^{-1/2}$$

where $\theta_{50/50}$ is the ductile-brittle transition temperature, α and C are constants, γ_1 is the energy for plastic tearing for high angle deviations at the lath boundaries, d_p is the packet diameter, and ϵ_1 is the lath width. Using this equation, the authors also pointed out the effect of other factors, such as tempering and carbide precipitation, on toughness through the energy term γ_1. Tempering reduced carbon content in solid solution and led to a decrease in the transition temperature by about 100°C in the investigated low carbon steel at all packet sizes and lath widths. However, if extensive carbide precipitation occurred, fracture toughness decreased. In other words, there exists a balance between carbon in solid solution and in the form of carbide for the optimum toughness in a steel. Contrary to the above trend, Brozzo[71] observed increases in fracture toughness as the martensite and bainite packet size was increased.

The role of the packet size in improving the toughness in duplex martensite and bainite microstructures was observed by Tomita and Okabayashi.[108] They showed that duplex structure with about 25% lower bainite had higher strength, ductility, and toughness than quenched and tempered martensite austenitized at the same temperature. The increase in strength was attributed to the refinement of the martensite substructure by lower bainite and the improvement in toughness was attributed to the crack arrest capability and stress relief capability of the acicular, ductile bainite particles. Using fractographic analysis, Tomita[81] demonstrated that the tempered martensite fractured in quasi-cleavage mode whereas duplex microstructure failed by predominantly dimple rupture. The reason that the duplex structure was tougher than lower bainite was not given. It may be possible that some untempered martensite had formed during cooling and contributed to the brittleness of the structure since the employed bainite transformation temperature was only 5°C above the M_s temperature of the steel and the transformed structure was not tempered.

1.3.2.3. Carbide Precipitation Toughening

Carbon is the most effective strengthening agent in martensitic and bainitic structures. The primary purpose of carbon addition to steels is to raise their strength level. Unfortunately, the strengthening is usually accompanied by a decrease in ductility and toughness.[104,112]

In martensite and bainite, carbon atoms stay in two places: bcc solid solution and carbides. In both cases carbon is detrimental to toughness. Carbon atoms in solid solution either occupy the octahedral interstices, increasing the tendency of brittle cleavage fracture by raising the critical resolved shear stress relative to the cleavage stress as the testing temperature is lowered,[104] or segregate to dislocations, increasing the difficulty in dislocation motion. Carbide precipitation reduces carbon content in solid solution but carbides may act as micro-cracks or crack initiation sites[113] or provide easy crack propagation paths to reduce toughness.[84]

In low carbon steels, carbide precipitation can be inhibited by the addition of alloying elements such as silicon and aluminum.[3] This practice eliminates the defect-like carbides and effectively improves fracture toughness.[84] In medium and high carbon steels, this approach may not work since a high degree of supersaturation of interstitial atoms in bcc solid solution reduces toughness. A possible solution is to retain a large amount of film shaped austenite to absorb the carbon atoms into the fcc solid solution.[82]

Many investigators[82,84,85,87,114] have successfully improved the fracture toughness of high strength steels by obtaining carbide free bainite through silicon additions. When carbide precipitation is not avoidable, Liu[115,116] has proved that it is better to have the carbides precipitate in bainite matrix than in tempered martensite. He observed some differences of carbide in these matrices. The bainitic carbide precipitates in a uniform fashion with fine size and small inter particle spacings whereas the martensitic carbide forms in an irregular distribution with coarse size and large inter particle spacings, especially when the matrix contains twins. These differences make the two types of carbides behave differently in fracture processes. The bainitic carbides participate in the fracture process leading a crack through a zigzag route and, therefore, raise the fracture energy. The martensitic carbides, on the other hand, usually do not interact with a propagating crack but leave it a straight path through a martensite plate. In fact, under the effect of the stress/strain field in front of a crack tip, coarse carbides crack or separate from the matrix easily, leading to micro-crack formation[63] or propagation[117] resulting in low toughness.

The above ranking of the structures, however, can be reversed. Bowen *et al*[86] showed that the carbide size, instead of its distribution or the matrix type, had a stronger effect on the fracture toughness of a A533B pressure vessel steel. The as-transformed auto-tempered martensite with a mean carbide width of 14 nm always had a higher toughness at all the test temperatures compared with a mixed lower and upper bainite structure which had a mean carbide width of 230 nm, even though the 0.2% proof strength of the former structure was almost twice that of the latter. In addition, the authors showed that there was a critical carbide size, about 110 nm for the A533B steel, below which the beneficial effect of reducing carbide size on toughness was insignificant.

Toughness ranking of microstructures opposite to general expectations due to the effect of carbide size was also observed by Bhadeshia and Edmonds[84] in bainite and by Pacyna and Witek in martensite.[85] In the former case, carbide free upper bainite showed a higher toughness than lower bainite containing carbide precipitates, whereas in the latter case toughness of martensite increased as the carbide size was decreased with the increase in carbon content below 0.47%C.

1.3.2.4. Retained Austenite Toughening

The beneficial effect of retained austenite on fracture toughness has been recognized by numerous investigators[3,23,35,80,82-84,87,94,95,105,114,118-125] although counter speculations[100] exist. The proposed retained austenite toughening mechanisms include plastic deformation[82,87,121], crack path deflection[87], and stress/strain induced martensitic transformation.[87,95,112,126]

Gerberich *et al*[112] estimated that stress induced martensite transformation consumed as much as five times more energy than the normal plastic dissipation processes occurring at a crack tip. Antolovich and Singh[126] attributed 77 to 84% fracture energy to transformation induced plasticity in a 9Cr-8Ni-2Mn-0.6C alloy.

Webster[123] observed another effective austenite toughening mechanism: "Cracks growing through martensite were arrested on reaching an area of austenite and then under increasing load were seen to branch and grow around the area of austenite."

Other indirect benefits of retained austenite are also realized.[125] The coherent γ/α interface is a lower energy boundary compared to the rotation lath boundary formed by lateral impingement of ferrite laths; it reduces impurity segregation and carbide precipitation tendencies. The existence of interlath retained austenite film also prevents interlath carbide formation. In tempered martensite, however, if retained austenite decomposes into ferrite and carbides, which can act as crack initiation sites, both strength and fracture toughness decrease.[113]

The key to the maximum toughening effect is to obtain thermally and mechanically stable retained austenite. Two forms of retained austenite are frequently observed: film shaped retained austenite and blocky shaped retained austenite. Film shaped retained austenite, distributed between the bainite/martensite laths or plates, is usually stable due to its higher carbon content and its geometrical relationship with bainite/martensite laths.[84,87] Hence fracture toughness of steels increases with increasing amount of retained austenite and thickness of austenite films.[127] However, when volume fraction of retained austenite increases to a certain level, blocky shaped retained austenite occurs.[82,128] In this form, the retained austenite is not stable. It can transform to twinned martensite or decompose to ferrite and carbides during cooling, upon tempering or deforming, and therefore promotes brittle fracture. It has been suggested that the volume fraction ratio of film over blocky retained austenite should be maximized.[84] In fact, the higher toughness of bainite than that of martensite in some steels can be partly attributed to the higher tendency of retaining film shaped, stable austenite in bainite than in martensite.

1.4. Effect of Alloying Content

The most commonly used alloying elements in low alloy steels are manganese, chromium, nickel, silicon, and molybdenum. The total amount of these elements in low alloy steels is less than 5 wt%. Hence it is important to understand the role of the elements and to use them effectively.

Manganese ties up sulfur atoms to form sulfides in relatively unharmful form and increases hardenability of steels. It suppresses M_s temperature and reduces martensite auto-tempering tendency, thereby, increases strength[62] of ferrite by solid solution strengthening but reduces plasticity. Manganese is an austenite stabilizer; it increases retained austenite volume fraction in as-quenched structures.[125]

Chromium is a transient γ loop closing element. With less than 7 or 8% addition, it lowers the temperature range of $\gamma \rightleftarrows \alpha$ transformation. It greatly increases hardenability of steels. In alloys with medium and high carbon content, chromium increases the tendency for twinned martensite formation.[129] Although a ferrite former, chromium helps the retention of austenite.[82,119] This effect is stronger when nickel is present.

Nickel largely dissolves in ferrite, even with high carbon content, and hence is useful in strengthening unhardened steels by the solid solution strengthening mechanism. When used alone, it has a mild effect on hardenability. When used together with other elements such as chromium, it greatly increases hardenability of alloys. In effective amounts in medium and high carbon steels, nickel also tends to retain austenite, thereby improves toughness.

Silicon promotes graphitization but inhibits cementite formation in martensitic and bainitic structures.[25,84,114] This effect eliminates crack-like defects from the structures and leaves more carbon atoms in solid solutions. Although carbon and silicon stabilize austenite, their effects are not enough to retain austenite. Therefore, manganese, nickel, and chromium are added to increase austenite stability.[82,87,119] When carbon enriches the existing austenite, the stability of the retained austenite is further increased.

Molybdenum raises austenite grain coarsening temperature, high temperature strength, and creep resistance. It greatly increases hardenability and contributes to deep hardening but promotes the formation of twins in martensite.[105]

1.5. Effect of Heat Treatment

The relevant heat treatment parameters to this study are austenitizing temperature, bainite transformation temperature, and bainite transformation time. The effect of austenitizing time is not studied since, in a proper austenitizing time range, grain size and chemical homogeneity of austenite are assumed to be functions of temperature only. The effect of tempering is also considered.

1.5.1. Effect of Austenitizing Temperature

In conventional heat treatment, low austenitizing temperature is preferred because it results in the smallest prior austenite grain size and presumably the best combination of mechanical properties.[130] However, in the 1970's investigators[90,95,110,118-120,125,130,131] repeatedly demonstrated that higher austenitizing temperature produced higher fracture toughness with no loss in strength and, therefore, better property combinations. The responsible microstructural changes included dissolution of residual alloy carbides,[118-120,130,131] elimination of twins in martensite structure,[95,105,118,130] obliteration of undesired high temperature transformation products,[85,97] and an increase in retained austenite volume fraction.[95,105,120,130]

Bodnar *et al* [88] found that increasing austenitizing temperature from 900 to 954°C increased the upper shelf energy of steam turbine forging steels by 61 J and attributed the effect to the dissolution of residual alloy carbides. Yield strength was also increased by up to 100 MPa at the expense of increasing FATT when austenitizing temperature was increased from 840 to 1040°C. In Fe/Mo/C steels, on the other hand, the marked increase in fracture toughness was due to reduction of internal twins in the martensite structure.[105] Many workers found an increase in retained austenite to be responsible for toughness improvement.

1.5.2. Effect of Bainite Transformation Temperature

Bainite transformation temperature determines the transformation product type and the substructural details. With decreasing transformation temperature, strength and toughness of bainite usually increase due to bainite packet size refinement.[82,107] However, bainite in different alloys behaves differently. Miihkinen and Edmonds[87] have observed monotonic toughness increase with decreasing transformation temperature in a Mn alloy. In a Ni alloy, however, toughness increases with decreasing transformation temperature and reaches a maxima at about 300°C. Further decreasing temperature leads to a decrease in toughness. The difference lies in the size of bainitic carbides. In the Mn alloy, carbides are fine; toughness is controlled by bainite packet size which monotonically decreases with decreasing temperature. In the Ni alloy, on the other hand, carbide size varies with transformation temperature, carbides of different size participate in the fracture process in different manner and cause fracture toughness to vary.

In silicon containing steels where carbide precipitation is partially or totally inhibited, Bhadeshia and Edmonds[84] correlated toughness to the volume fraction of retained austenite. Reducing transformation temperature increased volume fraction of bainite thermodynamically allowed and decreased the amount of retained austenite. As a result, the ratio of film over blocky shaped austenite, and therefore toughness, was increased. A slightly different phenomenon was observed in low alloy bainitic-austenitic alloys.[82] Here, both austenite volume fraction and the ratio of film over blocky shaped austenite increased with increasing transformation temperature below 320°C. Hence, ductility and toughness increased with transformation temperature between M_s and 320°C.

When different austenitizing temperatures were used, different trends between the toughness of bainite and the transformation temperature in a low alloy steel were observed.[110] If austenitizing temperature was high or prior austenite grain size was large, the ductile-brittle transition temperature of bainite decreased with decreasing transformation temperature to a minima at about 350°C and then increased with further decreasing transformation temperature. This behavior contrasted with the constant ductile-brittle transition temperature associated with low temperature austenitization.

1.5.3. Effect of Bainite Transformation Time

Bainite transformation time also affects mechanical properties. A short holding time above the M_s may interrupt bainite transformation and let more austenite transform to martensite. The transformed duplex microstructure in many cases[81,108,132] has better strength and toughness combinations than either martensite or bainite but there are examples where toughness is reduced due to the presence of martensite, the decrease in retained austenite,[82] and the decrease in austenite stability.[83] Prolonged holding after bainite transformation completion may lead to carbide growth, austenite stabilization due to carbon enrichment, or retained austenite decomposition.[83] These processes affect toughness in different directions; the net effect depends on the concerned steel composition and its bainite transformation kinetics.

1.5.4. Effect of Tempering Treatment

Bainite transforms at relatively high temperatures at which carbon diffusion rate is high. Carbon partitioning to surrounding austenite or dislocations and carbide precipitation may occur. Therefore, tempering of bainite is usually unnecessary. Nonetheless, experiments show that tempering of bainite at low temperatures may improve strength and toughness.[84,90] The effect may be due to partitioning of carbon or further stabilization of retained austenite. Another possibility is the tempering of the high carbon martensite formed subsequent to bainite transformation.

Tempering of bainite structure at high temperatures results in reduced mechanical properties. By tempering a 4340 steel at temperatures between 350 and 500°C, Smith and Hehemann[60] noticed a decrease in strength of martensite and bainite due to carbide coarsening and enlargement of cellular substructures. Viewing the effect of coarse carbide and retained austenite decomposition on toughness, a toughness degradation should be expected.

1.5.5. Summary

Bainite transformation is a complicated process. The transformation characteristics, the resulting microstructure, and the mechanical properties depend on the steel composition and the heat treatment. Many contradictory results exist in the literature. Some structure-property relationships have been observed, and the corresponding toughening mechanisms have been identified. Based on this progress, general guidelines for alloy and microstructural design have been proposed. However, the current knowledge of bainite and its various aspects is limited; detailed microstructure and property predictions are practically impossible. The extension of one toughening mechanism to a different class of steels is also difficult; experimental identification of the toughness controlling microstructure and the predominant toughening mechanism in a given steel is necessary. Accordingly, the best heat treating condition for a given steel cannot be reliably predicted but has to be experimentally determined in pre-selected heat treatment parameter ranges.

This work investigated the effect of austenitizing temperature, bainite transformation temperature, and bainite transformation time on fracture toughness in a low alloy steel. The range of austenitizing temperature was from 850 to 1050°C. Austenitizing temperatures greater than 950°C rarely find applications in mass production due to furnace design limitations. Here the high temperatures were included purely for academic interests. The bainite transformation temperature range was that in which lower bainite formed. Martensite/bainite duplex structure as well as only bainite were obtained by changing the transformation time. When fracture toughness and microstructure were changed upon varying heat treatment conditions, relationships among heat treatment parameters, microstructure, and fracture toughness could be deduced. Based on these relationships, the best heat treatment condition for the optimum strength and toughness could be obtained.

This study also investigated the effect of tempering on the fracture toughness of bainite by comparing toughness of specimens tempered at 200°C for two hours with that of the as-transformed specimens.

1.6. Fracture Mechanisms

Fracture mechanics is a relatively young, yet active, field of study. Many publications have been accumulated since World War II, especially after 1960. Detailed derivation and development is found in text books and articles elsewhere.[133-135] Only the commonly observed fracture modes are included here, since they are often referred to in later chapters. These modes are microvoid coalescence, cleavage, intergranular fracture, and fatigue failure, Figure 1.1. These are discussed separately.

1.6.1. Microvoid Coalescence

Microvoid coalescence, also known as dimple rupture, is a failure process that contains several steps: formation of microvoids, growth of voids, and coalescence of adjacent voids. Microvoids nucleate at inclusions and large particles by splitting the particle/matrix interface or by cracking the particles.

In engineering materials, particles are divided into three categories:[134] (a) large particles of the size 1 to 20 μm, (b) intermediate particles of the size 500 to 5000 Å, and (c) precipitates on the order of 50 to 500 Å. The large particles are usually brittle and incapable of accommodating the plastic deformation of the surrounding matrix. As a result, they fail early on and nucleate microvoids, when the matrix has undergone only a small amount of plastic deformation. However, since large particles fail at a few per cent of strain, while the final fracture occurs at much higher strains, Broek[136] has concluded that although the cracking of the large particles reduces toughness, it is not essential to the fracture process, and the intermediate particles are responsible for the final fracture. These particles lose coherence with the matrix when extensive plastic flow takes place in their vicinity, and microvoids form between the particles and matrix. The voids grow by slip causing the material between the voids to neck down to the full 100 per cent. Figure 1.2 shows schematically the steps of microvoid coalescence. The necking takes place at a micro-scale and the resulting total elongation remains small. Microvoid coalescence is usually a ductile mode of fracture but it is not necessarily always true.

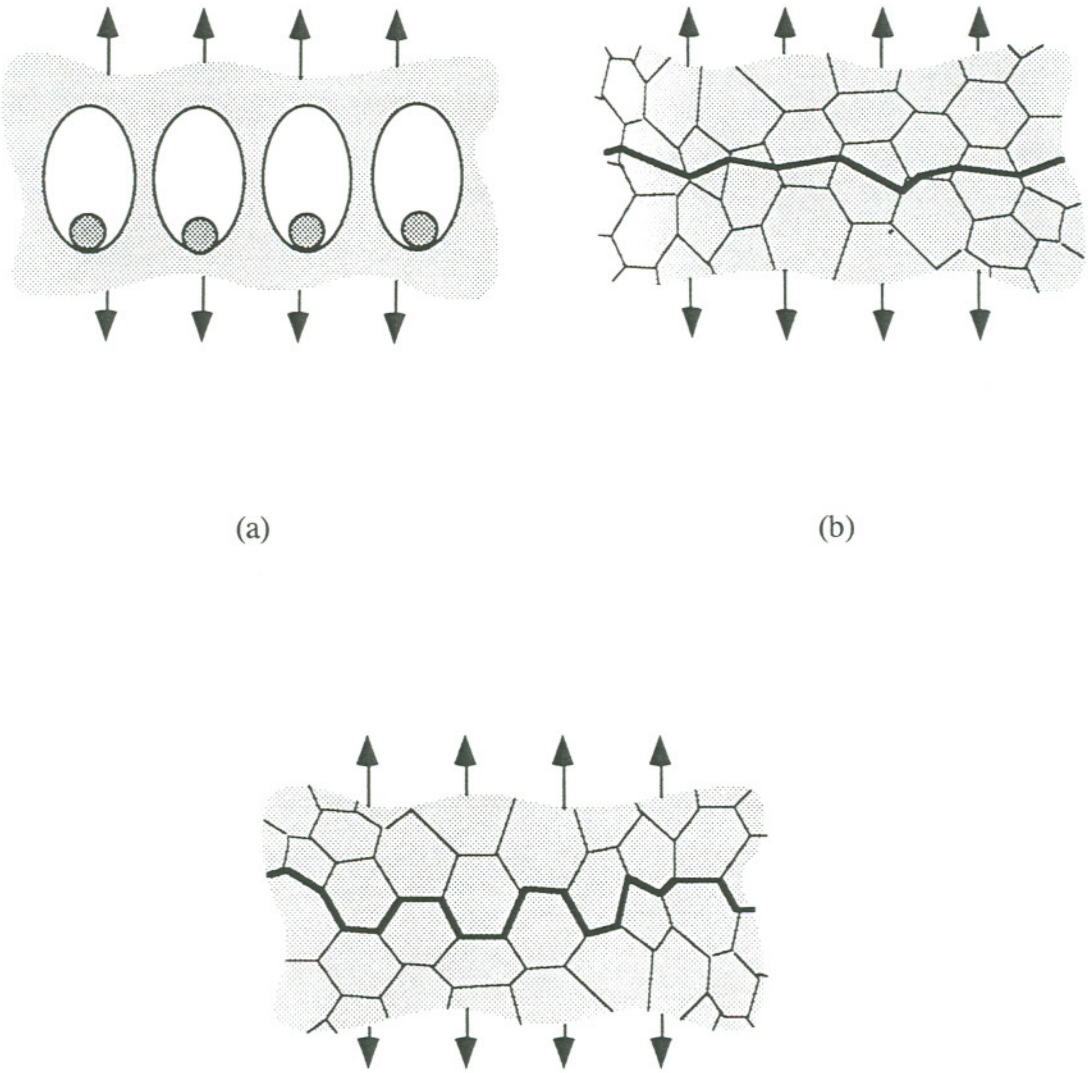

(a)

(b)

(c)

Figure 1.1. Three Micromechanisms of Fracture in Metals. (a) Microvoid Coalescence, (b) Cleavage, and (c) Intergranular Fracture.

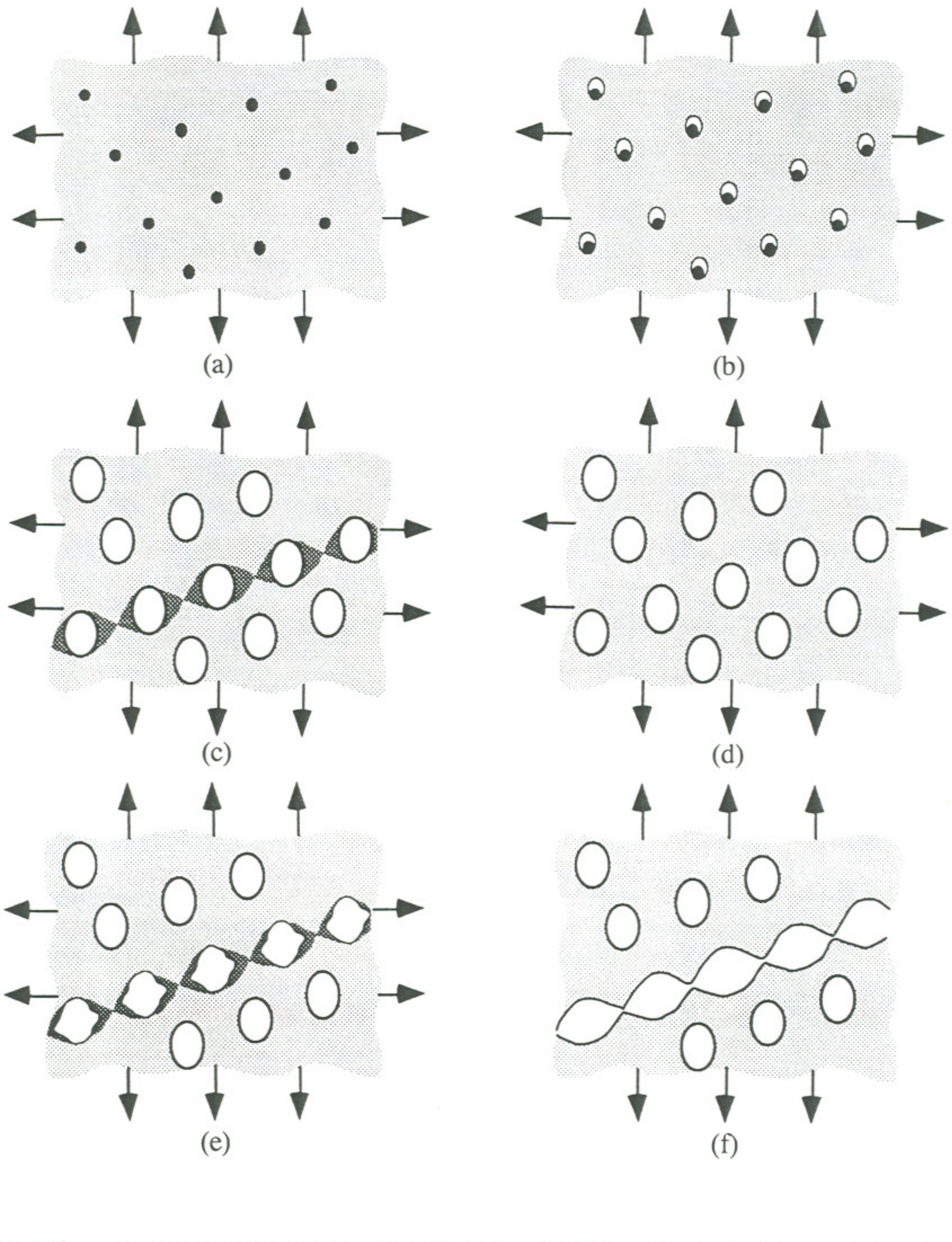

Figure 1.2. Stages of Microvoid Coalescence in Metals. (a) Inclusions in a Ductile Matrix, (b) Void Nucleation, (c) Void Growth, (d) Strain Localization, (e) Necking between Voids, and (f) Void Coalescence and Fracture.

1.6.2. Cleavage

Cleavage fracture of metals occurs by direct separation along crystallographic planes due to breaking of atomic bonds. This mechanism is usually associated with a particular crystallographic plane. Iron in bcc structure, for example, cleaves along {001} planes. Within one grain, the fracture surface is relatively flat. At grain boundaries the crack changes directions according to the misorientation of the grains and persists in the same type of planes in adjacent grains.

Several features often accompany cleavage fracture. The most observed is a so called river pattern because of its resemblance to a river and its tributaries. This river pattern is formed due to the merging of cleavage steps along parallel planes. It is more likely to occur at grain boundaries where a crack has to reorient to pass the boundary. This causes the next grain to cleave along several planes as shown in Figure 1.3. The steps are joined by secondary cleavage or by shear which raise the fracture energy. To minimize the fracture energy, the cleavage planes merge during propagation. Hence from the appearance of the river pattern one can deduce the crack propagation direction, which is the down stream direction.

Another feature is the cleavage tongue so named because of its apparent shape. A tongue is believed to form when cleavage along a (001) plane intersects a (112) twin, Figure 1.4. The main crack proceeds around the twin while a part of it propagates along the (112) plane for some distance, then fractures the twin and falls back to the original (001) plane.

The primary reason for cleavage fracture is that stress, especially local stress at the tip of micro-cracks, cannot be relaxed through plastic deformation. When local stress, σ_{yy}, increases beyond a critical cleavage stress, σ_f , over a characteristic distance defined by the material, cleavage occurs. Cleavage fracture usually happens to metals with bcc and hcp structures where there are fewer efficient slip systems,

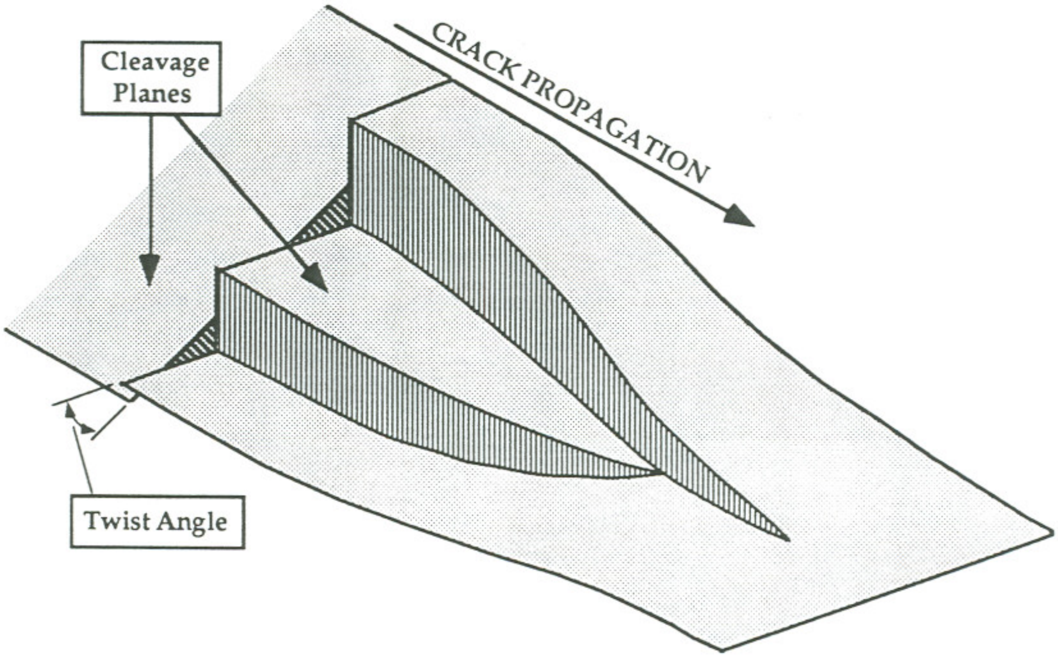

Figure 1.3. River Pattern Formation Mechanism.

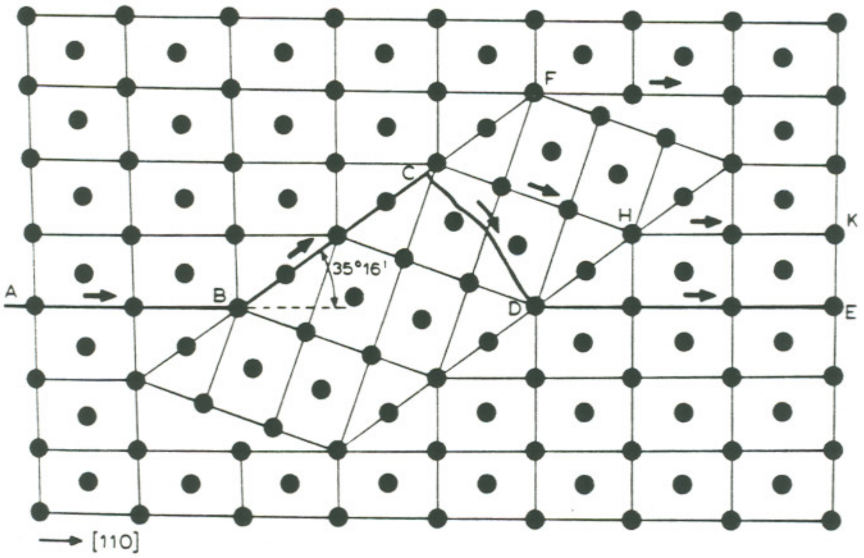

Figure 1.4. Formation of Cleavage Tongue due to Passage of Twin. Cut along (110) Plane through a Coherent Twin in bcc Lattice. (After Broek)

especially at low temperatures where active slip systems are lacking. Iron and steel, tungsten, molybdenum, chromium, zinc, beryllium, and magnesium are all susceptible to cleavage fracture. In many cases, crack initiation is the critical process. Once cracks are formed, propagation takes little energy. This is because cleavage proceeds at high speeds where plastic deformation is further suppressed.

A variation of cleavage fracture is the quasi-cleavage. In this process, some plastic deformation takes place at grain boundaries. In steels failed by quasi-cleavage, the fracture surface would contain relatively flat cleavage planes circumscribed by microvoid coalescence regions along ferrite grain boundaries and prior austenite grain boundaries. Cleavage is usually considered as a brittle fracture mechanism, quasi-cleavage is less brittle due to the ductile nature of the dimple rupture areas.

1.6.3. Intergranular Fracture

Intergranular fracture, as its name implies, occurs when grain boundaries are the preferred fracture path. There is no single mechanism for intergranular fracture. Rather, a variety of situations lead to cracking on grain boundaries, including

(a) precipitation of a brittle phase on the grain boundary,
(b) segregation of impurities such as sulphur and phosphorous to grain boundary,
(c) formation of brittle microstructure near grain boundary,
(d) hydrogen embrittlement and liquid metal embrittlement,
(e) environmental assisted cracking,
(f) intergranular corrosion, and
(g) grain boundary cavitation and cracking at high temperatures.

Briefly, precipitation of carbides on grain boundaries reduces grain boundary strength as compared to the grain interior. Fracture of the carbides also shift crack initiation sites to grain boundaries. Hence, grain boundary becomes the preferred crack path. This mechanism is responsible for martensite temper embrittlement (occurring at 250 to 350°C)[119] and temper embrittlement (occurring at 500 to 600°C).[119,131]

Segregation of sulphur and phosphorous to grain boundaries could also occur during step quenching and tempering. It has been proposed that impurities tend to be electronegative with respect to the matrix. They draw electronic charge off the metal atoms. This electronic charge transfer results in a weakening of the metal-metal bonds around the impurity. When impurities are segregated at the grain boundary, many metal-metal bonds will be weakened, and this weakening can give rise to intergranular fracture.[137]

In quenched or austempered steels, austenite is more likely to be retained along prior austenite grain boundaries. If the stability of austenite is not enough, the residual austenite transforms to high carbon martensite which is brittle and increases the possibility of intergranular fracture. Tempering reduces the brittleness of the martensite but low temperature tempering may not completely remove the twins while high temperature tempering may introduce other modes of embrittlement. Hence, these structures are susceptible to intergranular fracture.

1.6.4. Fatigue

Under the action of cyclic loads cracks can be initiated as a result of cyclic plastic deformation. Even if the nominal stresses are well below the elastic limit, locally the stresses may be above yield due to stress concentrations at inclusions or mechanical notches. Consequently, plastic deformation occurs locally on a micro-scale without a macroscopic sign.

Several models have been proposed to explain the initiation of fatigue cracks by local plastic deformation, that by Wood[138] is depicted in Figure 1.5. During the load-rising cycle, slip occurs on a favorably oriented slip plane. In the load-falling cycle slip takes place in the reverse direction on a parallel slip plane, since reverse slip on the original plane is inhibited by dislocation annihilation[139] and by oxidation of the newly created free surface. This first cyclic slip gives rise to an extrusion or an intrusion in the metal surface which may grow into a crack during subsequent cyclic loadings. Once a crack is formed, it propagates through a reversed slip, or a crack tip opening and resharpening mechanism[140]. During each stress cycle, the crack advances by a small distance and leaves a plastically deformed region, which on the fracture surface forms one striation. In ductile materials, fatigue striations are readily observable but in high strength steels they may not be as apparent.

Fatigue cracks usually start at corners, notches, steps and other places in structures where stress concentration exists. It also arises from surface roughness.[141] Since fatigue cracks initiate and grow under cyclic stresses below the general yield stress of a material, their existence and growth may be unexpected and undetected. When a crack reaches a critical size, it can cause catastrophic failure of an engineering structure.

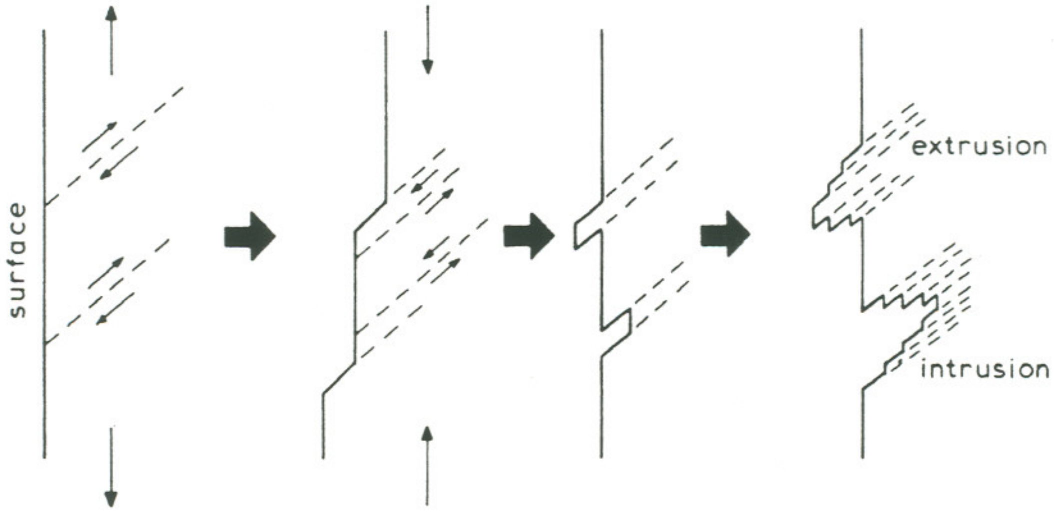

Figure 1.5. Wood's Model for Fatigue Crack Initiation.

CHAPTER 2

EXPERIMENTAL PROCEDURE AND DESIGN

2.1. Materials

The high carbon low alloy steel had the composition shown in Table 2.1.

Table 2.1. Composition of the Studied Steel.

C	Mn	Si	Cr	Ni	Mo	P	S
0.69	0.4	0.25	0.49	0.8	0.12	0.014	0.003

Samples were received in hot rolled and annealed conditions and in $127\times25.4\times1.5$ mm^3 strip form. Single Edge Cracked Tension (SECT) plate specimens for fracture toughness testing were machined according to ASTM STP 410.[142] Specimens for M_s measurement, grain size measurement, and time-temperature-transformation (TTT) diagram determination were also machined. In all cases the specimen thickness was 1.5 mm. All specimens received an initial quenching and tempering treatment to make the microstructure uniform except for half of the specimens for TTT diagram determination.

2.2. Martensite Transformation Start Temperature (M_s) Measurement

M_s temperature of the steel was measured using a Gleeble TMT system. Specimens of the size $127\times25.4\times1.5$ mm^3 were heat treated in an argon atmosphere. The average cooling rate of 80°C/s was achieved by blasting argon onto the specimen. A dilatometer with a 0.00037 mm resolution was used to monitor the specimen width change during heat treatment. The temperature and dilation data were recorded at a 0.4 hertz sampling frequency. The cooling rate between 300 and 200°C was about 10°C, therefore, the resolution of the measurement was ±4°C. Figure 2.1 shows typical temperature and dilation versus time curve.

The dimension of a specimen was quickly stabilized when the specimen was slowly heated to the austenitizing temperature. Upon cooling the specimen contracted. When martensite transformation took place, the specimen expanded. The temperature at which transformation induced expansion overcame thermal contraction, or the temperature corresponding to the minimum specimen width, was regarded as M_s temperature of the steel.

The measured M_s was affected by many factors. The effect of the initial microstructure and austenitizing temperature on M_s was investigated using the arrangements shown in Table 2.2 in which 1st to 4th indicated the number of heat treatment.

Table 2.2. Sequence of M_s Measurements.

Group	Austenitizing Temperature, °C				
	850	875	900	925	950
I	1st, 4th		2nd		3rd
II		all			
III	3rd		1st, 4th		2nd
IV				all	
V	2nd		3rd		1st, 4th

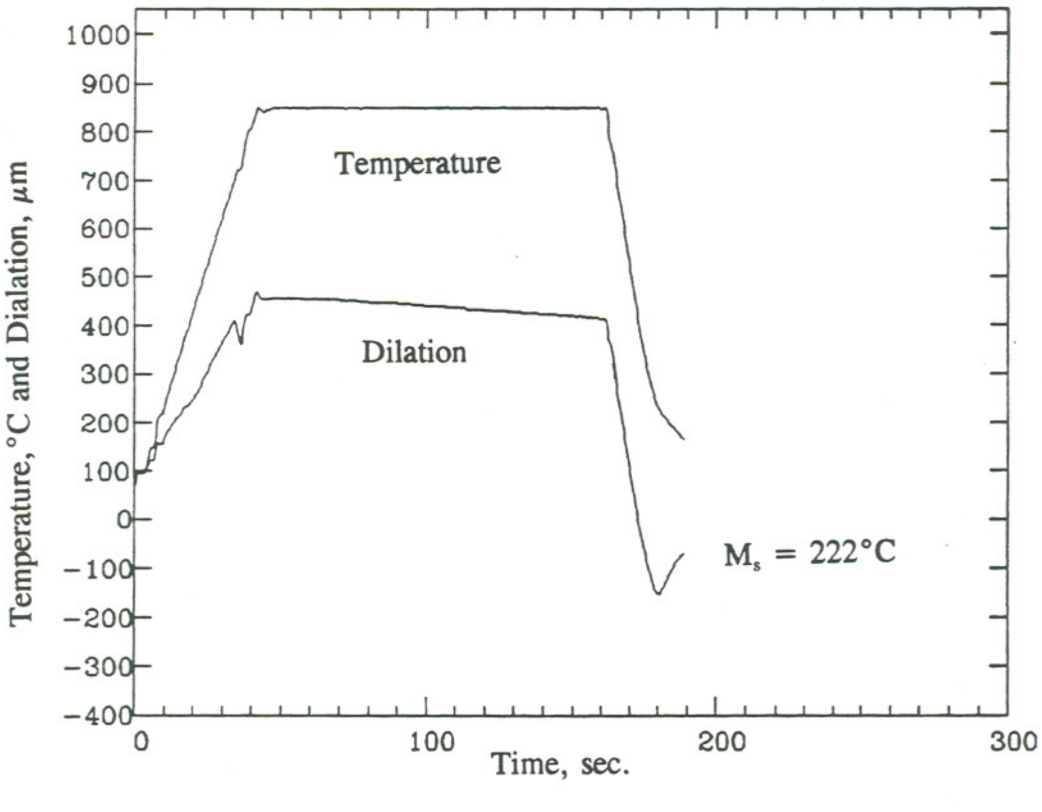

Figure 2.1. A Typical Temperature and Dilation versus Time Curve Obtained from M_s Temperature Measuring Heat Treatment.

The specimens were separated into five groups; each contained six specimens. Four measurements were taken from each specimen. The austenitizing temperature for the first measurement increased from Group I to Group V. It changed from test to test for groups I, III, and V but remained constant for groups II and IV. The latter two groups were designed to be the references. If the measured M_s kept changing for these two groups, the change was due to the repetition of the heat treatments and the associated grain refinement. Otherwise, the repeated heat treatment was expected to have no effect on the measurement. If the second case was true and if changes of M_s were observed for the other three groups, the change would be due to the change in the austenitizing temperature.

2.3. Grain Size Measurement

The delineation of prior austenite grain boundaries in high carbon steels is very difficult;[143] therefore, the grain size measurement was conducted using fractographic technique following ASTM E122-88.[144] The specimens used for this purpose were heat treated to a brittle microstructure, notched, and fractured under three point bending conditions. The fracture surfaces of the specimens were examined in a JEOL scanning electron microscope (SEM). The average diameter of the exposed grains was measured on micrographs and regarded as the prior austenite gain size of the steel at the applied austenitizing temperatures. Figure 2.2 shows a fracture surface of a specimen used in grain size measurement. The austenitizing temperature was 900°C and the prior austenite grain size was 20 μm or ASTM 8.4.

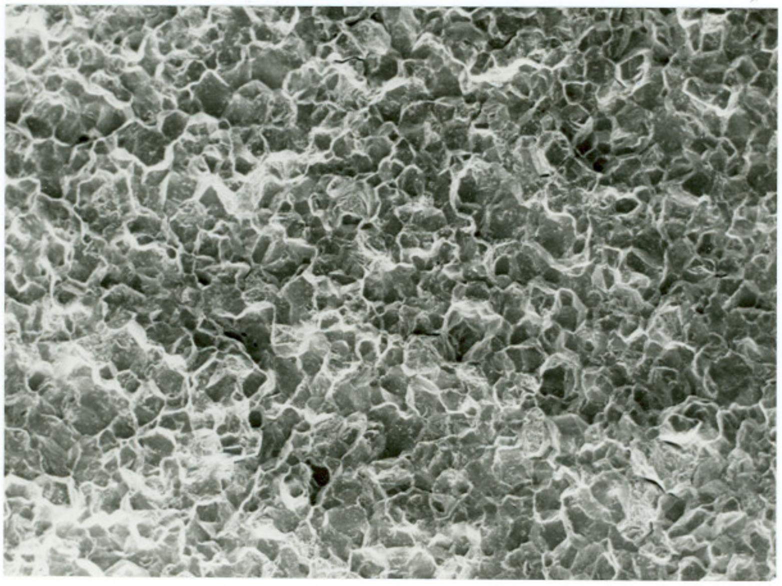

Figure 2.2. Fracture Surface for Prior Austenite Grain Size Measurement. The Austenitizing Temperature Is 900°C and the Prior Austenite Grain Size Is 20 μm.

2.4. Time-Temperature-Transformation (TTT) Curve Measurement

Two TTT diagrams of the steel were measured. One was measured using as received specimens, the other was determined on quenched and tempered specimens. Austenitization for both measurements were at 927°C for five minutes. Comparison of these diagrams would reveal the effect of initial microstructure on the austenite decomposition processes.

The size of the specimens was $64 \times 10 \times 1.5$ mm^3. During the heat treatments for TTT diagram measurement, the specimen width was continuously monitored using a cross strain gage with a 0.00025 mm resolution. A typical dilation curve is shown in Figure 2.3. The specimen dimension was stabilized during austenitization. It contracted during cooling but quickly settled down and maintained a constant value at the isothermal holding temperature before transformation took place. After an incubation time, represented by A, transformation started and the specimen width kept increasing until transformation finished, at the time represented by B, either because all austenite had been transformed or the maximum amount of transformation product allowed by thermodynamics had been obtained. The instants corresponding to A and B were determined by computer analysis. The program calculated the average specimen dilation at the holding temperature prior to transformation and detected the time at which the dilation increased beyond a pre-set window of 0.0015 mm over the average. This time was defined as the incubation time. The transformation finish time was determined in a similar way. The computer determined times were validated by visual inspection of the graph printed using the dilation data file. The TTT diagram was constructed by plotting the transformation initiation and finish times at different temperatures on a logarithm scale.

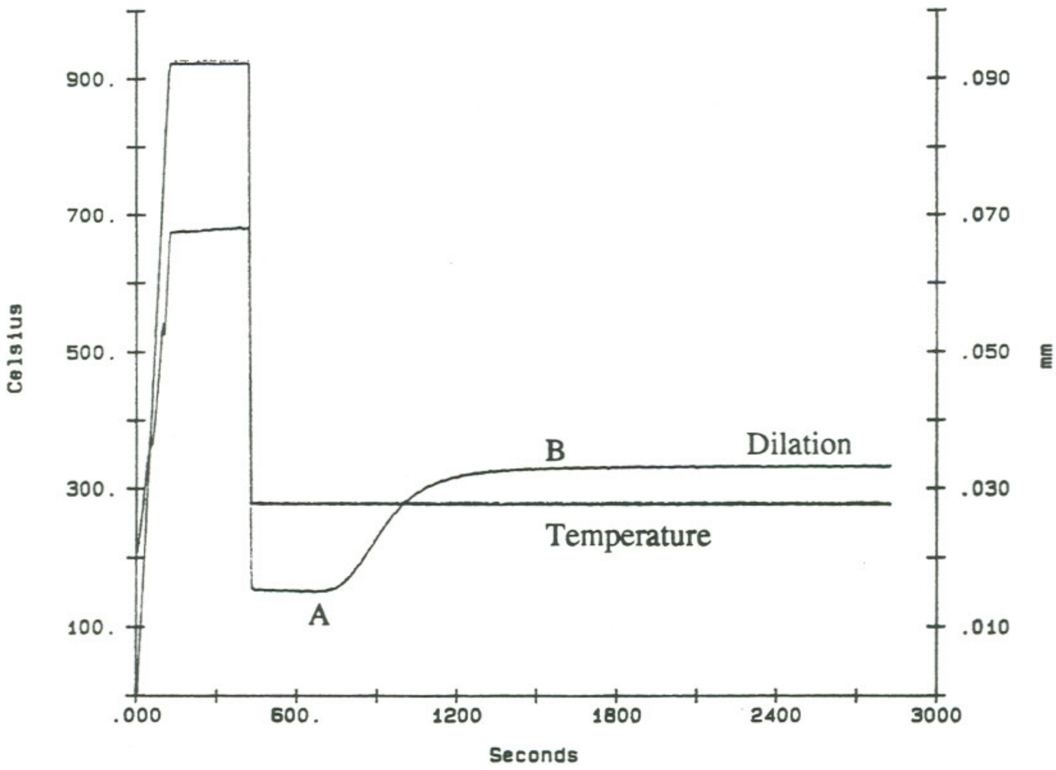

Figure 2.3. A Dilation Curve Resulted from Isothermal Heat Treatment.

2.5. Isothermal Bainite Transformation Kinetic Study

Bainite transformation kinetics was studied using the Johnson-Mehl-Avrami[145,146] equation of the following form:

$$X = 1 - \exp[-k(t-\tau)^n] \tag{2.1}$$

where X is volume fraction of the product phase, t is time, τ is reaction incubation time, and k and n are constants. The term n is called curve shape constant. Its value is determined by the dimensionality of a transformation; for a three dimensional transformation, n is between 3 and 4. For two dimensional and one dimensional transformations, n reduces to between 2 and 3, and between 1 and 2, respectively.[147] Within each range, n depends on the nucleation site and nucleation mode. For brevity, equation (2.1) is referred to as the Avrami equation hereafter.

Microstructural analysis revealed that primarily only one transformation product existed after every heat treatment. This characteristic allowed the volume fraction of the product to be approximated using

$$X = \frac{\Delta L}{\Delta L_{MAX}} \tag{2.2}$$

where ΔL_{MAX} was the maximum dilation of a specimen due to phase transforation and ΔL was the dilation at any time between transformation initiation and finish.

Upper and lower bainite transform in their respective temperature ranges. As the transformation temperature varies, the nucleation rate and transformation rate of the reactions change. The relationships between transformation temperature and the constants may be deduced.

Rearrange equation (2.1) to

$$ln ln(\frac{1}{1-X}) = ln k + n ln(t-\tau) \tag{2.3}$$

The slop of the linear portion of a lnln[1/(1-X)] versus ln(t-τ) plot is n and the intersection of the curve with the vertical axis equals k. The value of k is on the order of 10^{-3} to 10^{-4} and is subject to more factors and greater experimental errors than n. Therefore, only the relationship between n and transformation temperature was investigated.

2.6. Fracture Toughness Evaluation

2.6.1. Specimen Configuration

The as-received material geometry limited the fracture toughness test specimen configuration possibilities to only a few. Among these, single edge cracked plate tension specimen (SECT) was selected for its simplicity. In a set of feasibility tests, this specimen proved to be capable of differentiating fracture toughness of specimens with different microstructures.

The American Society for Testing and Materials recommends the following specimen dimensional requirements[142,148,149] for a plane strain fracture toughness test:

$$16B < W < 45B \tag{2.4}$$

$$a \geq 2.5\left(\frac{K_C}{\sigma_{ys}}\right)^2 \tag{2.5}$$

$$B \geq 2.5\left(\frac{K_C}{\sigma_{ys}}\right)^2 \tag{2.6}$$

where a is crack length, K_C is the apparent fracture toughness, σ_{ys} is yield strength, B and W are the specimen thickness and width, respectively. For single edge cracked plate tension specimens, a span-to-width ratio of three was also suggested.[142] Except the thickness requirement all other requirements were fulfilled. The measured K_C

values could not be compared with the published plane strain fracture toughness data but the comparisons of the toughness of the present steel under different heat treating conditions or with steels with the same thickness and similar strength were valid. Figure 2.4 provides detailed dimensions of the SECT specimen.

Toughness calculation followed that by Brown and Srawley.[142]

$$K_C = \frac{P_f}{BW}\sqrt{\pi a}\; Y\left(\frac{a}{W}\right) \tag{2.7}$$

where P_f was the load at failure, W and B were specimen width and thickness, respectively, a was crack length, and

$$Y\left(\frac{a}{W}\right) = 1.12 - 0.231\,\frac{a}{W} + 10.55\left(\frac{a}{W}\right)^2 - 21.72\left(\frac{a}{W}\right)^3 + 30.39\left(\frac{a}{W}\right)^4$$

The effective crack size correction due to McClintock and Irwin[150] was implemented through an iteration procedure.[135] Yield strength of the steel, needed for the plastic zone size estimation, was calculated from the measured hardness value using the linear equation by Squirrell et al[151]

$$\sigma_{ys}(ksi) = 0.145*[3.25*HV(10kg) - 349] \tag{2.8}$$

where HV(10kg) is Vickers hardness number using a 10 kg load. The calculated yield strength agreed with measured value very well.

2.6.2. Experimental Design

This investigation employed two types of experimental arrangements, i.e., factorial analysis and systematic analysis, to study the effect of heat treatment parameters on fracture toughness and hardness. The factorial analysis was used at the primary stage of the research and was followed by the systematic analysis. This setup allowed a wide range for each variable yet the total number of tests was low.

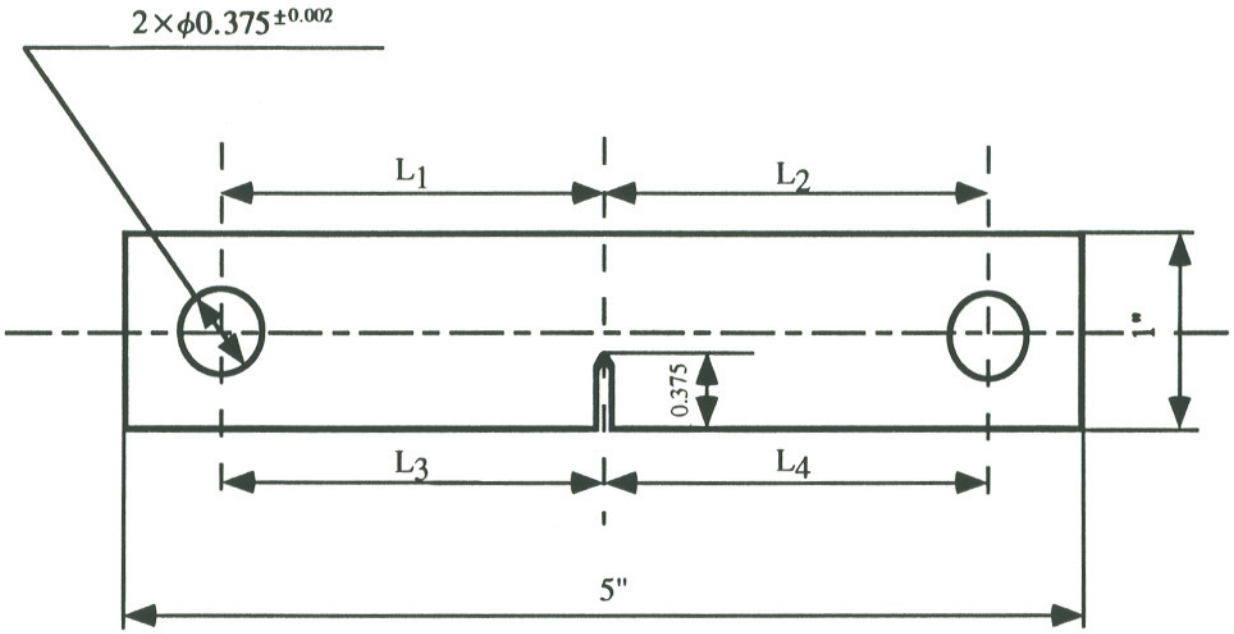

$L_1 = L_2 = L_3 = L_4 = 1.91^{\pm 0.002}$

Figure 2.4. Single Edge Crack Plate Tension Specimen Configuration.

2.6.2.1. Factorial Analysis

A three factor, three level fractional factorial analysis was used to establish rough relationships between the heat treatment parameters and fracture toughness. The investigated variables were austenitizing temperature (AT), bainite transformation temperature (BT), and bainite transformation time (Bt). The levels of the factors and the arrangements are listed in Table 2.3. The numbers in parentheses indicate the level of each factor. Ten specimens were heat treated under each condition. The specimens were then tempered at 200°C for two hours.

Table 2.3 shows the part of a standard four factor, three level factorial analysis table, $L_9(3^4)$, employed.

Table 2.3. Factorial Heat Treating Matrix.

Heat Treatment	AT °C	BT °C	Bt min
A	950 (1)	220 (1)	10 (1)
B	950 (1)	250 (2)	50 (2)
C	950 (1)	280 (3)	25 (3)
D	850 (2)	220 (1)	50 (2)
E	850 (2)	250 (2)	25 (3)
F	850 (2)	280 (3)	10 (1)
G	900 (3)	220 (1)	25 (3)
H	900 (3)	250 (2)	10 (1)
I	900 (3)	280 (3)	50 (2)

2.6.2.2. Systematic Study

To explore the effects of heat treatment parameters on the microstructure and fracture toughness more precisely, a systematic research was conducted. The studied heat treatment parameters were austenitizing temperature ranging from 900 to 1050°C and bainite reaction temperature between 250 and 320°C.

Table 2.4 shows the temperatures of the heat treatments. Each row contains heat treatments with a common austenitizing temperature, therefore, the difference in fracture toughness is brought about by the change in bainite transformation temperature. Similarly, the heat treatments in each sub-column under the bainite transformation temperature category have the same bainite reaction temperature but different austenitizing temperatures; the change in fracture toughness is due to the variation in austenitizing temperature. In the table, an x signifies a selected treatment, while a 0 means an omitted condition.

Table 2.4. Heat Treatments for Systematic Analysis.

Austenitizing Temperature, °C	Bainite Transformation Temperature, °C			
	250	280	300	320
900	x	x	x	0
950	x	x	x	x
1000	x	x	x	0
1050	0	x	0	0

Three specimens were heat treated under every condition. Three additional specimens were austenitized at 1000°C, austempered at 300°C and, tempered at 200°C for two hours. Tempering was not applied to other specimens of this test; the comparison of the toughness from this test and that from the factorial analysis would reveal the effect of tempering on toughness.

2.6.3. Fracture Toughness Testing

The preparation of the specimens for fracture toughness testing involved heat treatment according to the above experimental design, electric discharge machining of a single edge notch with a 0.15 mm root radius, and fatigue precracking to extend the notch into a sharp crack. The total crack length over specimen width, a/W, was controlled between 0.45 and 0.55 as previously suggested.[142]

Fatigue pre-cracking was carried out in an Instron machine of a capacity of 20,000 pounds under tension-tension conditions using a sine wave. The minimum load was fixed at 20 pounds, while a maximum load of 425 to 450 pounds was first used to initiate a crack. As the crack propagated, the maximum load was gradually reduced to 200 pounds. This procedure guaranteed a sharp crack with a minimum plastic zone at the crack tip.

Fracture toughness tests were carried out using the same Instron machine at room temperature. The load output was recorded using a 486 computer at a sampling rate of 10,000 hertz. Crack size, a, at the onset of fracture was measured using a traveling microscope on fracture surface from the edge of a specimen to the fatigue precrack front since no stable crack propagation was observed.

2.6.4. Loading Rate Effect

The effect of loading rate on the measured fracture toughness was studied by varying the cross-head displacement speed from 0.025 to 254 mm/sec. on a separate set of specimens. A 486 computer was used to record the load at 10,000 hertz frequency for tests with a displacement speed at and above 2.54 mm/sec. For slower tests an oscilloscope was used. At least two measurements were taken at every displacement speed.

2.6.5. Bainite Volume Fraction Effect

The effect of bainite volume fraction on fracture toughness was investigated by testing specimens with approximately 25%, 50%, 75%, and 100% bainite transformed at the same temperature. Volume fraction of bainite was manipulated by controlling the reaction time. To a certain degree these experiments repeated the study of the effect of bainite transformation time on toughness carried out in the factorial analysis but were in a more systematic manner and were also extended to shorter transformation time regime. Three specimens were tested under every microstructural condition.

2.7. Hardness Measurement

Hardness was measured on mounted specimens. A 0.5 mm thick surface layer was removed from every specimen. Then metallographic specimen preparation procedure was applied to achieve a smooth surface. Final polishing was done using 1200 grit abrasive paper. Knoop micro hardness of the specimens was measured using a LECO M-400 instrument with 1 kg load. Five measurements were taken on each specimen and the average was used to represent hardness of the specimen under the corresponding heat treating condition.

2.8. Fractography

All fracture surfaces were immediately coated with a protective clear plastic "Hi-Tech" spray paint to prevent extensive oxidization. The coating was dissolved in acetone and the specimen was rinsed in methanol and dried before examination.

Fracture surfaces of the specimens involved in the factorial analysis were examined in a JEOL scanning electron microscope (SEM) operated at 15 kV while the others were studied in a ZEISS SEM, also at 15 kV.

The observation was focused on the fracture mode change from one heat treating condition to another. Small surface roughness changes were also noticed for a qualitative correlation to the toughness.

2.9. Microscopy

2.9.1. Optical Microscopy

The specimens for optical microscopic examination were ground successively on 120, 240, 400, 600, 800, and 1200 grit abrasive papers and then polished with 6 μm and 1 μm diamond pastes. Final polishing was carried out by repeatedly polishing the specimens with 0.05 μm alumina particles suspended in glycerin and ethanol and lightly etching in a 4% picric acid in ethanol till all the disturbed metal was removed. To delineate martensite and bainite the final etching was carried out by submerging a polished surface in 4% picric acid for 6 to 8 seconds and then in LePera etchant[152] for 6 to 8 seconds. The solution was prepared by mixing 4% picric acid in ethanol and 1% sodium metabisulfite in distilled water in 1:1 volume ratio just before etching. Fresh solution was prepared for each specimen. The examinations were performed on a Nikon instrument.

2.9.2. Scanning Electron Microscopy

Scanning electron microscopy was performed in the Zeiss SEM in both back scattered electron (BSE) mode and secondary electron (SE) mode for microstructural feature identification and characterization. The specimen preparation procedure was the same as that used in optical microscopy work.

2.9.3. Transmission Electron Microscopy (TEM)

Specimens of the size $25 \times 10 \times 1.5$ mm^3 cut from the fractured SECT specimens were ground to 0.5 mm thickness in a grinder by removing a 0.5 mm layer from each side in a coolant to prevent over heating. The feeding rate was 0.01 mm per pass. The specimens were then manually thinned to 150 μm thickness by grinding successively on 120, 240, 400, 600, 800, and 1200 grit papers. Three millimeter diameter disks were punched from the foils. A shallow crater of 1.5 mm diameter and 50 μm depth was ground in the center of each disk using a dimpler. The disks were electro-polished at 50 volts in 5% perchloric acid in methanol maintained at -40°C in a double jet unit. TEM studies of the foils were conducted in a Hitachi H-800 electron microscope operated at 200 kV.

2.10. Heat Treatment

Two types of heat treatments were applied. The first type was quenching and tempering, the purpose of which was to prepare the specimens for further treatments and tests. Austenitizing of the specimens for quenching was carried out in a Lucifer furnace at 850°C for 12 hours with the specimens sealed in argon filled capsules. Quenching was done by transferring and breaking the capsules in room temperature fresh water. The specimens were then tempered at 200°C for two hours.

The second type was the final heat treatment and was carried out in a Gleeble model 1500 system in an argon atmosphere. The heating rate was 7.7°C/s. The austenitizing time was 5 minutes at all the involved temperatures. The cooling rate of 150°C/s was achieved by blasting 35 psi helium at the specimen. The differences in the final heat treatments for different purposes are detailed in the following sections.

2.10.1. Heat Treatment for Grain Size Measurement

To measure prior austenite grain size as a function of austenitizing temperature, the specimens were austenitized at 800 to 1200°C , cooled to 220°C and held for 10 minutes, then quenched to room temperature. This heat treatment was found to promote intergranular fracture.

2.10.2. Heat Treatment for TTT Curve Measurement

The austenitizing temperature for TTT curve measurement was 927°C. The isothermal reaction temperature ranged from 250 to 700°C. Holding time was varied to allow transformation to finish at each temperature.

2.10.3. Heat Treatment for Fracture Toughness Measurement

The specimens used for fracture toughness tests were first quenched and tempered to provide the ends of the specimens with some strength. The final heat treatment parameters are detailed in Tables 2.3 and 2.4.

A separate set of specimens was heat treated to the same condition for the study of loading rate effect on toughness. The austenitizing and bainite transformation temperatures were 950 and 280°C, respectively. Bainite transformation proceeded to finish.

Another set was heat treated using the same heat treatment parameters except the bainite transformation time was varied to obtain different bainite volume fraction. Fracture toughness testing of these specimens was expected to reveal the effect of bainite volume fraction on toughness.

CHAPTER 3

EXPERIMENTAL RESULTS

3.1. M_s Measurement

As described in Chapter 2, the M_s temperature was measured four times on each specimen. The first measurements always produced higher M_s values and a greater scatter than the subsequent measurements, especially when austenitizing temperature was low, Table 3.1. This phenomenon was attributed to the nonuniform structure of the as-received samples, heterogeneous alloying element distribution, and incomplete austenitization during the two minute austenitization. As temperature was increased, austenitization proceeded to a greater level, M_s value and the associated standard deviation decreased. Prolonged holding also enhanced austenitization and reduced M_s. Measurements after 5 and 30 minute austenitization at 850°C, yielded M_s of 255 and 239°C, respectively, as opposed to 260°C after 2 minute treatment.

In subsequent measurements, the specimens had more uniform and homogenous initial microstructures. As a result, the M_s clustered to 227°C regardless of the austenitizing temperature and the number of measurements. Calibration of the temperature measuring system showed that at the time the measurement was carried out, the machine consistently produced an error of 4°C below the actual temperature in the range 200 to 300°C. Hence, the M_s temperature of the steel was 231°C. Figure 3.1 depicts M_s temperature of the first and the fourth measurements as functions of austenitizing temperature. It was clear that above 900°C, two minutes was nearly adequate for the initial austenitization. After the first treatment, M_s temperature became a constant and did not vary with austenitization temperature.

Table 3.1. The Measured M_s and the Associated Standard Deviation of the Five Specimen Groups.

Sequence of Measurement	M_s Temperature and Standard Deviation, °C									
	I		II		III		IV		V	
	M_s	SD$^+$	M_s	SD$^+$	M_s	SD$^+$	M_s	SD$^+$	M_s	SD$^+$
First	260	15	244	9	235	5	232*	3	230	6
Second	228	4	229	4	225	6	227	4	223	6
Third	227	4	226	5	224	6	226	5	227	8
Fourth	231	9	227	5	227	5	229	4	228	8

* An abnormal data point of 264°C was rejected based on Chauvenet's criterion[153] since a t-test showed that the probability for a value to deviate from the mean by the observed amount (0.5%) was less than 1/(N), where N is the number of measurements. In other words, it was very unlikely that the value 264°C belonged to the population.

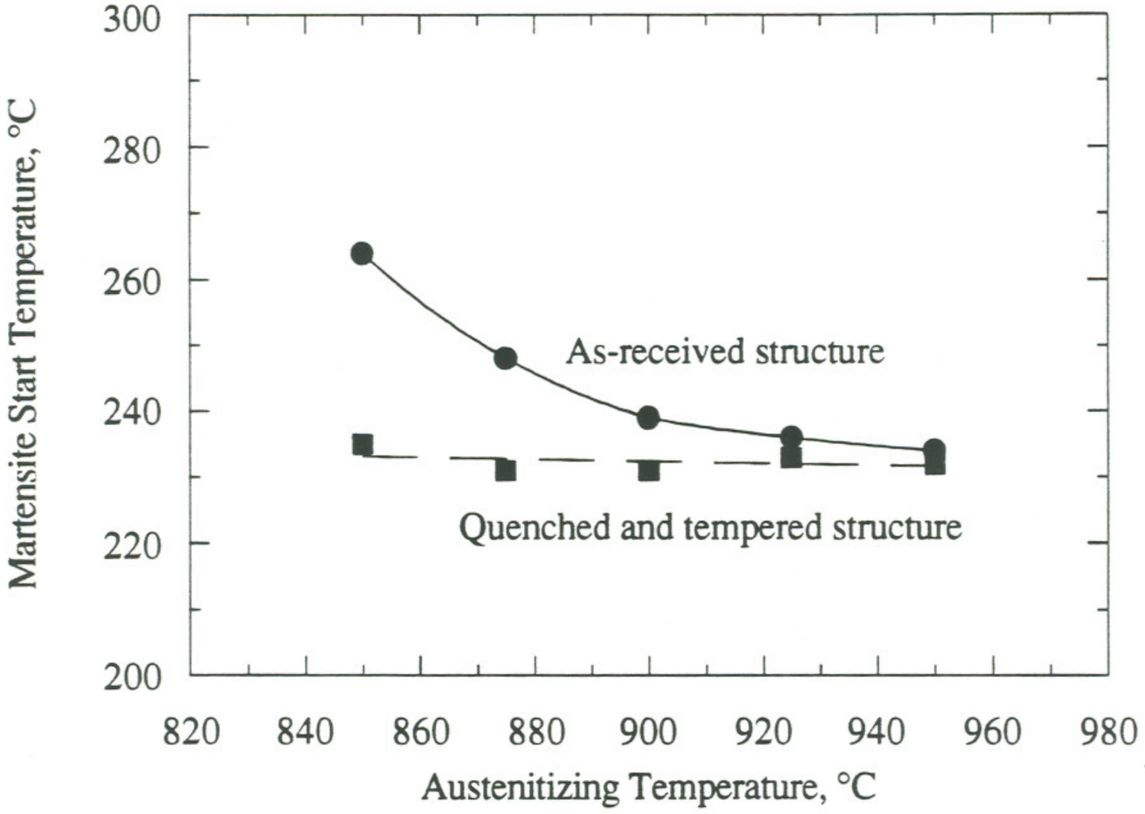

Figure 3.1. Variation of Martensite Transformation Start Temperature with Austenitizing Temperature.

3.2. Grain Size Measurement

Prior austenite grain size increased with austenitizing temperature, Table 3.2 and Figure 3.2. It grew slowly from 8 μm at 850°C to 38 μm at 1050°C and then grew quickly with further increase in austenitizing temperature. When austenitized at 1200°C, austenite grains were on the order of millimeters.

Table 3.2. Prior Austenite Grain Size at Different Austenitizing Temperatures.

Austenitizing Temperature °C	Prior Austenite Grain Size μm	ASTM Number
800	6	11.8
850	12	9.8
900	20	8.4
950	25	7.7
1000	28	7.5
1050	38	6.5
1100	121	3.2
1150	335	0.5

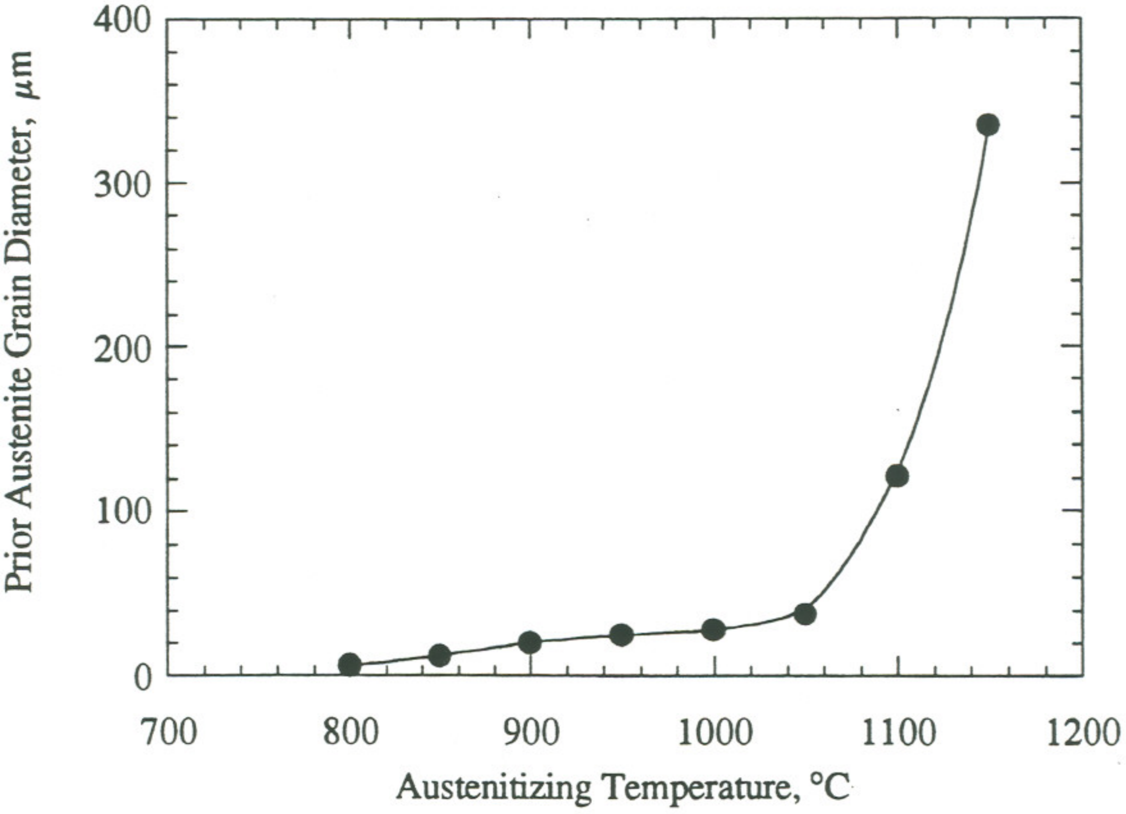

Figure 3.2. Prior Austenite Grain Size at Different Austenitizing Temperatures.

3.3. TTT Diagram Measurement

Time-temperature-transformation diagrams of the steel in as-received and in quenched and tempered conditions were almost identical after austenitization at 927°C for five minutes, Figure 3.3. This suggested that the initial microstructure did not affect the austenite decomposition process when similar austenitization condition was reached. As expected, the transformation start C curves of pearlite, upper bainite, and lower bainite overlapped due to low alloy additions. The reaction finish C curves, however, were somewhat separated.

A slight reaction acceleration at temperatures just above M_s was observed. This phenomenon was not due to the "swing back" effect associated with isothermal martensite transformation.[44,154,155] Instead, it arose from lower bainite transformation as will become clear in Chapter 4. In fact, the first three data points above M_s, formed part of the lower bainite C curve.

3.4. Fracture Toughness Measurement

3.4.1. Factorial Analysis

The experimental arrangement in the factorial analysis was such that the levels of more than one variables changed simultaneously from one test condition to another. Hence, one could not directly compare the test results. Rather, the average property with a certain variable being fixed at one level was compared against the average property of the same variable at another level.

The variable in consideration was called a reference variable. In calculating the mean properties of the reference variable at any level, each level of the other variables appeared once and only once. The effects of other variables on the mean properties of the reference variable were considered equivalent and were canceled out

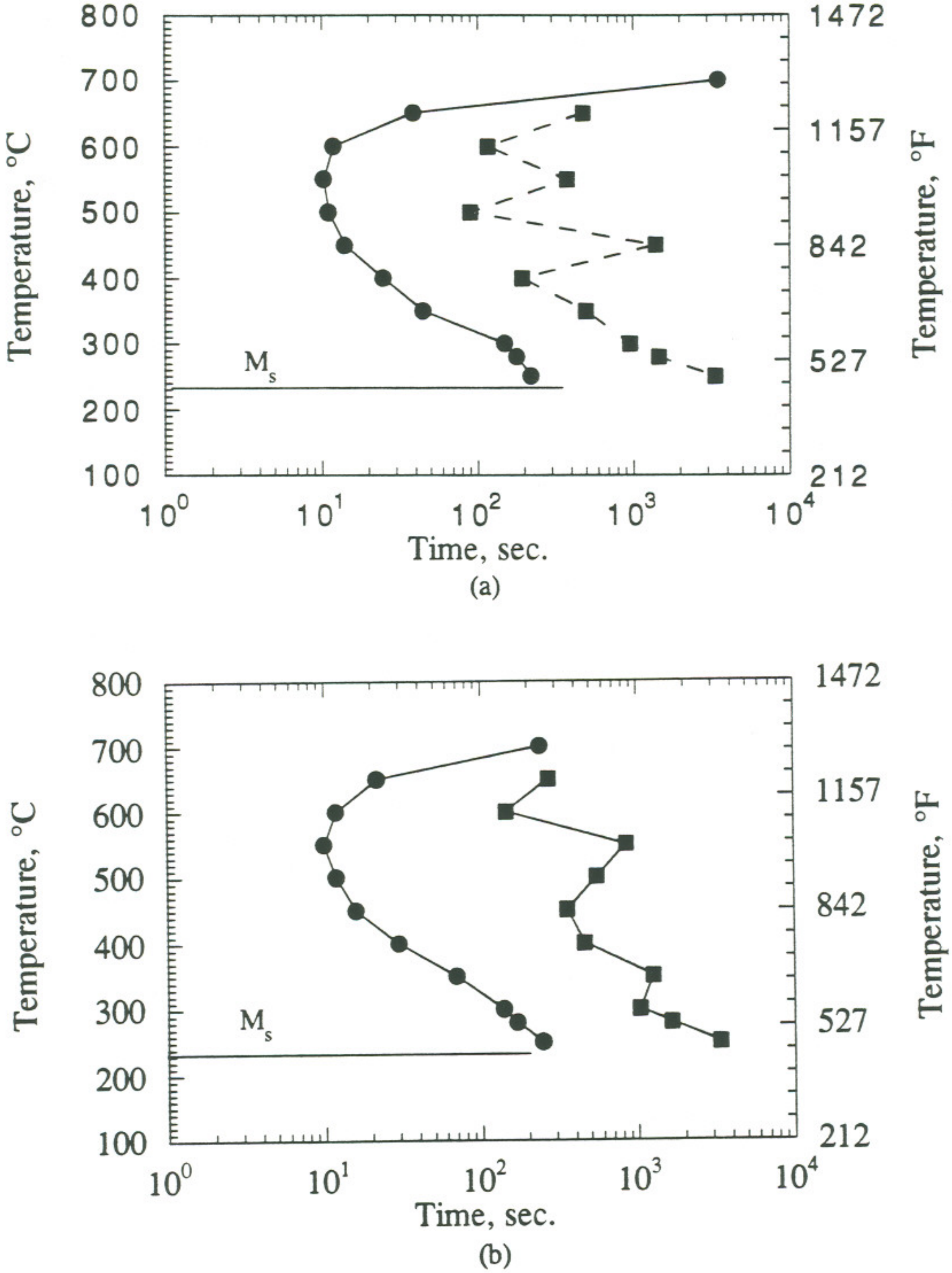

(a)

(b)

Figure 3.3. Time-Temperature-Transformation Diagrams of the Steel in (a) As-Received Condition and (b) after Quenching and Tempering.

when the mean properties of the reference variable were compared. The observed changes, hence, were due to the change of the reference variable itself. If the change was significant, the variable was a strong factor. Otherwise it was a weak variable.

The measured toughness values did not show any systematic dependence on the heat treatment parameters (see the right most column in Table 3.3) but the mean toughness clearly demonstrated an increase with both austenitizing and austempering temperatures. The third row of the table summarizes the mean toughness of each reference variable at the indicated levels, while the bottom row shows the maximum difference in the mean fracture toughness caused by changing the level of each variable. Apparently, bainite transformation temperature affected fracture toughness the most, austenitizing temperature ranked the second. Bainite transformation time imposed little effect. Figure 3.4 depicts the relationships between fracture toughness and the heat treatment parameters.

A linear regression analysis on the data in the third column of Table 3.3 yielded the following equations

$$\begin{aligned} K_{IC} &= 0.27BT-30.67 \\ K_{IC} &= 0.10AT-53.67 \\ K_{IC} &= 0.05Bt+35.06 \end{aligned} \tag{3.1}$$

From these equations the ranking of the effect of the variables on fracture toughness was clear.

In factorial analysis, the selection of a test matrix table is based on the number of variables and their levels considered. An ideal table contains the same number of columns as the number of variables; each column hosts one variable. If an available table has more columns than the number of variables, the extra columns are simply eliminated. The elimination does not affect the assessment of the effect of each

Table 3.3. Factorial Analysis of Fracture Toughness Results

Heat Treatment	Fracture Toughness, ksi$\sqrt{in}$			
	A.T.	B.T.	B.t.	K_c
A	950	220	10	33
B	950	250	50	41
C	950	280	25	53
D	850	220	50	27
E	850	250	25	32
F	850	280	10	37
G	900	220	25	25
H	900	250	10	36
I	900	280	50	43
I	42	28	35	
II	32	36	37	
III	35	44	37	
R	10	16	2	

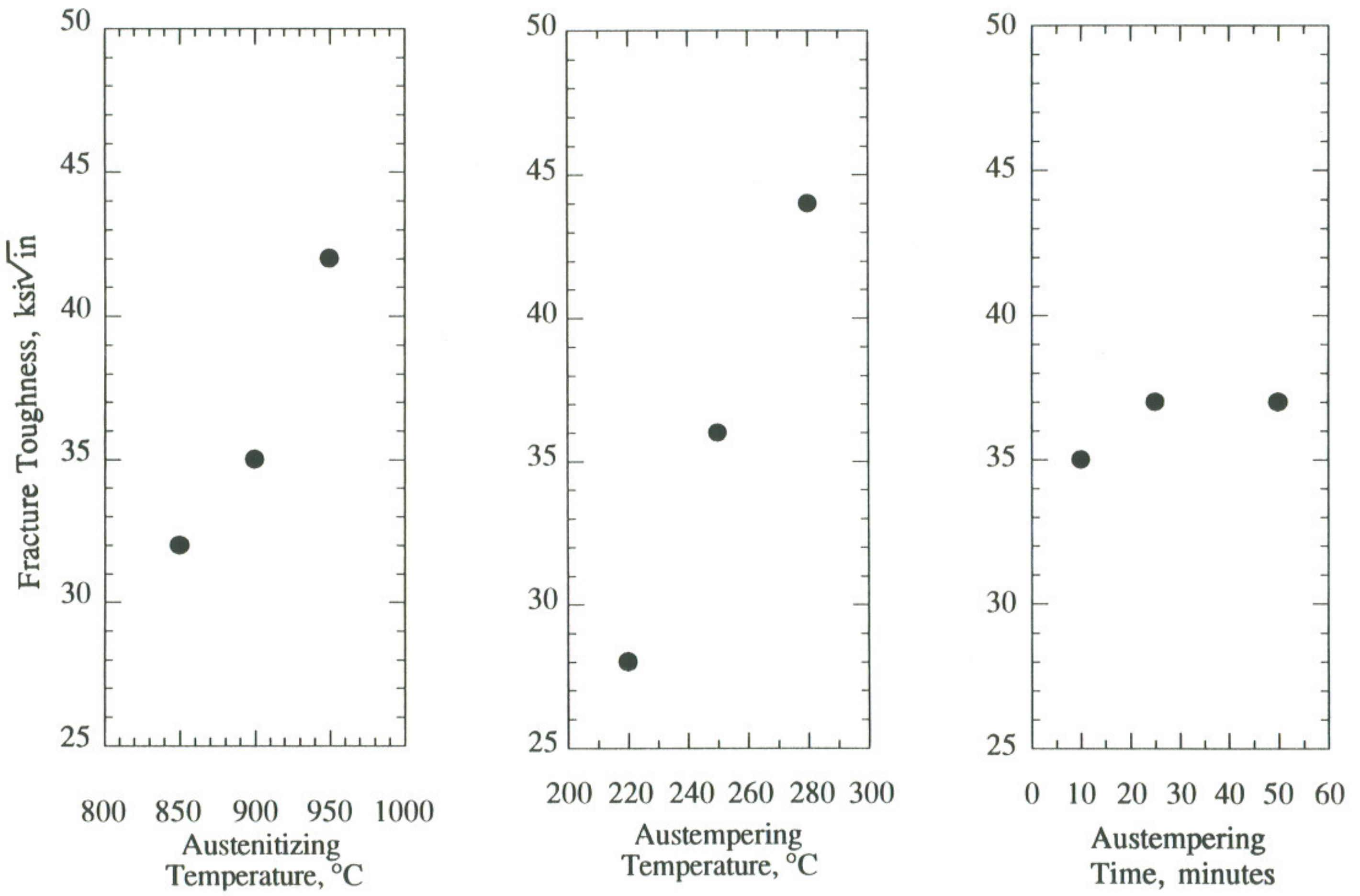

Figure 3.4. Relationship between Fracture Toughness and The Heat Treatment Parameters.

variable on the studied properties but it may impede the analysis of the interactions of the factors.

The factorial analysis table suitable for this study is $L_9(3^4)$, which is designed for four variable, three level situations. Since three variables are involved, three columns are needed; the fourth one is omitted. For a three level factorial analysis, each variable has two degrees of freedom. The study of the interaction of any two variables involves four degrees of freedom. The interaction is obtained from the other two columns not occupied by the variables under consideration. Since only three columns are available, the interaction of the variables cannot be investigated following the standard procedure.

However, it was noted that bainite transformation time exerted very little effect on toughness. Hence the interaction of austenitizing temperature and bainite transformation temperature could be assessed as in a two variable study, Table 3.4.

Table 3.4. Combined Effect of Austenitizing Temperature and Bainite Transformation Temperature on Fracture Toughness.

Fracture Toughness, ksi$\sqrt{\text{in}}$			
Austenitizing Temperature, °C	Bainite Transformation Temperature, °C		
	220	250	280
850	27	32	37
900	25	36	43
950	33	41	53

Figure 3.5 shows the trend of toughness with bainite transformation temperature. Relationships between fracture toughness and bainite transformation temperature at the three austenitizing temperatures are as follows:

$$\begin{array}{ll} 850^{\circ}C & K_c = 0.17BT - 9.67 \\ 900^{\circ}C & K_c = 0.30BT - 40.33 \\ 950^{\circ}C & K_c = 0.33BT - 41.00 \end{array} \tag{3.2}$$

It was clear that fracture toughness increased with increasing bainite transformation temperature and the rate was high when higher austenitizing temperatures were used. As expected, the average of the regression coefficients in equation (3.2) equaled the coefficient of bainite transformation temperature in equation (3.1) since the former was obtained from data at each austenitizing temperature, while the latter resulted from factorial analysis in which an average operation was applied.

The relationships between toughness and austenitizing temperature were

$$\begin{array}{ll} 220^{\circ}C & K_c = 0.06AT - 25.67 \\ 250^{\circ}C & K_c = 0.09AT - 44.67 \\ 280^{\circ}C & K_c = 0.16AT - 99.67 \end{array} \tag{3.3}$$

These equations repeated the observation that fracture toughness increased with increasing austenitizing temperature. A more important point was that the beneficial effect of high austenitizing temperature on fracture toughness was amplified by the use of high bainite transformation temperature. Hence, the austenitizing and bainite transformation temperatures were mutually supportive in the respective ranges tested.

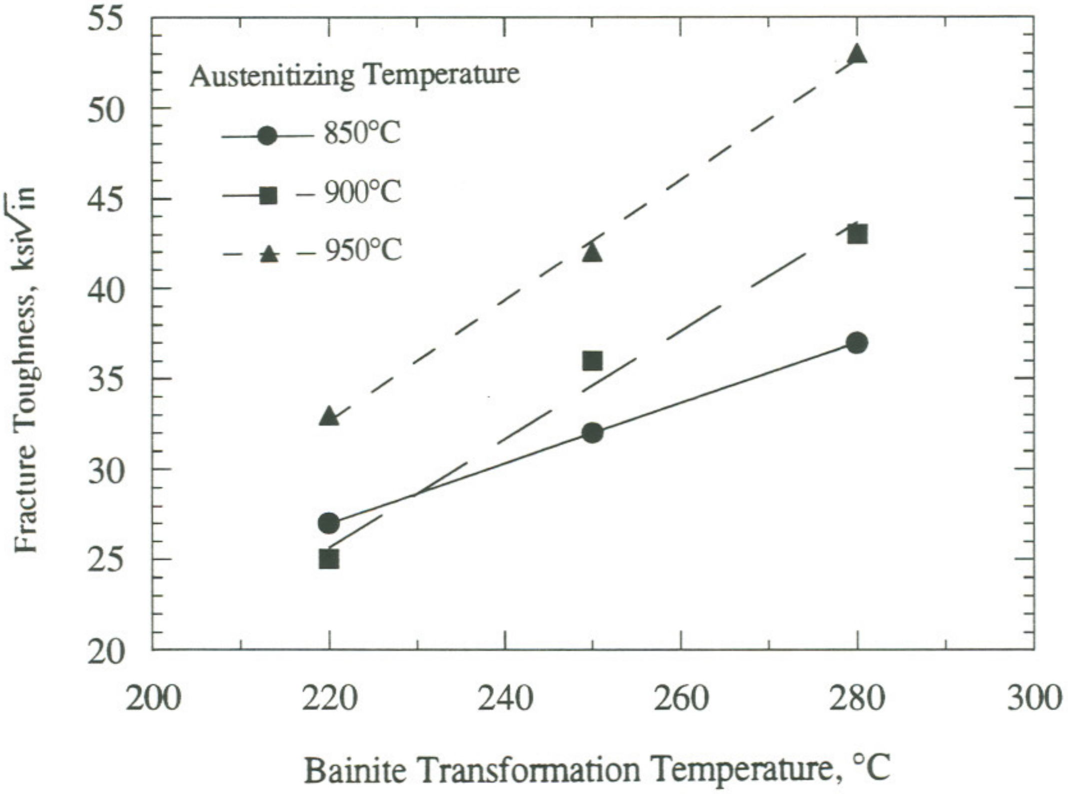

Figure 3.5. Fracture Toughness as a Function of Bainite Transformation Temperature.

3.4.2. Systematic Analysis

Systematic analysis results, Table 3.5, show that toughness increased with austenitizing temperature until the austenite grain growth temperature was reached. Toughness also increased with bainite transformation temperature to 320°C.

Table 3.5. Systematic Analysis Results.

Fracture toughness, ksi$\sqrt{in}$				
Austenitization Temperature, °C	Bainite Reaction Temperature			
	250°C	280°C	300°C	320°C
900	34	43	50	
950	35	45	49	55
1000	36	53	54/63*	
1050		52		

*Fracture toughness measured after tempering at 200°C for two hours.

Fracture toughness did not continuously increase with the austenitizing temperature. It formed a plateau at 53 ksi$\sqrt{in}$ when the specimens were austenitized at 1000°C. Further increase in austenitizing temperature reduced toughness.

The temperature at which fracture toughness started to decrease with increasing bainite transformation temperature was not clear. The temperature 320°C was in the upper/lower bainite transition temperature region. Since upper bainite was believed to reduce toughness, only one heat treatment was carried out at 320°C and no austempering was conducted at higher temperatures. The result, however, showed that toughness continuously increased with austempering temperature. The hardness of the specimens austempered at 320°C was below the required level for the application, hence, even though further toughness improvement could be obtained by increasing bainite transformation temperature, the overall mechanical properties were not acceptable. For this reason, no temperatures higher than 320°C were considered.

The application of a multiple linear regression analysis related fracture toughness to austenitizing and bainite transformation temperatures as

$$K_{IC} = 0.05AT + 0.33BT - 97 \tag{3.4}$$

The formula implied that the effect of increasing bainite transformation temperature was over six times greater than the increasing of austenitizing temperature.

3.4.3. Effect of Tempering Treatment on Fracture Toughness

The fracture toughness tests were carried out on tempered specimens in the factorial analysis but on as-austempered specimens in the systematic analysis. By comparing the measured fracture toughness of specimens heat treated to similar conditions in the two tests, the effect of tempering treatment on toughness could be deduced, Table 3.6. Tempering increased fracture toughness by 10 to 20% if the austenitizing temperature was higher that 900°C but had little effect if the austenitizing temperature was at or below 900°C, Figure 3.6. For example, specimens austenitized at 950°C and austempered at 250°C had a toughness of 41 ksi$\sqrt{\text{in}}$ in tempered condition but 35 ksi$\sqrt{\text{in}}$ in as-austempered condition. Confirmation tests showed that tempering at 200°C for 2 hours increased fracture toughness of specimens austenitized at 1000°C and austempered at 300°C from 54 to 63 ksi$\sqrt{\text{in}}$, a 17% improvement. On the other hand, the specimens austenitized at 900°C exhibited about the same toughness with or without tempering.

Table 3.6. Effect of Tempering on Fracture Toughness.

Fracture Toughness of As Austempered (N) and Tempered (T) Conditions, $ksi\sqrt{in}$						
Austenitizing Temperature °C	Bainite Transformation Temperature, °C					
	250		280		300	
	N	T	N	T	N	T
900	34	36	43	43		
950	35	41	45	53		
1000					54	63

3.4.4. Effect of Loading Rate on Fracture Toughness

The measured fracture toughness values at different loading rates are tabulated in Table 3.7 which clearly shows that fracture toughness maintained a relatively constant value through the loading rate range.

The corresponding strain rate, $\dot{\epsilon}$, was approximated using[133]

$$\dot{\epsilon} = \frac{2\sigma_{ys}}{tE} \qquad (3.4)$$

where σ_{ys} was yield strength and t was loading time.

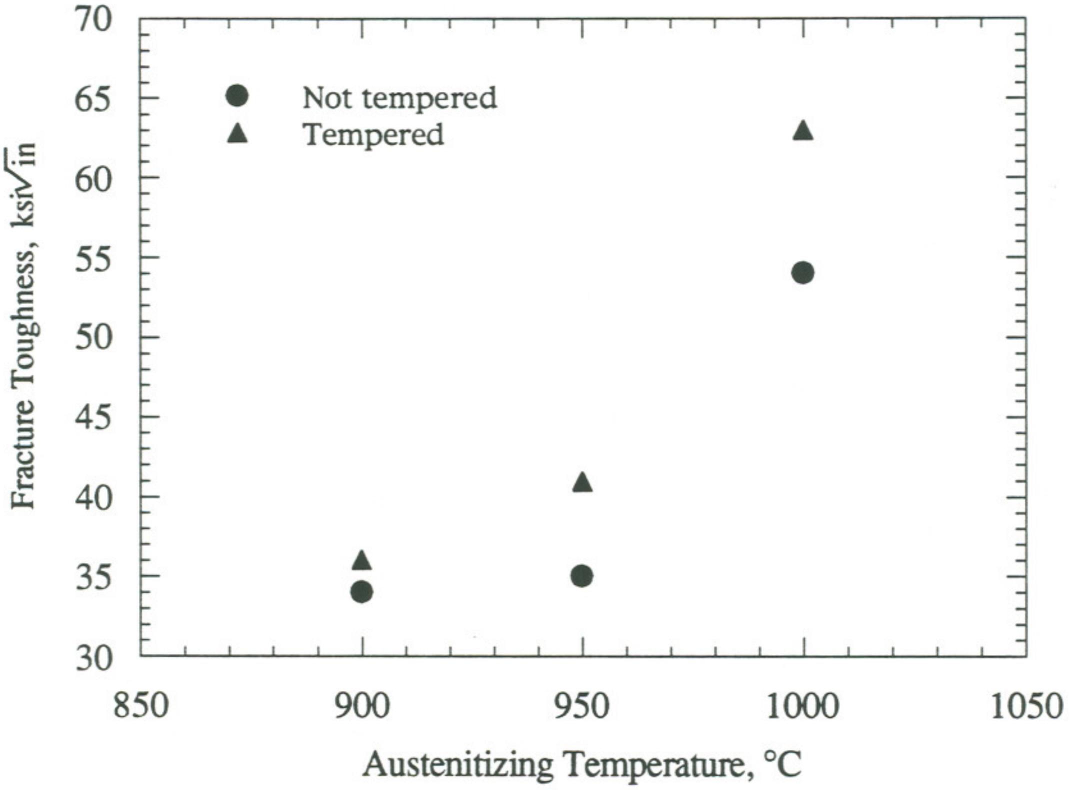

Figure 3.6. Effect of 200°C Tempering Treatment on Fracture Toughness.

Table 3.7. Loading Rate Effect on Fracture Toughness.

Fracture Toughness at Different Loading Rates		
Displacement Speed mm/s	Strain Rate 1/s	Fracture Toughness $\mathrm{ksi}\sqrt{\mathrm{in}}$
254	1.0×10^{-3}	40
50.8	6.6×10^{-4}	40
25.4	3.1×10^{-4}	40
0.254	9.0×10^{-6}	41
0.025	1.7×10^{-6}	46

According to Rolfe and Barsom,[132] fracture toughness tests are classified by strain rate as follows:

Static	$\dot{\epsilon} \approx 10^{-5}$/sec.
Intermediate	$\dot{\epsilon} \approx 10^{-1}$/sec.
Dynamic	$\dot{\epsilon} \approx 10$/sec.

Hence, the toughness tests were conducted in static to intermediate strain rate conditions.

Fracture toughness usually decrease with increasing loading rate and decreasing test temperature since these changes shift the transition temperature region to higher temperatures. High strength materials, however, respond much less to the changes of these variables either because the difference between the upper and lower energy shelves is small or because the transition temperature range is above room temperature, i.e., the tests are carried out in the lower shelf region. The relatively constant toughness at various loading rates found in this study might indicate that the tests were conducted below the transition temperature as expected. Following this argument, further increase in loading rate and decrease in test temperature should not affect fracture toughness. The opposite adjustment of these variables, on the other hand, might increase toughness by moving the test condition from lower energy shelf to the transition range. The somewhat higher toughness at the lowest loading rate might be due to this type of test condition change.

3.4.5. Effect of Bainite Volume Fraction on Fracture Toughness

The factorial analysis compared mean properties of each reference variable. When bainite transformation time was the reference variable, the effect of bainite transformation temperature on toughness was averaged out. This simplification helped the assessment of the effect of bainite transformation time on toughness but obscured the detection of the effect due to microstructure. The factorial analysis involved very different microstructures due to the change of heat treatment parameters including bainite transformation time. Simply averaging out the effect of one or more factors might lead to erroneous conclusions.

This part of the test was designed to study the effect of bainite transformation time on toughness more carefully. It was focused on the effect of bainite volume fraction on toughness. The result showed clearly that fracture toughness increased with bainite volume fraction, Table 3.8. This trend was contradictory to the factorial analysis results which showed no effect of bainite transformation time on fracture toughness. It was also different from the results of Tomita *et al*[81,108] who obtained the highest toughness from duplex structures with 75% martensite and 25% bainite.

The volume fractions approximated in Table 3.8 were the target volume fractions based on the TTT diagram developed using 927°C austenitizing temperature, Figure 3.3; while the austenitizing temperature used here was 950°C. The small difference in transformation characteristics due to the different austenitizing temperature was not expected to strongly influence bainite volume fraction. Even though some deviation from the target values occurred, the general conclusion would still hold since what was of interest was the trend between fracture toughness and bainite volume fraction, not the toughness at a particular bainite volume fraction.

Table 3.8. Bainite Volume Fraction Effect on Toughness.

Reaction Time, min.	Volume Fraction	Toughness, $\mathrm{ksi}\sqrt{\mathrm{in}}$
6.92	25%	44
8.17	50%	49
9.9	75%	49
25	100%	53

It should be pointed out that a careful analysis of the toughness values from the factorial analysis could also lead to the conclusion that toughness was controlled by microstructure. A microstructure based toughness ranking was extracted from the data in Table 3.3 and is presented in Chapter 5.

3.5. Hardness Measurement

Since an increase in toughness is usually accompanied by a decrease in hardness, hardness measurement served to monitor potential hardness reduction, when toughness was improved. The hardness was also used to calculate yield strength, which was needed for effective crack size correction for toughness calculation and stress state estimation. The equation developed by Squirrell *et al*[151] was selected, since it calculated values that agreed very closely with the measured yield strengths. For example, the yield strength of the steel under condition *I* was measured to be 244 ksi, while the calculated was 224 ksi; the underestimation was less than 10%. Considering the small errors that could stem from this approximation and the time that could be saved using the calculated yield strength, no further yield strength measurements on specimens from other conditions were carried out. Only calculated values were used in this work.

The hardness of the steel in the conditions used in the factorial analysis is tabulated in Table 3.9. The analysis showed that increasing either bainite transformation temperature or extending bainite transformation time suppressed hardness. Increasing austenitizing temperature, on the other hand, had much less influence on hardness. The effects of the heat treatment parameters on hardness were evaluated as

$$\begin{aligned} HRC &= 0.003AT+54 \\ HRC &= -0.067BT+74 \\ HRC &= -0.071Bt+59 \end{aligned} \tag{3.5}$$

Hardness and yield strength of the conditions used in the systematic analysis were also tabulated, Tables 3.10 and 3.11. The effect of the austenitizing and austempering temperatures on hardness of bainite in as transformed conditions was formulated as

$$HRC = -0.013AT-0.09BT+92.75 \tag{3.6}$$

Hardness decreased faster with bainite transformation temperature than with austenitizing temperature. This trend was retained in the yield strength and temperature relationships since linear hardness-yield strength correlation was assumed.

Table 3.9. Hardness under the Factorial Analysis Conditions.

Heat Treatment	Knoop	HRC	Yield Strength ksi
A	755	61	289
B	673	57	248
C	616	54	223
D	651	56	238
E	662	57	244
F	646	58	236
G	737	60	280
H	711	59	267
I	618	54	224

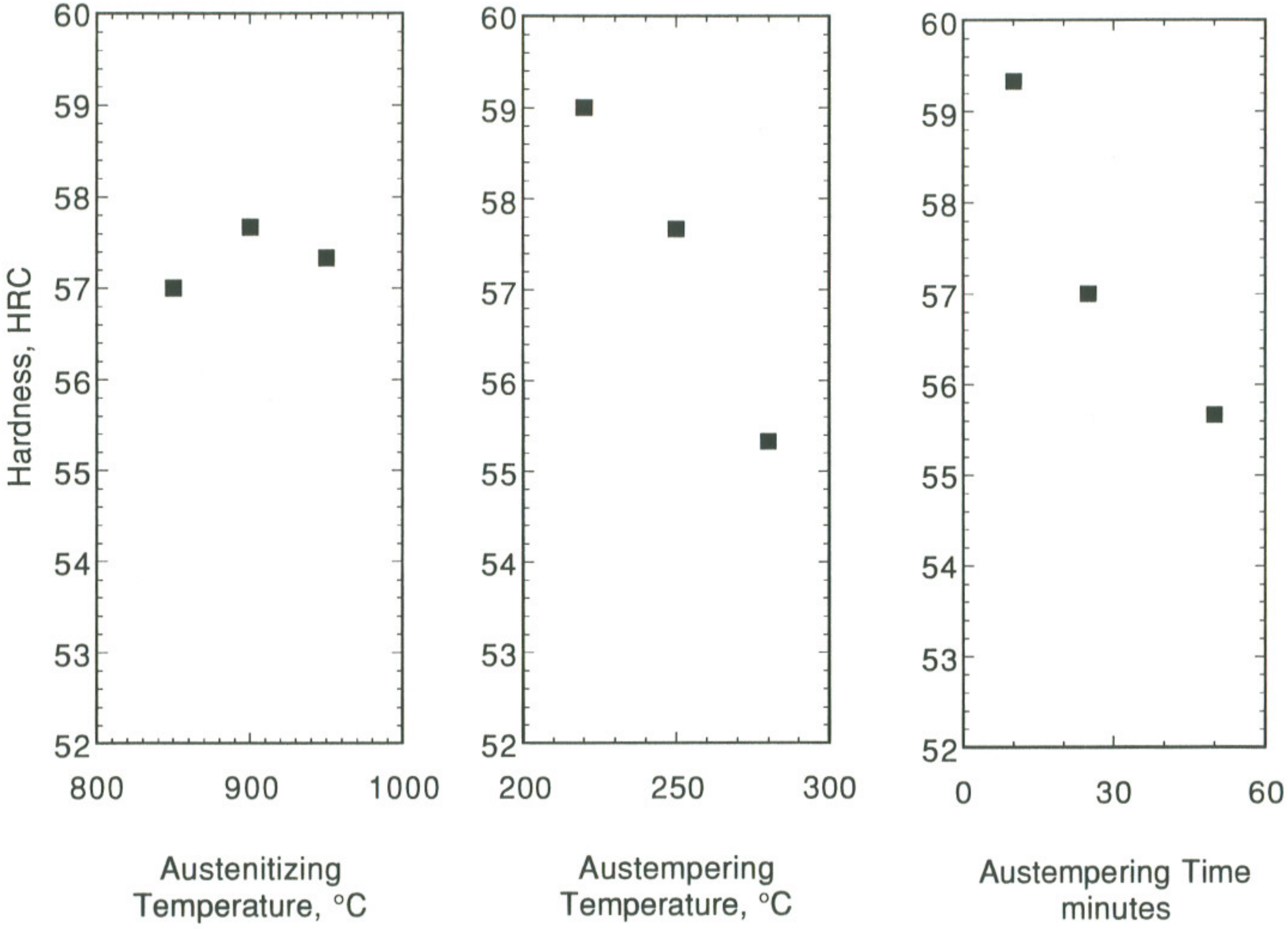

Figure 3.7. Effect of Heat Treatment Parameters on Hardness

Table 3.10. Hardness under the Systematic Analysis Conditions.

Micro-hardness, Knoop				
Austenitizing Temperature, °C	Bainite Transformation Temperature, °C			
	250	280	300	320
900	674	613	588	
950	662	613	582	541
1000	645	603	562	
1050		608		

Table 3.11. Yield Strength under the Systematic Analysis Conditions.

Yield Strength, ksi				
Austenitizing Temperature, °C	Bainite Transformation Temperature, °C			
	250	280	300	320
900	250	222	211	
950	244	222	208	199
1000	236	218	200	
1000		219		

3.6. Microscopy

3.6.1. Optical Microscopy

Longitudinal sections of the specimens were examined. As expected for a commercial grade alloy, the steel contained relatively large number of inclusions, the size, distribution, and volume fraction of which were not affected by the applied heat treatments. The effect exerted on the steel by the inclusions in all the tested conditions was assumed to be the same; the exact magnitude of the effect was not of interest since only one steel was considered. Dark and bright bands, which were presumably due to segregation,[156] were also observed in the as-received material. The bands disappeared after the initial quenching and tempering treatment. Although segregation might still exist, its extent should be negligible, especially after the austenitization of the final heat treatments; the effects of the non-observable bands and the disappearing segregation were not studied.

The microstructures from the heat treatments used in the factorial analysis are described next. The applied etchant attacked ferrite/carbide interface and etched bainite darker than as-quenched martensite. If tempering was applied, both martensite and bainite contained carbides; the etchant could not delineate them. When volume fractions of both structures were close, especially when both structures were evenly distributed and well mixed, the whole surface was etched more or less evenly. This was the case with heat treatment *F* which included austempering at 280°C for 10 minutes, Figure 3.8. Specimens under conditions *C* and *I* were austempered at the same temperature as that of *F* specimens but were held for longer times to allow bainite transformation to finish. Not much contrast could be obtained from these specimens either (Figures 3.9 and 3.10) since only one phase was present. The mechanism for the low contrast in these specimens was different from that in *F*.

Specimens under conditions *B*, *E*, and *H* were austempered at 250°C. White matrix and dark etching second phase were observed. The nature of these structures, however, was different and the contrast was due to different mechanisms even though the optical microstructures looked very similar. Specimen *B* was austempered for 50 minutes, i.e., bainite transformation had almost completed. The residual austenite transformed to martensite during cooling. This produced a bainite matrix plus martensite particles, Figure 3.11.

Specimens *E* and *H* were austempered for 25 and 10 minutes, respectively, while bainite transformation finish time was about an hour. A large amount of residual austenite was left at the end of isothermal treatment and was transformed to martensite. Hence the structures contained martensite matrix and bainite as the second phase, Figures 3.12 and 3.13. More bainite was formed in *E* than in *H* due to longer holding times; this agreed with the observed volume fraction ratio of the dark etching phase in Figures 3.12 and 3.13.

By comparing Figures 3.11, 3.12, and 3.13, it was obvious that the matrix in *B* was different than that in *E* and *H*. Transmission electron microscopy confirmed that specimen *B* contained mainly bainite, while *E* and *H* contained primarily martensite.

Specimens under *A*, *D*, and *G* conditions were austempered at 220°C which was below M_s. Some primary martensite would form but since martensite transformation in normal steels was athermal, it could not proceed without further cooling. During isothermal holding lower bainite formed. However, only small amounts of lower bainite could be obtained at such a low temperature in the time allowed. Secondary martensite formed during cooling subsequent to bainite transformation. The final microstructure contained martensite matrix with lower bainite as the second phase, Figures 3.14, 3.15, and 3.16.

The differentiation between the primary and secondary martensite might be artificial but when bainite formed, carbon partitioning into the residual austenite could happen. At higher temperatures, carbon atoms could diffuse further away into residual austenite so that all austenite contained more or less even carbon content. When the transformation temperature was low, on the other hand, carbon might build up in austenite close to the bainite/austenite interface. The carbon enriched austenite had a higher tendency to transform to twinned martensite and led to lower toughness.

In Figures 3.14, 3.15, and 3.16, the white etching matrix was martensite and the dark plates were lower bainite. Volume fraction of lower bainite increased in the order *A*, *G*, and *D*, correctly reflecting the length of the isothermal holding time as shown in Table 3.12, where 'M' and 'B' stand for martensite and bainite, respectively. The lower case letters 'l', 'm', and 'h' indicated the transformation temperatures of lower bainite; 'l' was 220, 'm' was 250, and 'h' was 280°C. The significance of bainite transformation on toughness is discussed in Chapter 5.

Table 3.12. Volume Fraction of Second Phase Structure.

Heat Treatment	Matrix Type	Second Phase Type	Volume Fraction, %
A	M	l B	18
B	m B	M	12
C	h B	-	-
D	M	l B	36
E	M	m B	20
F	h B	M	30*
G	M	l B	26
H	M	m B	9
I	h B	-	-

*Calculated bainite volume fraction.

The contrast observed in the specimens probably arose more from electrochemical reaction than from chemical reaction. Two micro-cells existed and competed against each other during etching. Martensite, due to its higher dislocation density and carbon supersaturation, had a slightly higher electro-potential than bainite; it acted as anode while bainite behaved as cathode. The electric current was the same at the anode and the cathode; volume fraction of the structures played the major role in determining the current density and the etching rate of different structures. When martensite volume fraction was low, e.g., condition *B*, the anode current density was high; martensite was etched (oxidized) more than bainite and became darker. When martensite and bainite had comparable volume fraction, as in condition *F*, both structures were etched to about the same degree; not much contrast occurred. When bainite volume was low, on the other hand, cathode current density was high. However, instead of generating a large amount of hydrogen due to the accelerated reduction process, a second micro-cell composed of bainitic ferrite and carbides became active. The operation of this cell oxidized the bainitic ferrite and attacked the ferrite/carbide interface, changing the color of bainite structure dark. The relatively low current density in the martensite region, on the other hand, left martensite lightly etched. Hence, martensite matrix was light and bainite particles was dark. This contrast generating mechanism applied to conditions *A*, *D*, *E*, *G*, and *H*.

Bainite transformation time for all the specimens used in the systematic analysis was adequate for bainite transformation to finish. Very little martensite was formed. The effect of the martensite on toughness of all specimens should be about the same. The observed toughness changes were due mainly to bainite substructures and, in part, to prior austenite grain size variation. The bainite substructural changes, however, had to be studied at higher magnifications, i.e., by transmission electron microscopy. For comparison purpose, the optical microstructure of bainite transformed at 280°C after 1000°C austenitization was shown in Figure 3.17.

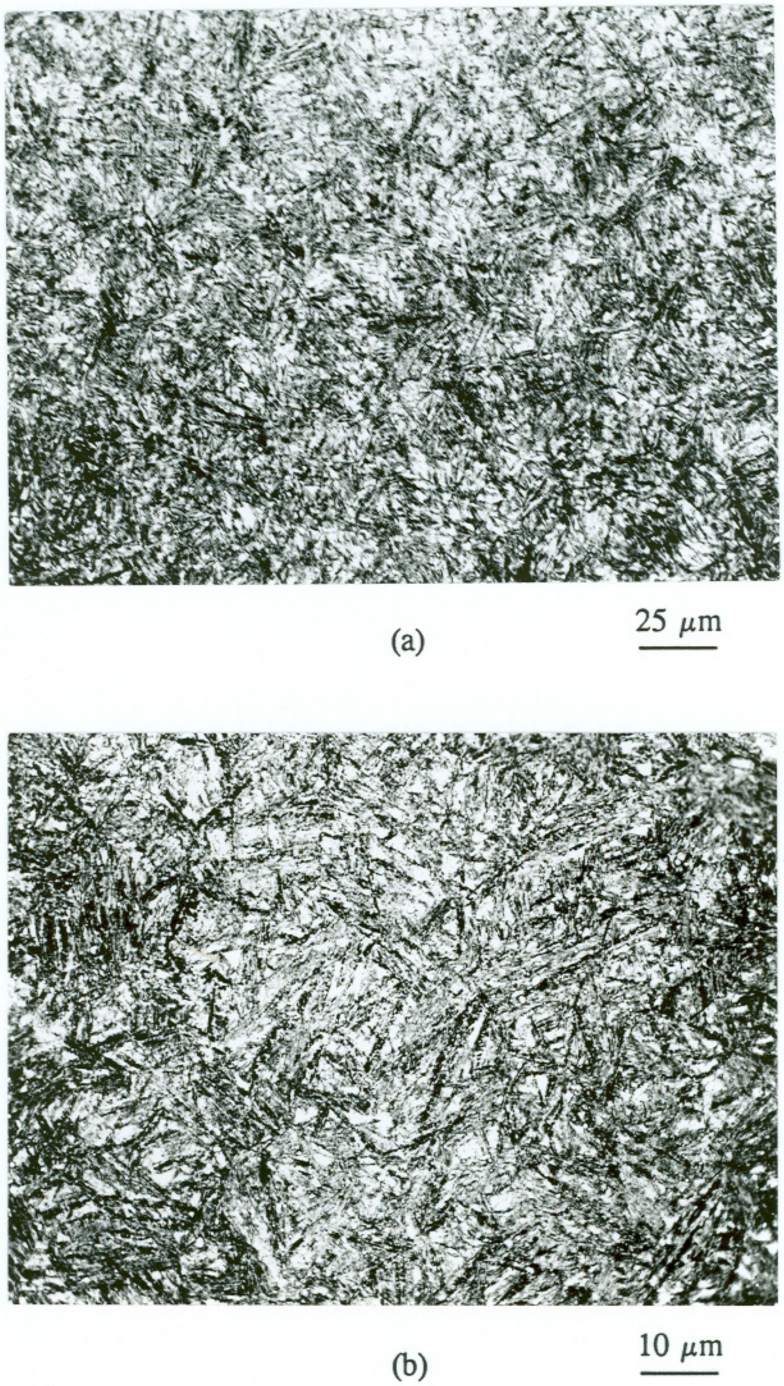

Figure 3.8. Optical Microstructure of Specimen F at (a) 400× and (b) 1000× Magnifications.

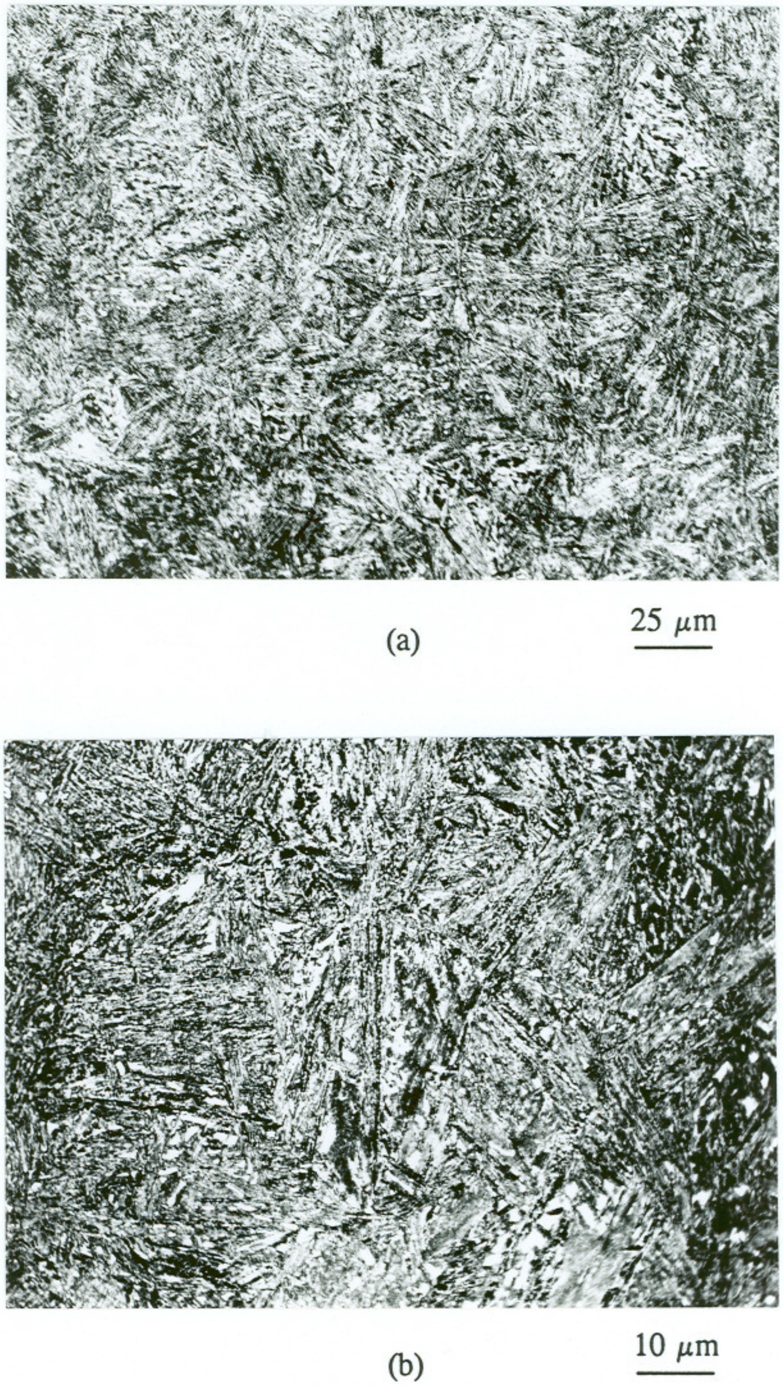

Figure 3.9. Optical Microstructure of Specimen C at (a) 400× and (b) 1000× Magnifications.

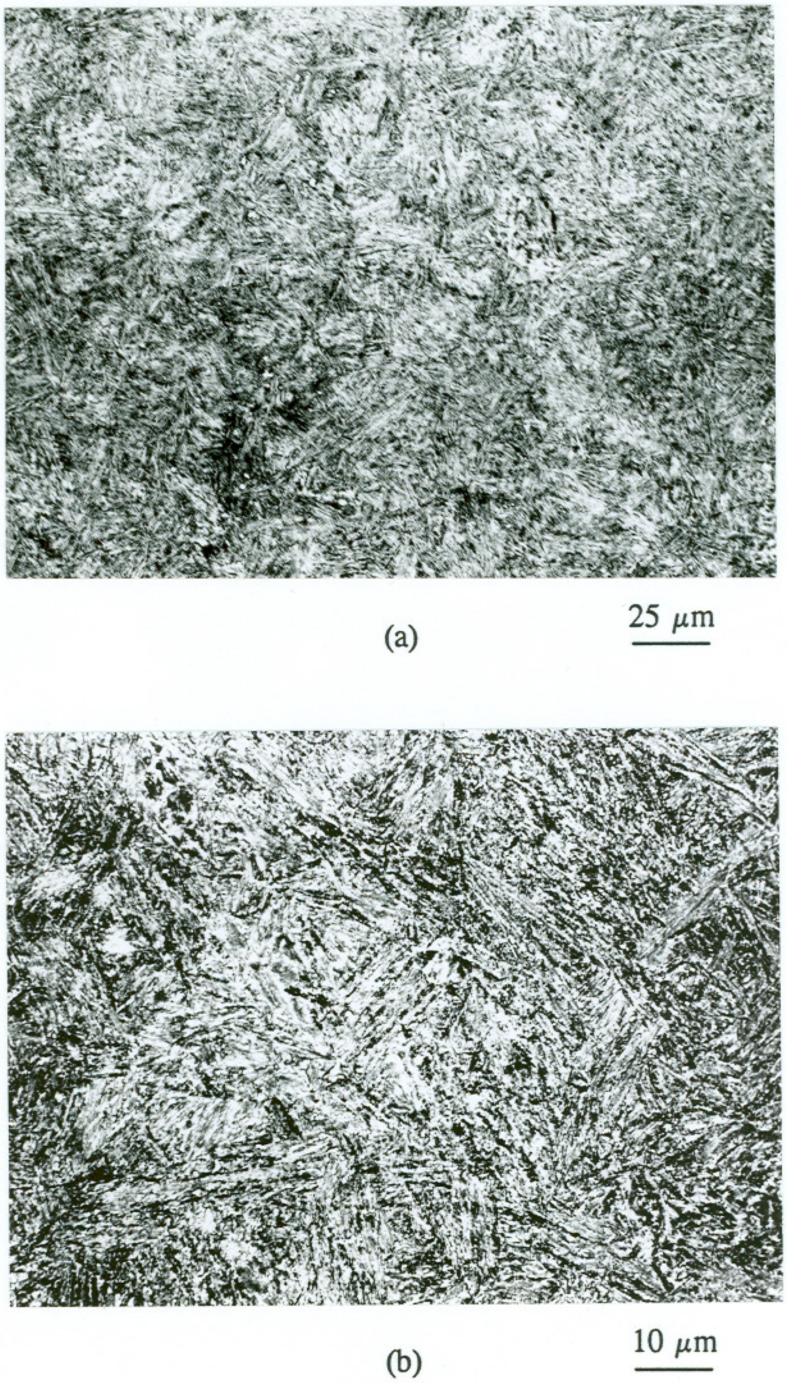

(a)

(b)

Figure 3.10. Optical Microstructure of Specimen I at (a) 400× and (b) 1000× Magnifications.

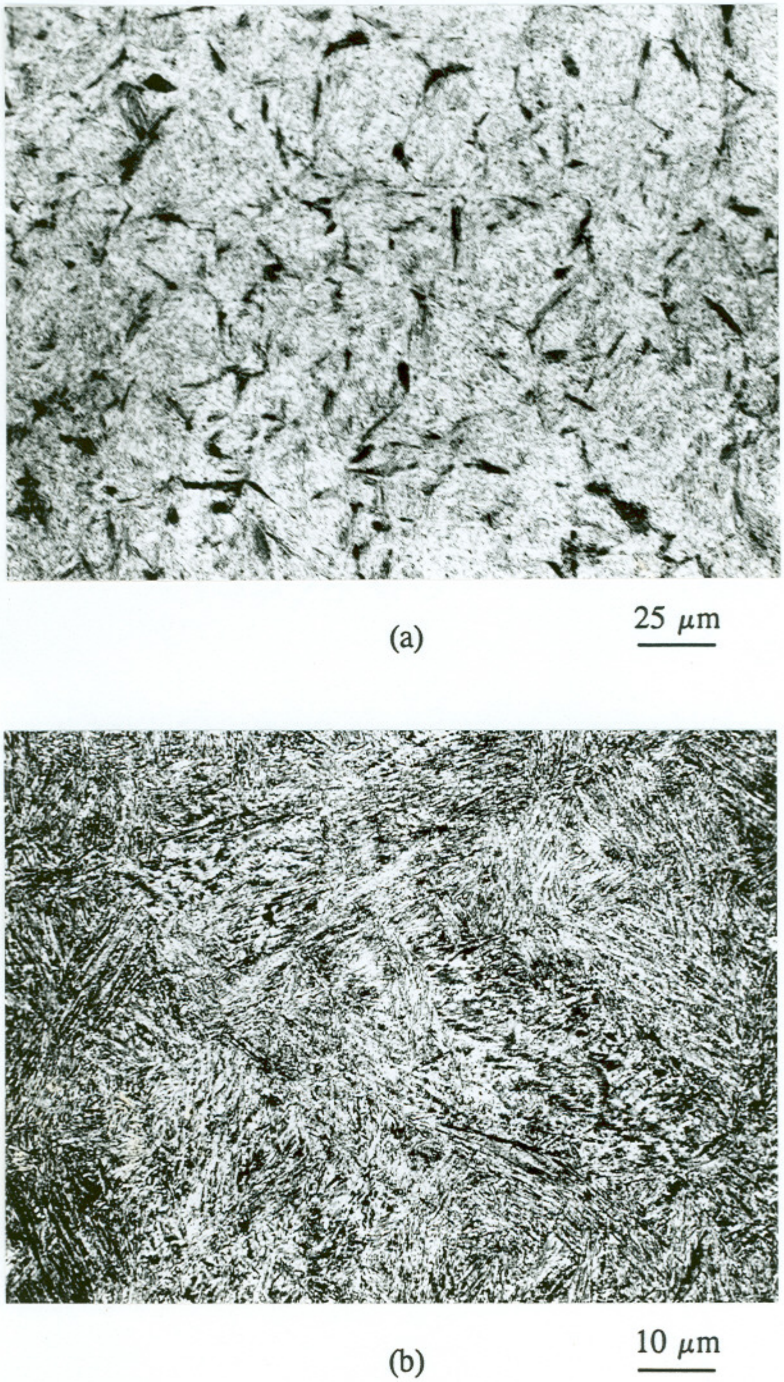

(a)

(b)

Figure 3.11. Optical Microstructure of Specimen B at (a) 400× and (b) 1000× Magnifications.

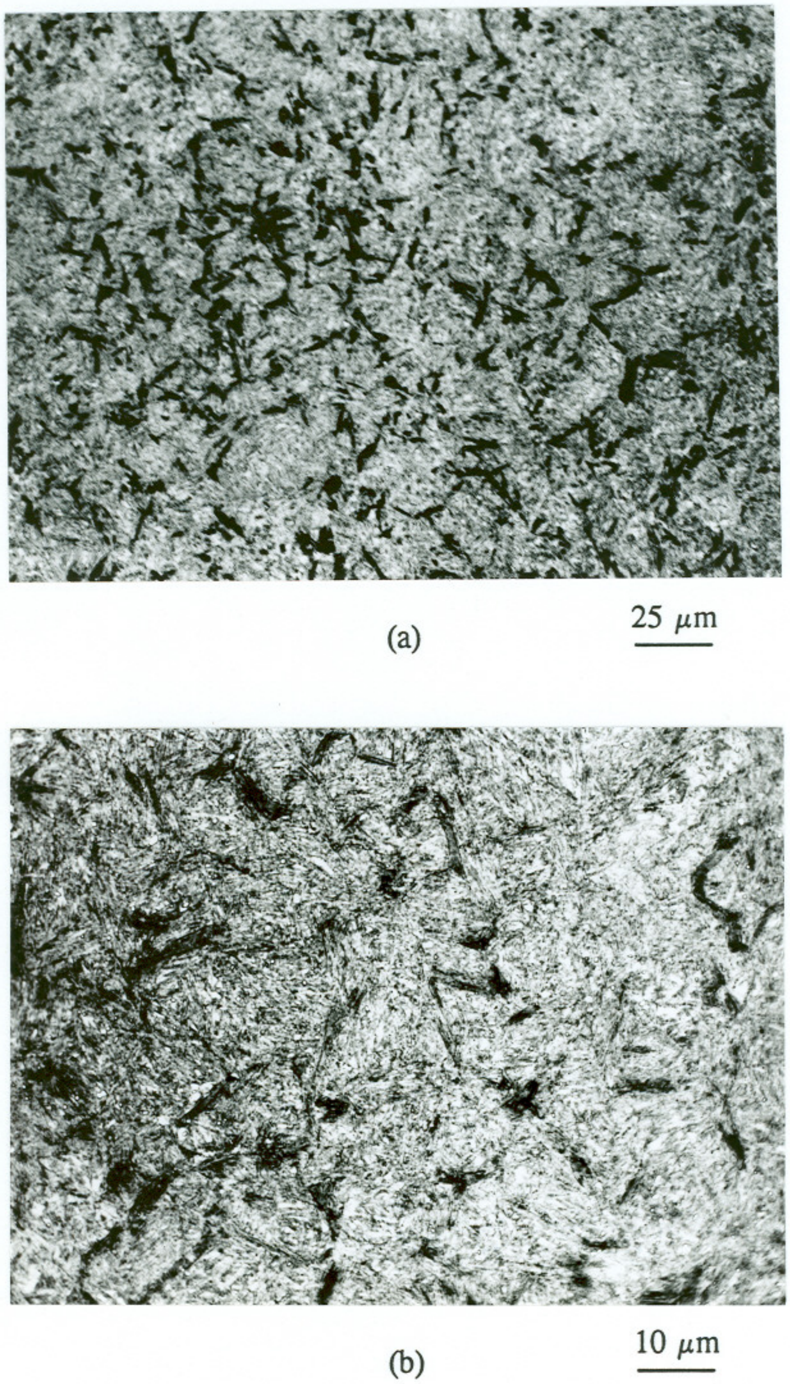

Figure 3.12. Optical Microstructure of Specimen E at (a) 400× and (b) 1000× Magnifications.

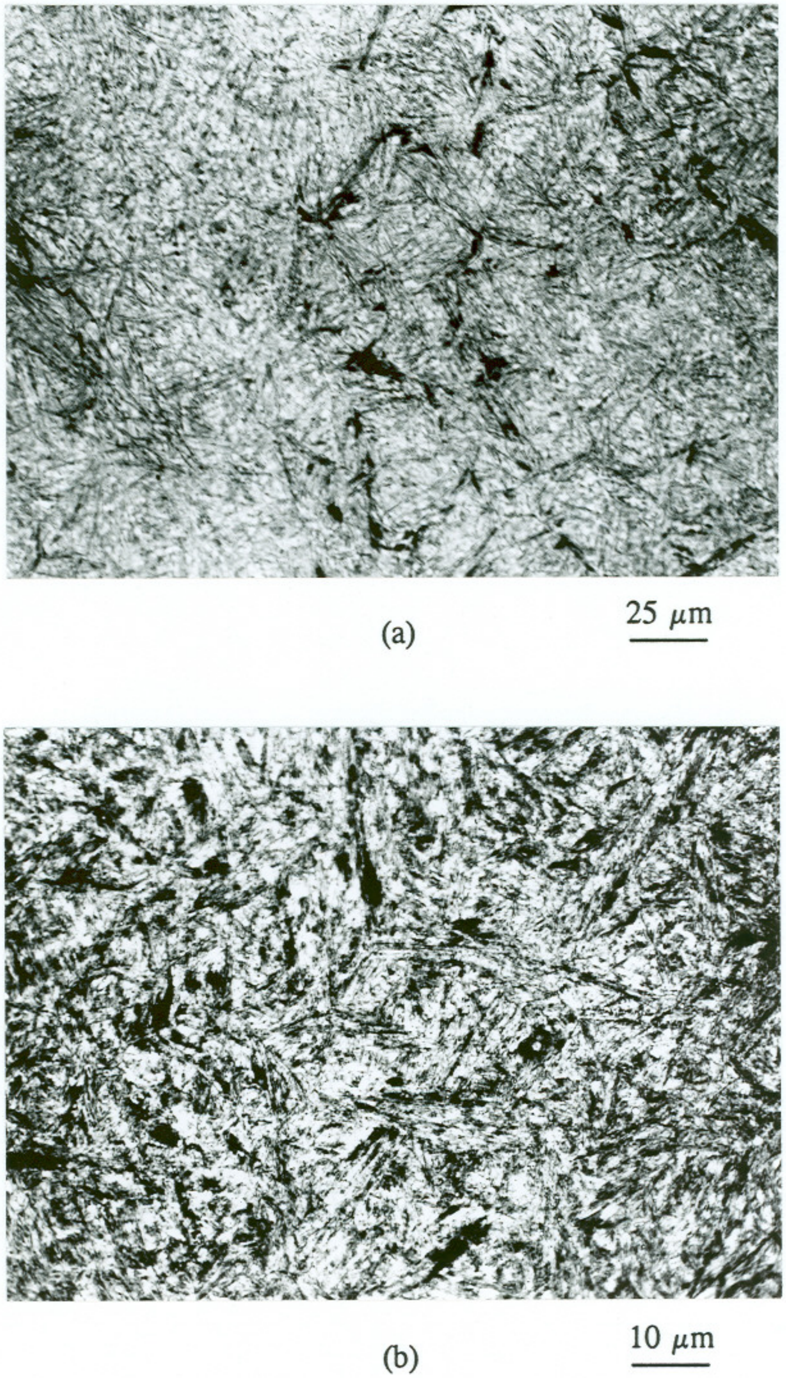

Figure 3.13. Optical Microstructure of Specimen H at (a) 400× and (b) 1000× Magnifications.

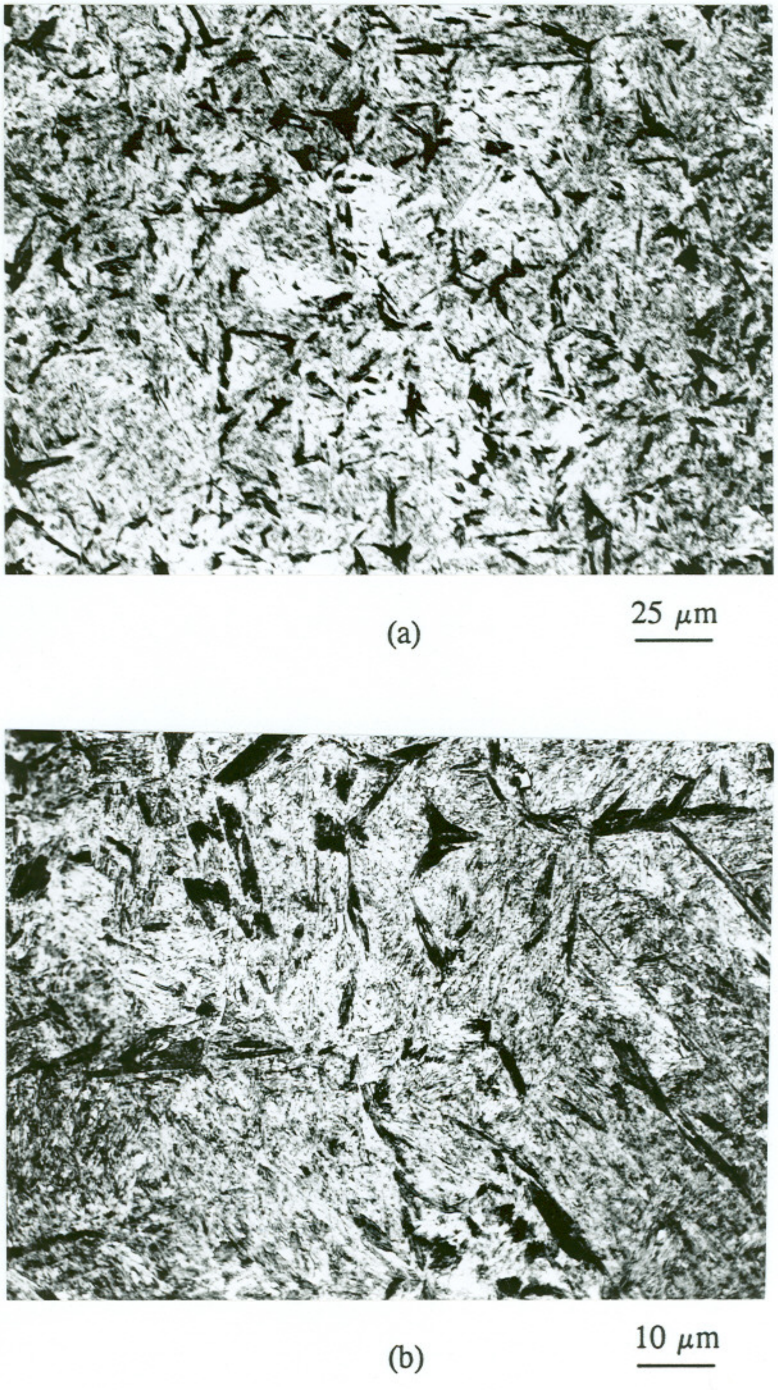

Figure 3.14. Optical Microstructure of Specimen A at (a) 400× and (b) 1000× Magnifications.

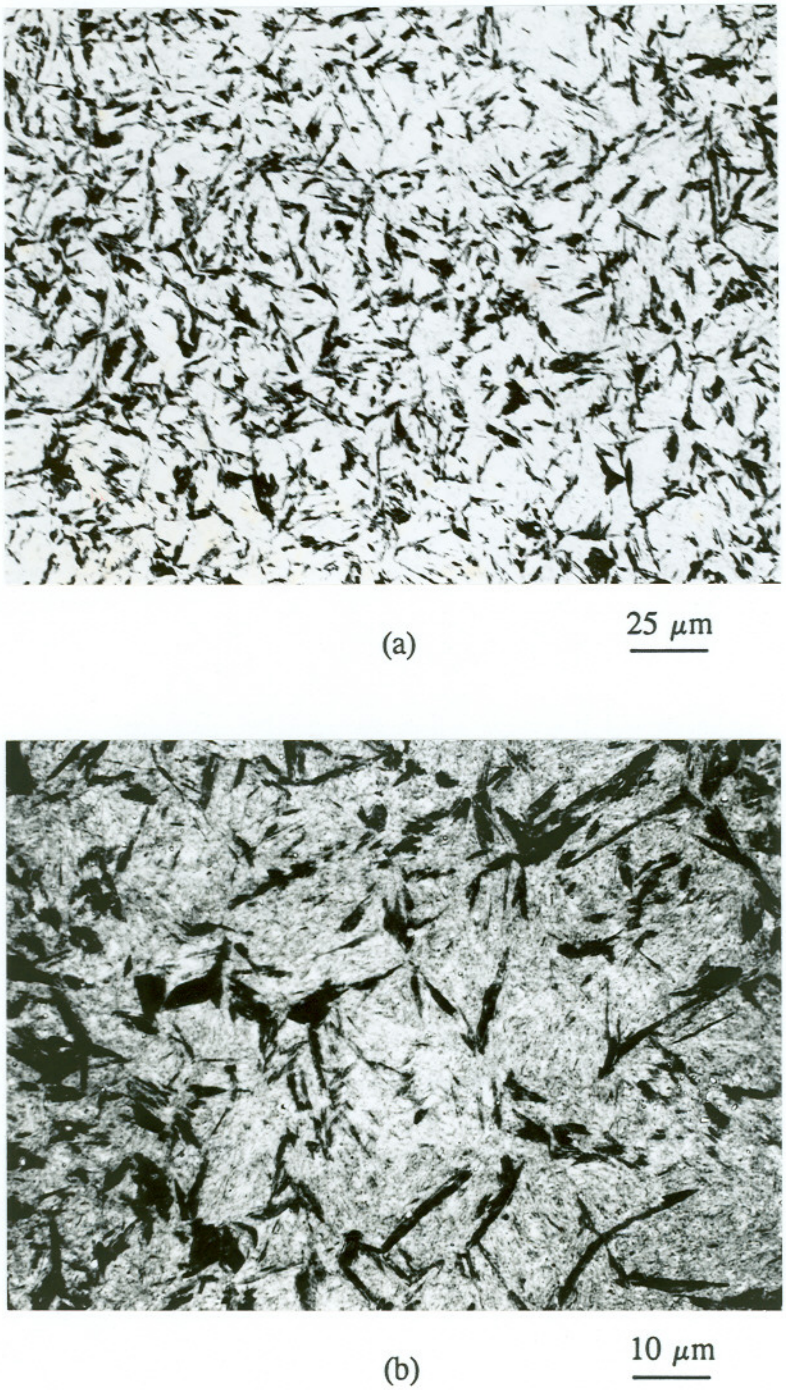

(a)

(b)

Figure 3.15. Optical Microstructure of Specimen G at (a) 400× and (b) 1000× Magnifications.

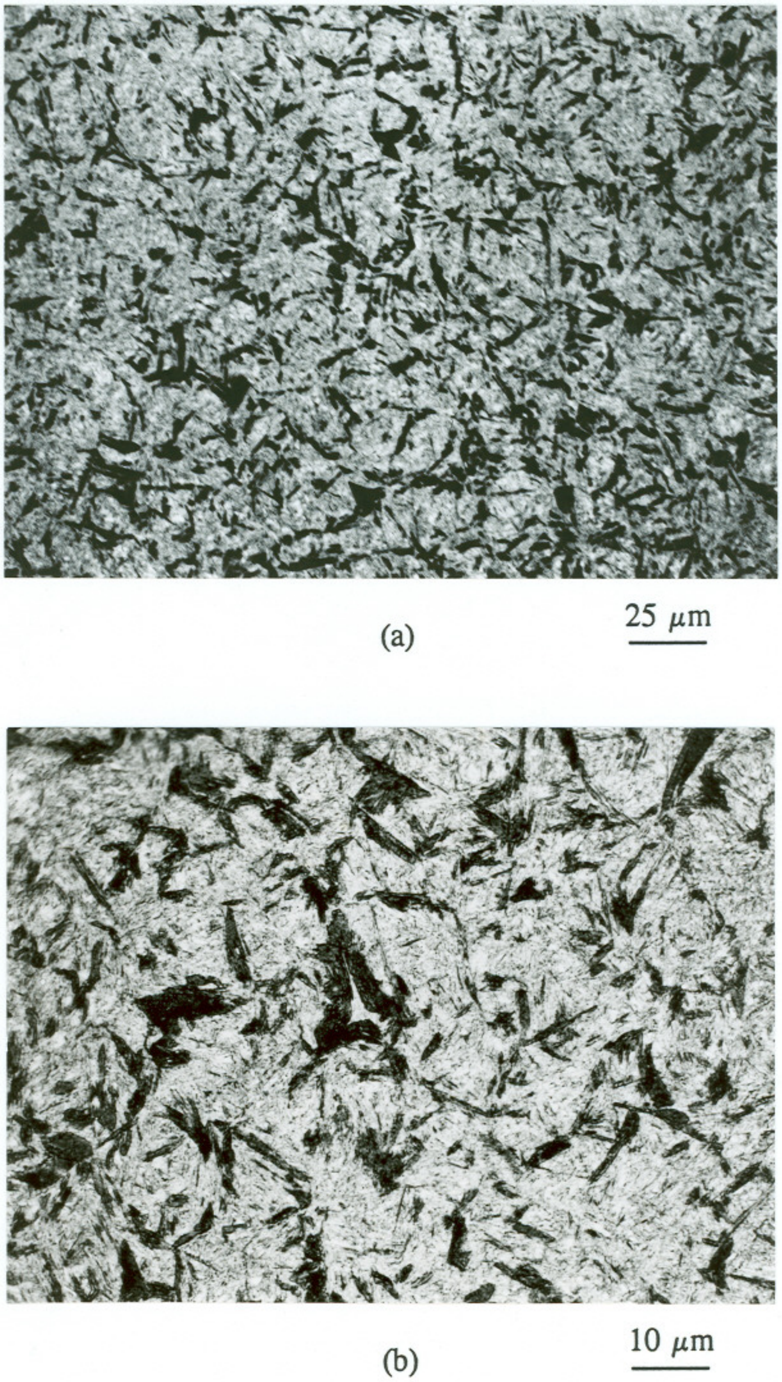

(a)

(b)

Figure 3.16. Optical Microstructure of Specimen D at (a) 400× and (b) 1000× Magnifications.

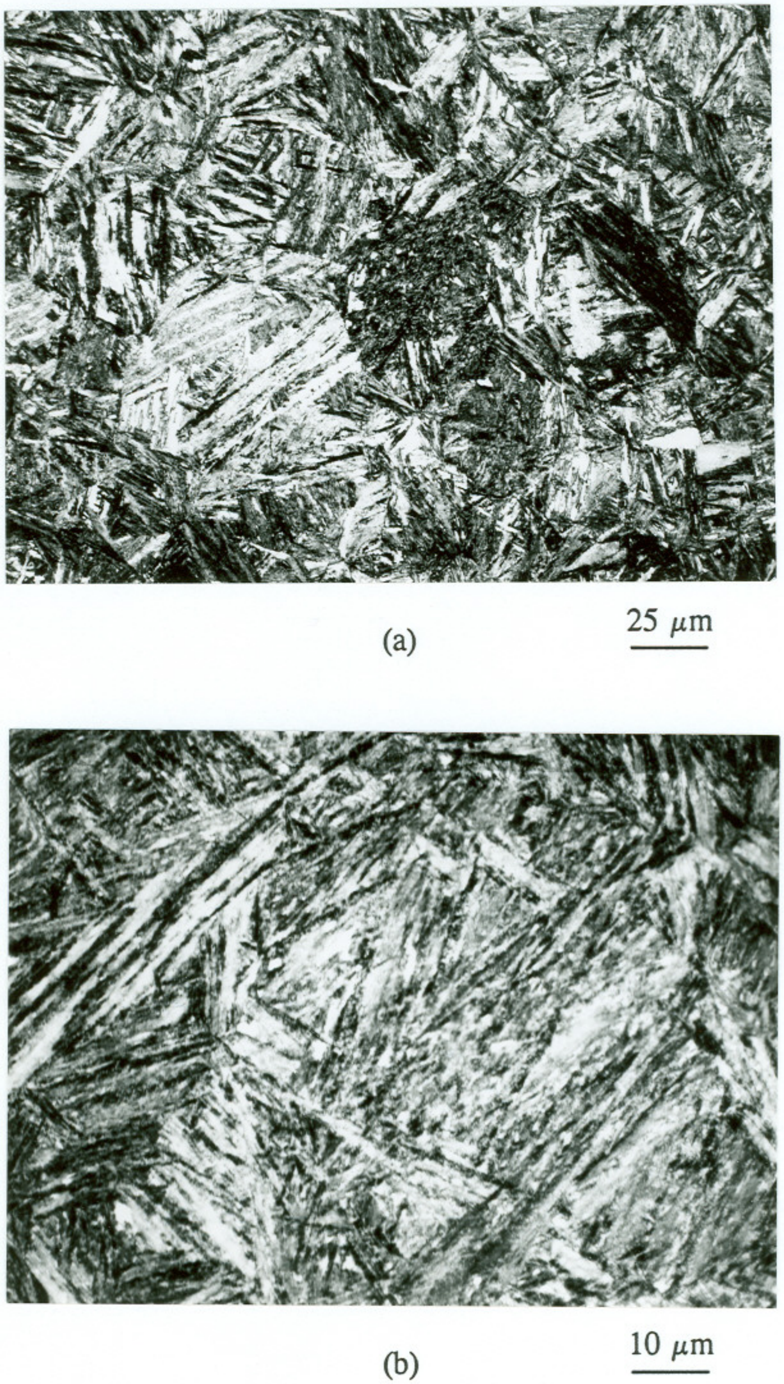

Figure 3.17. Optical Microstructure of a Specimen Austenitized at 1000° C and Austempered at 280°C. (a) 400× and (b) 1000× Magnifications.

3.6.2. Scanning Electron Microscopy

Back scatter mode operation failed to distinguish bainite from martensite unless the volume fraction of bainite was low. Secondary electron mode operation was not effective.

3.6.3. Transmission Electron Microscopy

Many of the heat treatments used in the factorial analysis produced low temperature tempered martensite matrix which contained a high density of dislocations, Figure 3.18a, and fine carbides, Figure 3.18b. Both dislocated and twinned martensite were present, the former occurred more frequently although the carbon content of the steel was high. Since the specimens tended to fail in intergranular mode, TEM work was carried out to search for phases such as continuous carbides which might form on prior austenite grain boundaries and reduce the grain boundary strength.

The grain boundaries, however, were mostly clean and free from continuous carbides, Figure 3.19. Occasionally very fine, unidentified structures were observed on the grain boundaries. Since density of these structures was very low, they were not expected to contribute to intergranular fracture tendency. Both martensite and lower bainite plates nucleated at grain boundaries. In Figure 3.19a, a bainite plate was formed on one side of the boundary, while martensite formed on the other side. The boundary itself was straight and non-decorated. The black phase surrounded by a lower bainite plate in Figure 3.19b was a martensitic plate. The boundaries in all the specimens were similar; no criterion could be devised to differentiate the prior austenite grain boundaries due to different heat treatments.

Segregation of impurity elements such as phosphorus to the grain boundaries was speculated to be the cause of intergranular fracture but calculations based on the

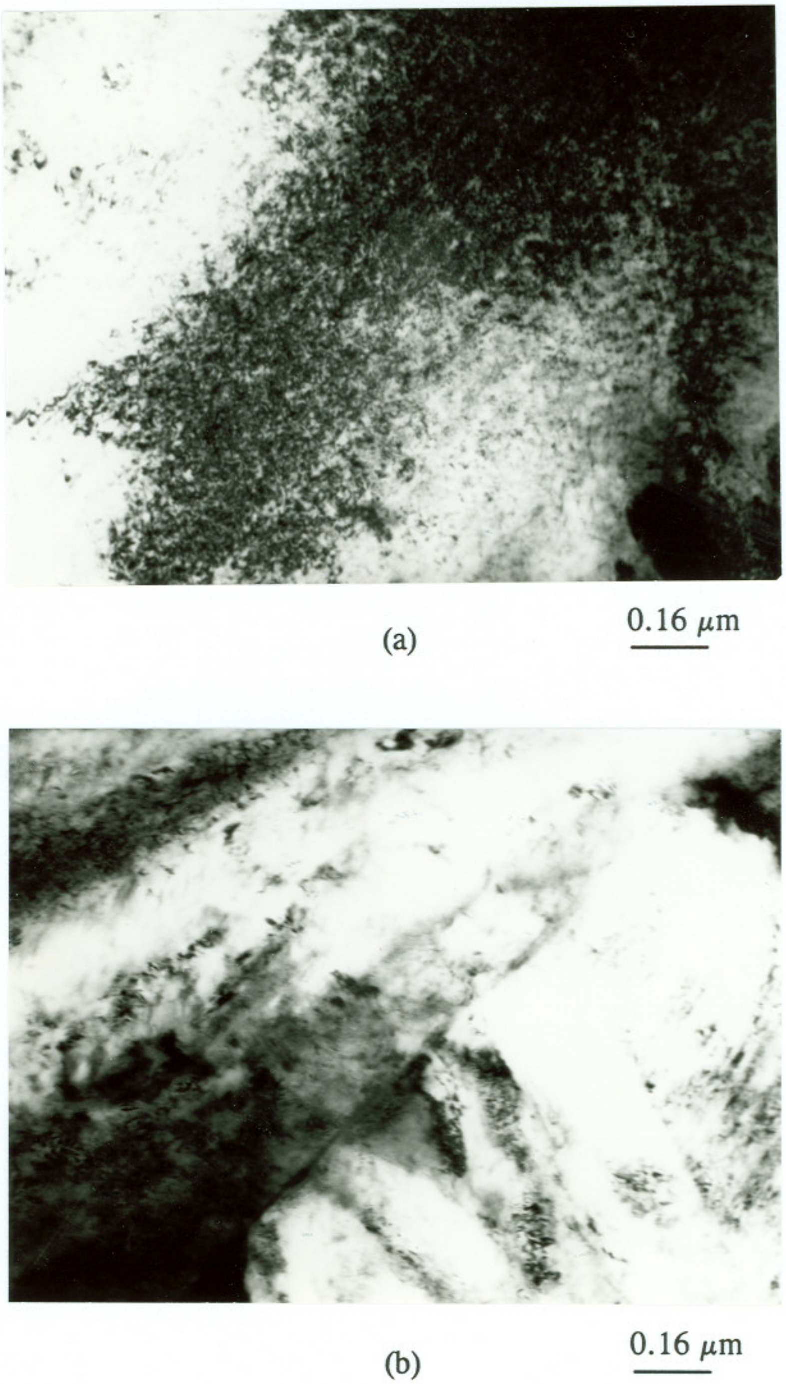

(a)

(b)

Figure 3.18. Characteristic of Low Temperature Tempered High Carbon Martensite. (a) High Dislocation Density (b) Fine Carbide.

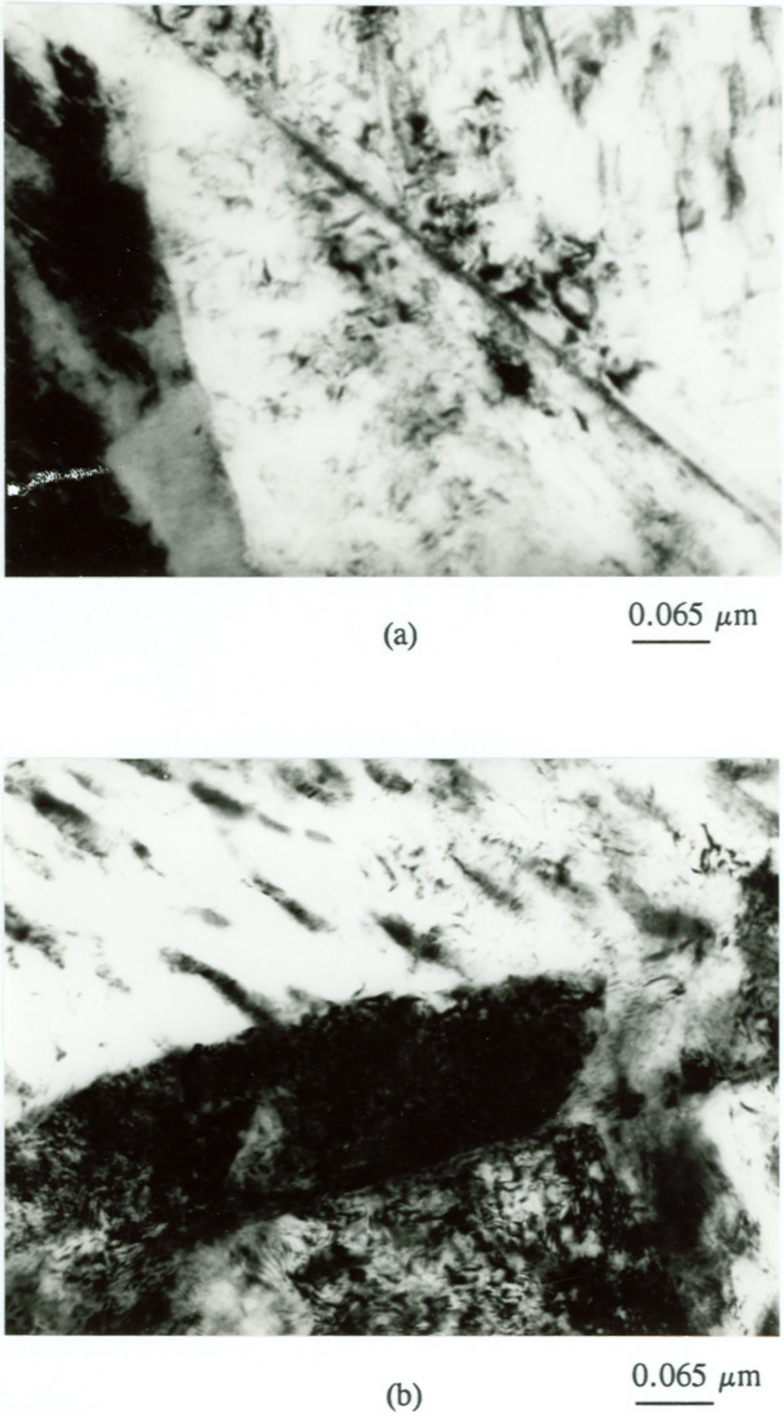

Figure 3.19. Prior Austenite Grain Boundaries. (a) Condition A (b) Condition F.

non-equilibrium segregation theory showed that segregation could not occur during quenching and tempering. This conclusion was confirmed by *in situ* Auger analysis. Logically, austempering at higher temperatures would increase the level of segregation. If segregation was the cause, toughness would decrease with increasing austempering temperature. However, the opposite toughness-temperature relationship was observed; therefore, intergranular fracture could not be due to grain boundary precipitation or segregation but was because of other factors, e.g., the fracture characteristics of martensite in ultra high strength steel.

In the systematic analysis, only bainite was formed after each heat treatment; intergranular fracture was not the predominant fracture mode. Hence, attention was focused on the bainitic structure and property relationship. Lower bainite had a typical lath morphology with carbides precipitated unidirectionally within the ferrite lath at an angle about 55 to 65° from the longitudinal direction of the lath. The interface between the carbides and ferrite was ragged indicating that it could either be totally incoherent or semi-coherent with dislocations to accommodate the stresses between ferrite and cementite, Figure 3.20a.

The diffraction pattern in Figure 3.20c consists of reflections from both ferrite and cementite. The orientation relationship determined as shown in Figure 3.20d was $(\bar{1}\ 1\ \bar{2})_\theta \parallel (1\ \bar{3}\ 0)_\alpha$ and $[2\ 0\ \bar{1}]_\theta \parallel [3\ 1\ \bar{2}]_\alpha$, which, by using stereographic analysis, could not lead to any of the cementite-ferrite orientation relationships frequently observed in martensite and bainite. The (102) cementite reflection was used in the centered dark field image, Figure 3.20b, to reveal the carbides.

The bainite lath width and carbide length were determined on TEM micrographs and are tabulated in Tables 3.13 and 3.14, respectively. Due to the relatively large experimental errors involved, these values could only be used in a semi-quantitative manner. The correlation between transformation temperature and

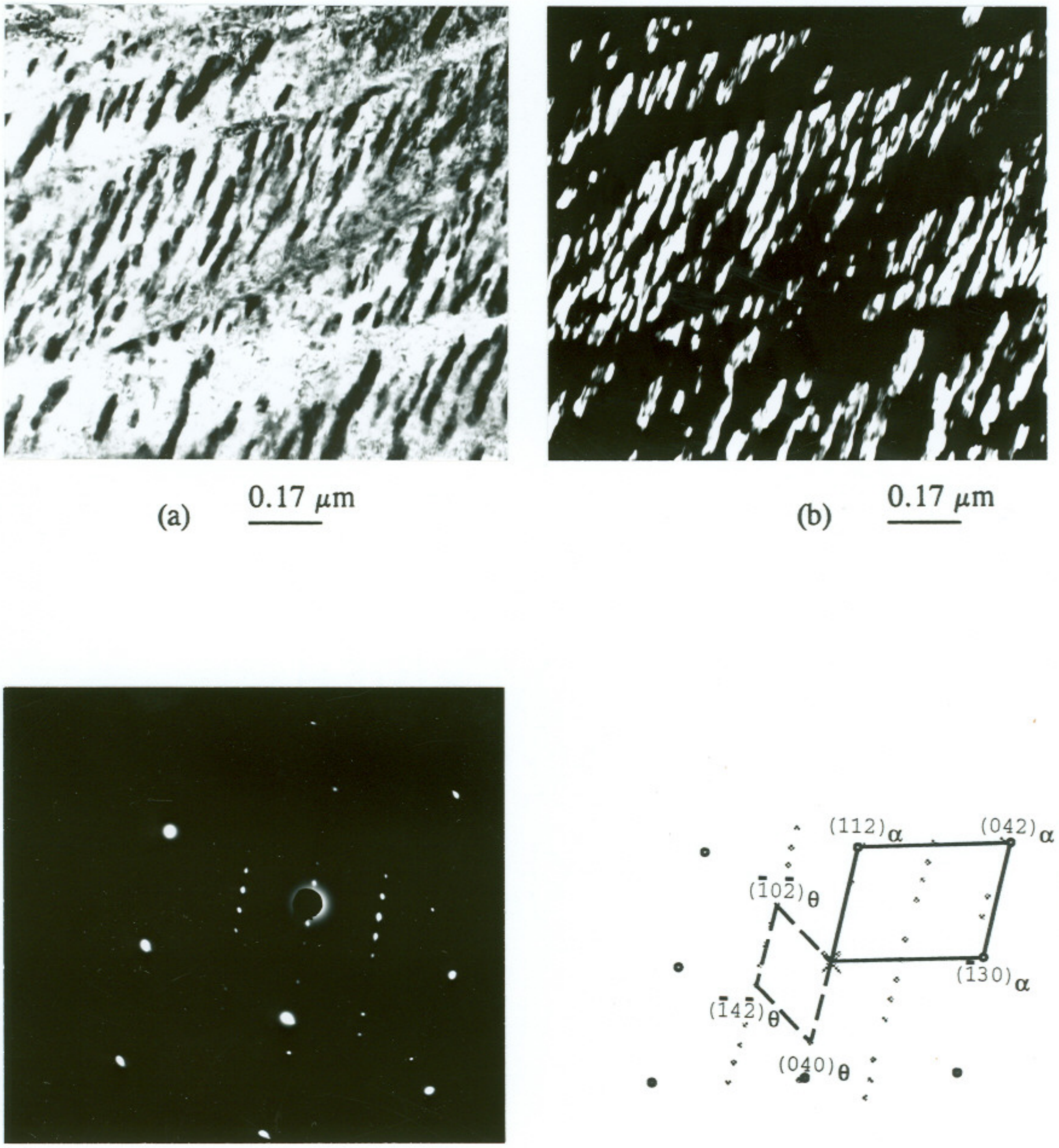

(a) (b)

(c) (d)

Figure 3.20. Lower Bainite Transformed at 280°C. (a) Bright Field Image (b) Dark Field Image (c) Diffraction Pattern and (d) Interpretation of the Diffraction Pattern.

bainite lath width was clear, Table 3.13. With increasing transformation temperature, bainite lath width increased.

Carbide length also increased with transformation temperature. Carbide width, however, remained constant at about 22 nm. The lengthening of carbides led to an increase in carbide volume fraction. The volume fraction of carbide was roughly

Table 3.13. Temperature Dependence of Bainite Lath Width.

Bainite Lath Width, μm				
Austenitizing Temperature °C	Bainite Transformation Temperature, °C			
	250	280	300	320
900	0.59	0.99	1.03	
950	0.54	0.88	1.31	1.42
1000	0.73	0.73		

Table 3.14. Temperature Dependencies of Carbide Length.

Carbide Length, nm			
Austenitizing Temperature °C	Bainite Transformation Temperature, °C		
	250	280	300
900	110	190	260
950	150	185	210
1000	194	240	

0.063, 0.072, and 0.091, respectively when lower bainite was transformed at 250, 280, and 300°C, while the theoretical carbide volume fraction in the steel was 0.010. Figure 3.21 shows representative micrographs at these temperatures.

Another structural change in lower bainite with increasing transformation temperature was the formation of sub-lath boundaries. Some planar defects were seen to partition a bainite lath into sub-regions, Figure 3.22. The carbides in all the sub-regions grew in the same direction but stopped growing at the sub-lath boundaries. The sub-division of bainite lath and restriction of carbide growth might affect the mechanical properties of bainite. However, due to the low density and non-even distribution of the sub-lath boundary, its effect on toughness was difficult to evaluate.

When transformation temperature was increased to 320°C, upper bainite started to transform. Carbides precipitated parallel to ferrite lath, Figure 3.23. The orientation relationship was $(1\ 1\ 3)_\theta \parallel (0\ 0\ 2)_\alpha$ and $[8\ 1\ \bar{3}]_\theta \parallel [1\ 3\ 0]_\alpha$. Again, Bagaryatski relationship was not satisfied. The centered dark field image was obtained using $(0\ 3\ 1)_\theta$.

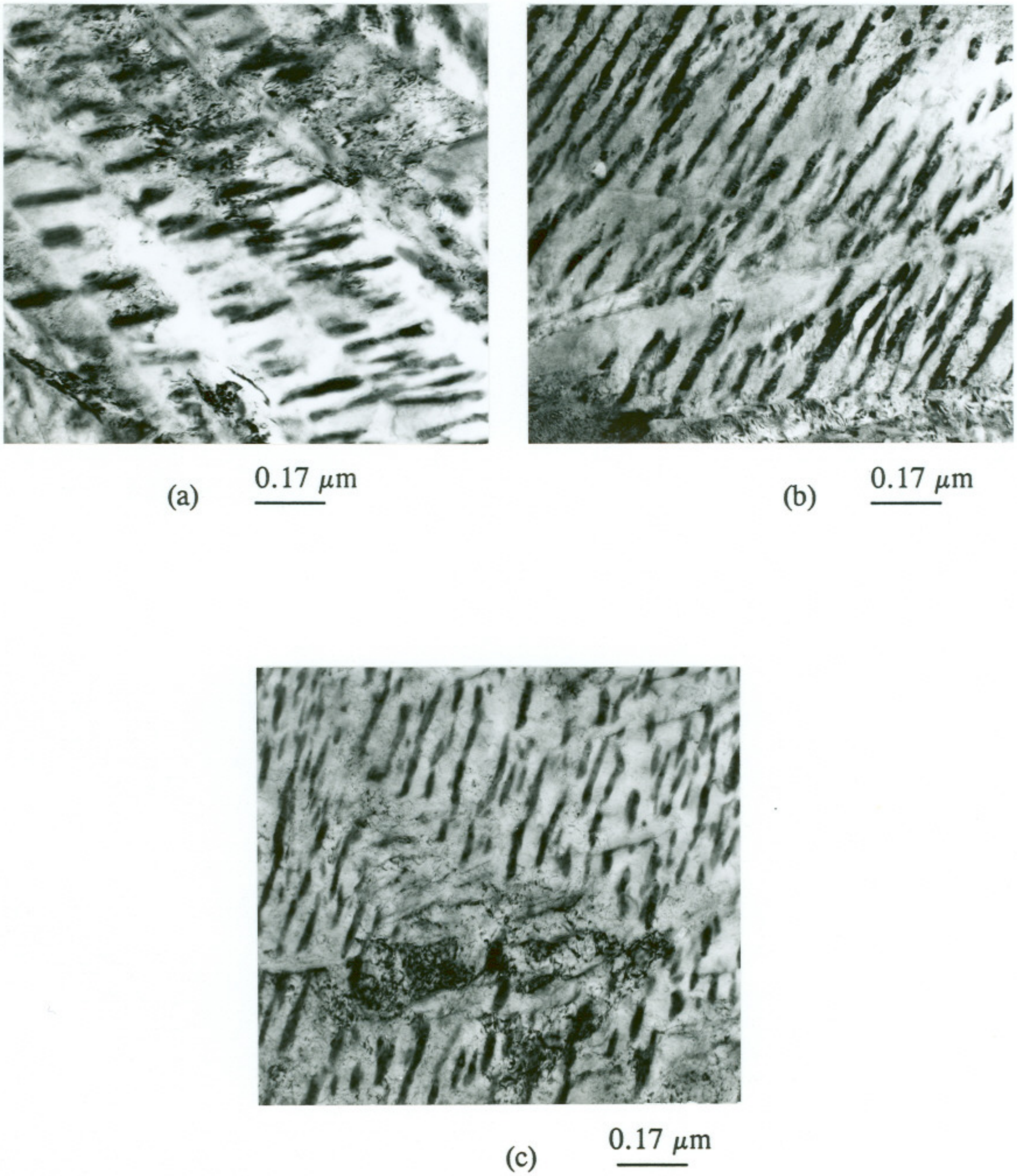

Figure 3.21. Lower Bainitic Carbide Morphology at (a) 250°C (b) 280°C and (c) 300°C.

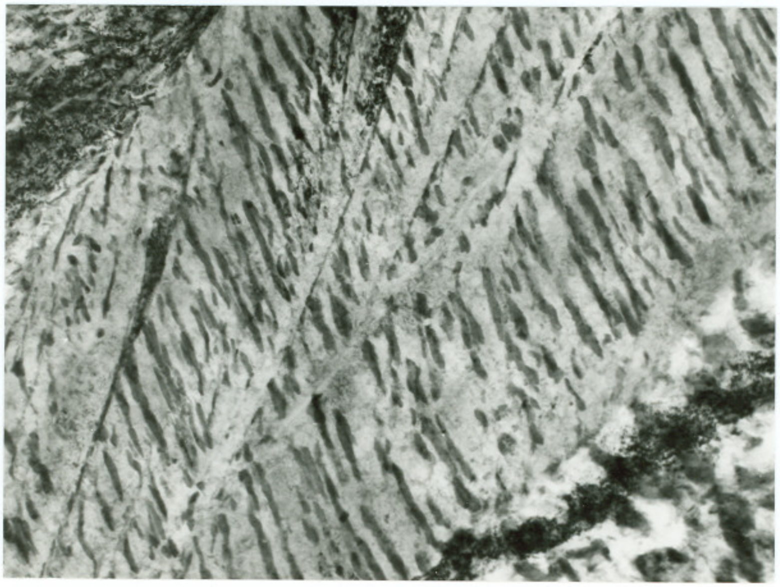

(a) 0.22 μm

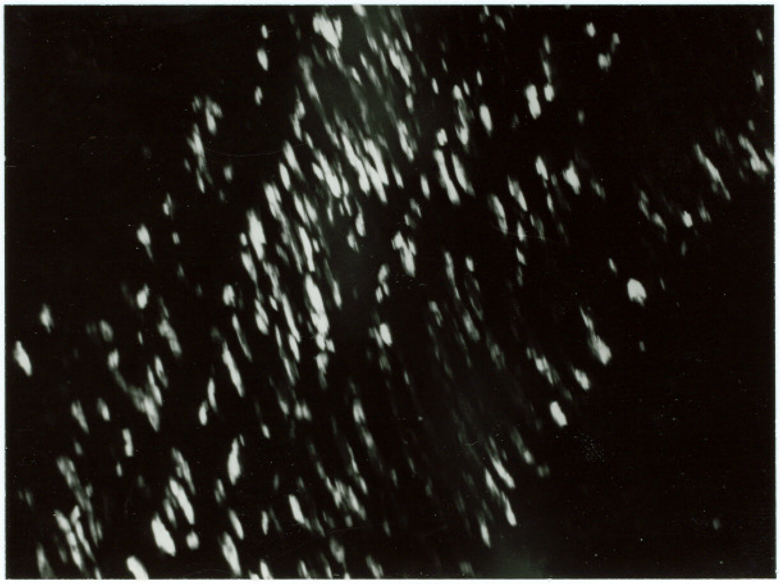

(b) 0.22 μm

Figure 3.22. Sub-Lath Boundaries in A Lower Bainite Lath. (a) Bright Field (b) Dark Field.

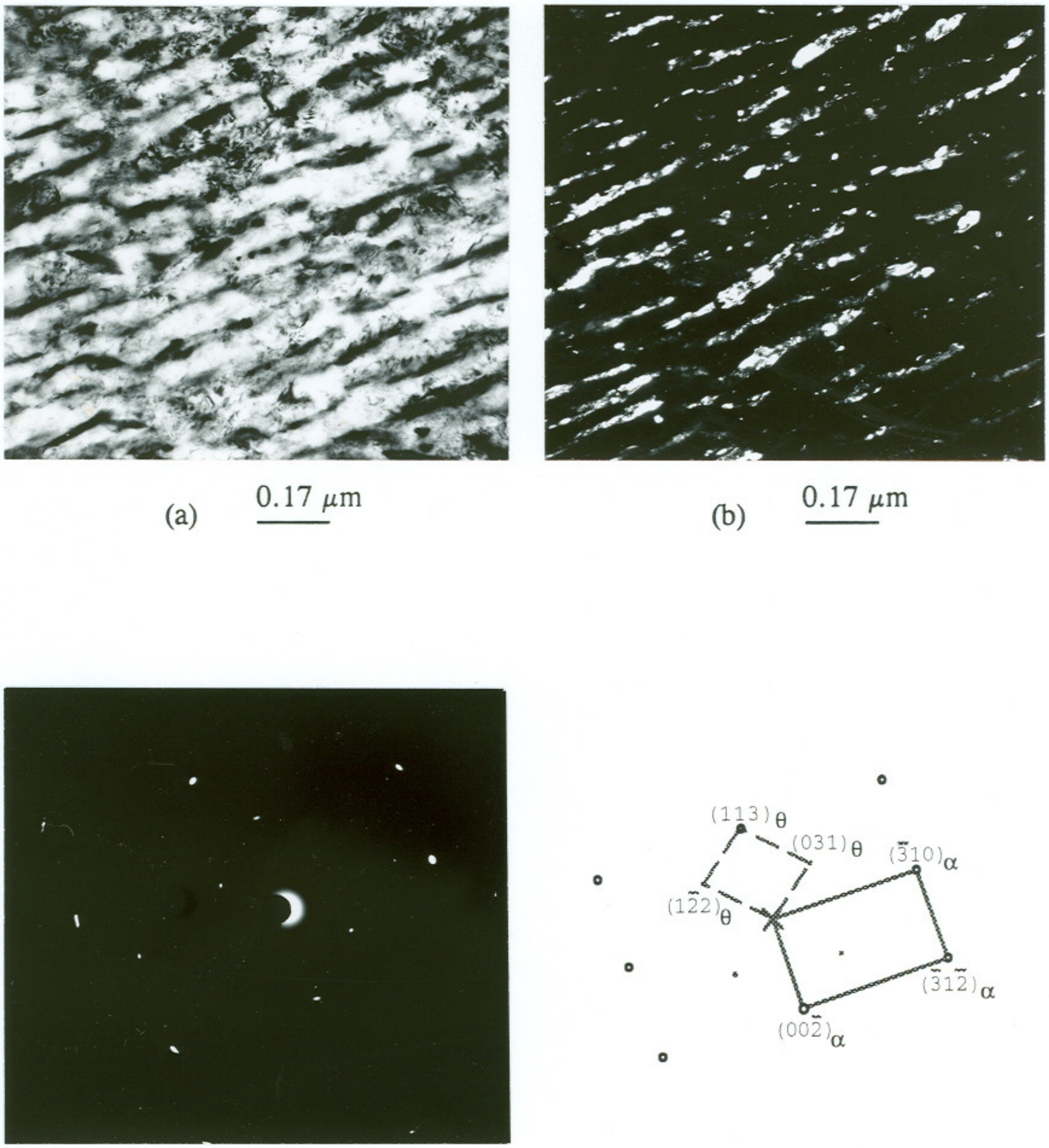

(a) (b)

(c) (d)

Figure 3.23. Upper Bainite Formed at 320°C. (a) Bright Field Image (b) Dark Field Image (c) Diffraction Pattern (d) Interpretation of Diffraction Pattern.

3.7. Fractography

Optical microscopy showed that the steel was heat treated to different conditions in the factorial analysis than in the systematic study. Most of the heat treatments in the former test produced martensite/bainite duplex structures, while those in the latter series gave the steel virtually only bainite structures. This difference was the primary reason for the observed different behaviors of the steel during toughness tests. In the following sections fractographic analyses of the two series are presented separately.

3.7.1. Fractography of Specimens Used in Factorial Analysis

All specimens except *C* failed in intergranular and transgranular mode in both fatigue pre-cracked region and fractured region. The fraction of intergranular fracture in the pre-cracked region was always higher than that in the fractured region in the same specimen. The fraction of intergranular fracture in the fractured region appeared to be a strong toughness controlling factor; when fraction of intergranular fracture increased, toughness was reduced, Table 3.15. When no intergranular fracture was observed, i.e., under condition *C*, fracture toughness was the highest.

Fraction of intergranular fracture was not the only variable that controlled fracture toughness; the substructure in the transgranularly fractured regions also influenced toughness. Figure 3.24 shows fracture surface of specimen *A* in both intergranular and transgranular fractured regions. Two different transgranular fracture surface appearances were observed in the fractured region. Figure 3.25a exhibits a region due to microvoid coalescence, while Figure 3.25b reveals a quasi-cleavage mode of fracture.

The quasi-cleavage region of the present steel differed from typical quasi-cleavage mode fractures in other steels in that instead of having cleavage planes circumscribed by tear ridges, the fracture surface contained grooves and mounds of the size of bainite lath, giving an impression that the transgranular fracture proceeded by the separation of bainite laths along the lath boundaries. Similar quasi-cleavage fracture mode was also observed in specimen B, Figure 3.26a, and C, Figure 3.26b. An increase in the depth of the grooves and the height of the steps seemed to result in an increase in toughness.

Table 3.15. Fracture Toughness and Intergranular Fracture Relationship.

Heat Treatment	Fracture Toughness, $ksi\sqrt{in}$	Intergranular Fraction, %
C	53	0
I	43	1
B	41	2
F	37	3
H	36	17
A	33	23
E	32	20
D	27	40
G	25	63

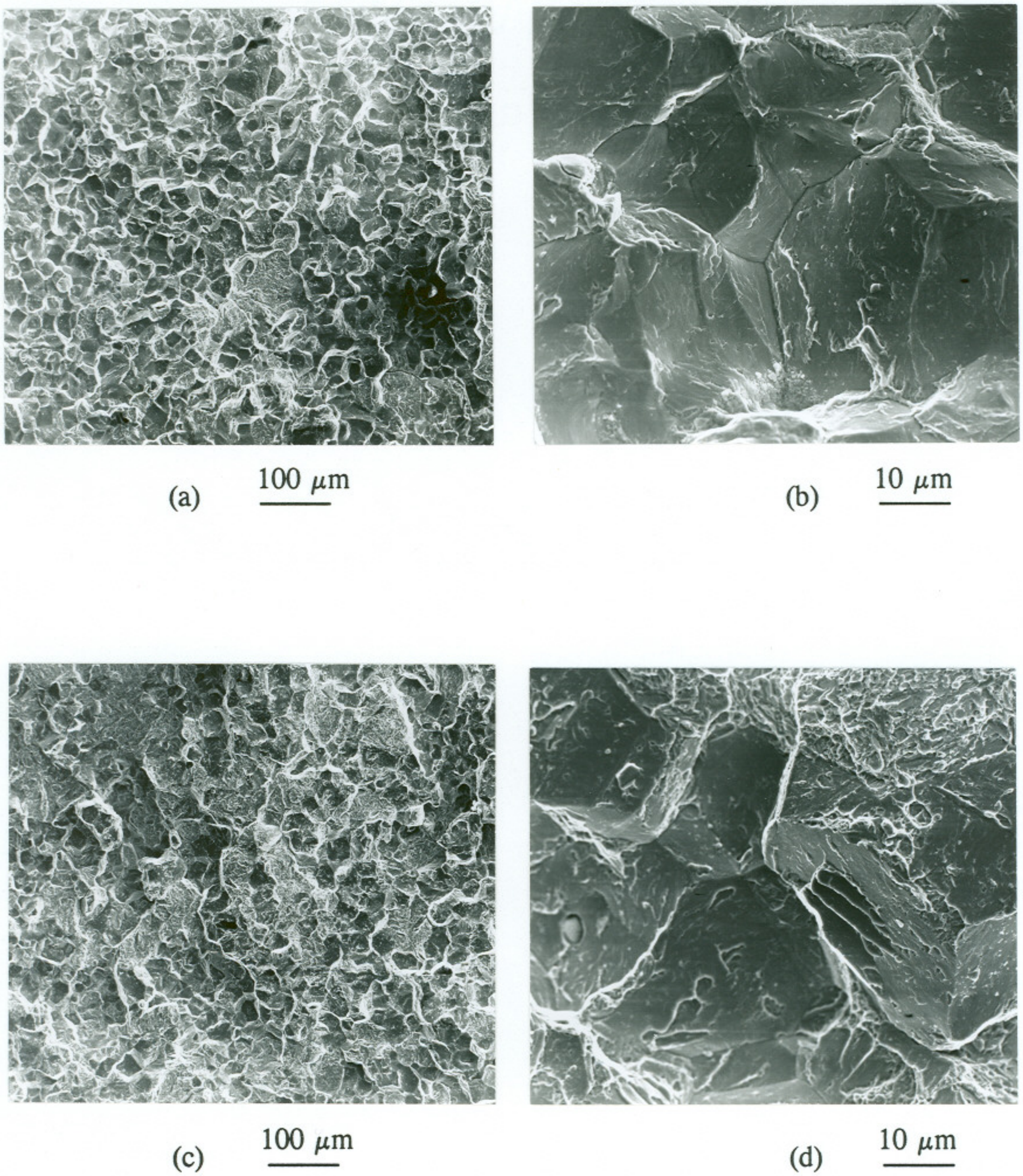

Figure 3.24. Fracture Surface of Specimen *A* in Fatigue Pre-crack Region at (a) Low and (b) high magnifications and in Fractured Region at (c) Low and (d) High Magnifications.

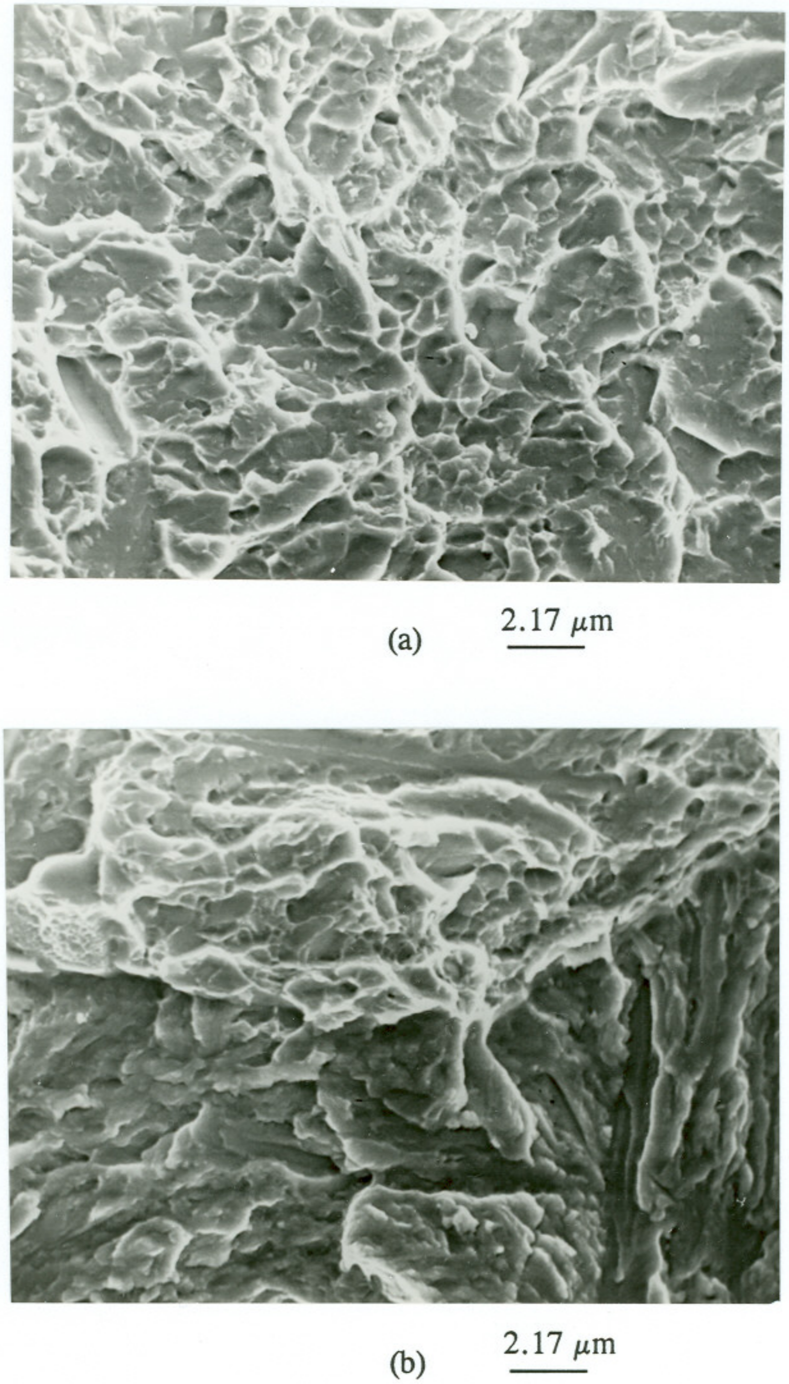

Figure 3.25. Transgranular Fracture by (a) Microvoid Coalescence and (b) Quasi-Cleavage modes.

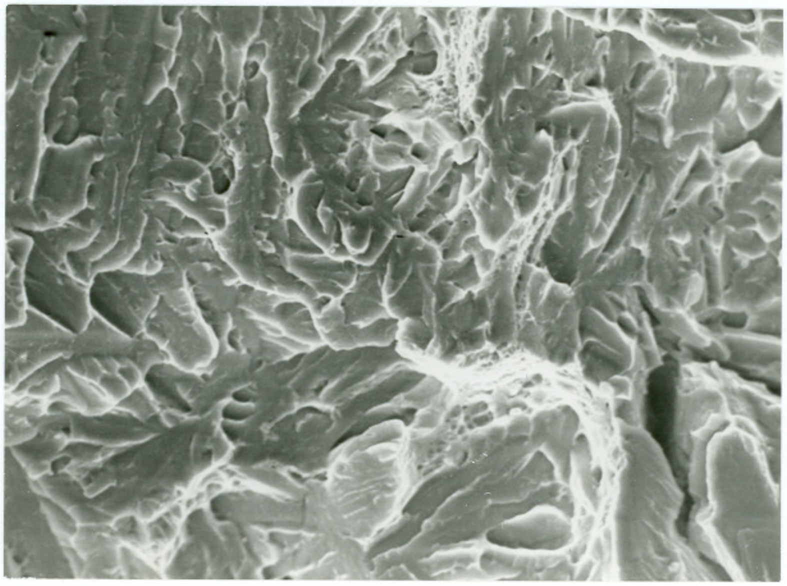

(a) 3.25 μm

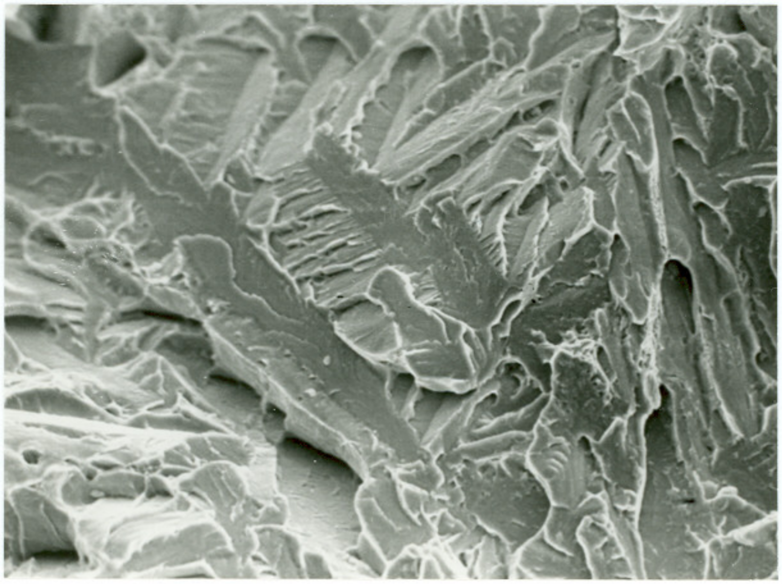

(b) 3.25 μm

Figure 3.26. Fracture Surface of Specimens Heat Treated under (a) B and (b) C Conditions.

3.7.2. Fractography of Specimens Used in Systematic Analysis

The specimens used in the systematic analysis fractured mainly in a transgranular fashion. When transformation temperature was raised to 280°C, fracture was almost 100% transgranular. At low magnifications, some black areas similar to intergranular fractured region were observed, Figure 3.27a. These, at high magnifications, were seen to be the areas where deep holes were formed on the fracture surface, Figure 3.27b.

Quasi-cleavage was the predominant transgranular fracture mode. A comparison of the appearance of the fracture surfaces under different heat treating conditions suggested that fracture toughness could be related to fracture surface roughness. On a macroscopic level, fracture surface of 250°C austempered specimens appeared flat, Figure 3.28a, while that of 300°C austempered specimens was much rougher, Figure 3.28b. On microscopic scale, besides the surface roughness changes, the quasi-cleavage unit size, which closely matched with bainite lath width, also increased with transformation temperature, Figure 3.29.

The quasi-cleavage units were surrounded by tear ridges which were presumably formed by localized plastic deformation. Tear ridges could be seen on two levels, i.e., along bainite lath and around prior austenite grain, with the latter being seen only occasionally, Figure 3.30. Tear ridges along bainite packet boundaries were of the same magnitude as those along bainite lath boundaries, indicating that ferrite grain boundaries participated in fracture processes to the same extent as bainite lath boundary, not as much as what Brozzo *et al*[71] had observed. The bainite lath boundary tear ridges accounted for over 95% of all the observed ridges; they were the main energy absorbers. The prior austenite grain boundary tear ridges were sparse but, when present, they appeared wider and contained more microvoids, suggesting that they dissipated more energy per unit length than lath boundary tear ridges. These two types of ridges should be incorporated into the toughness-structure relationship study.

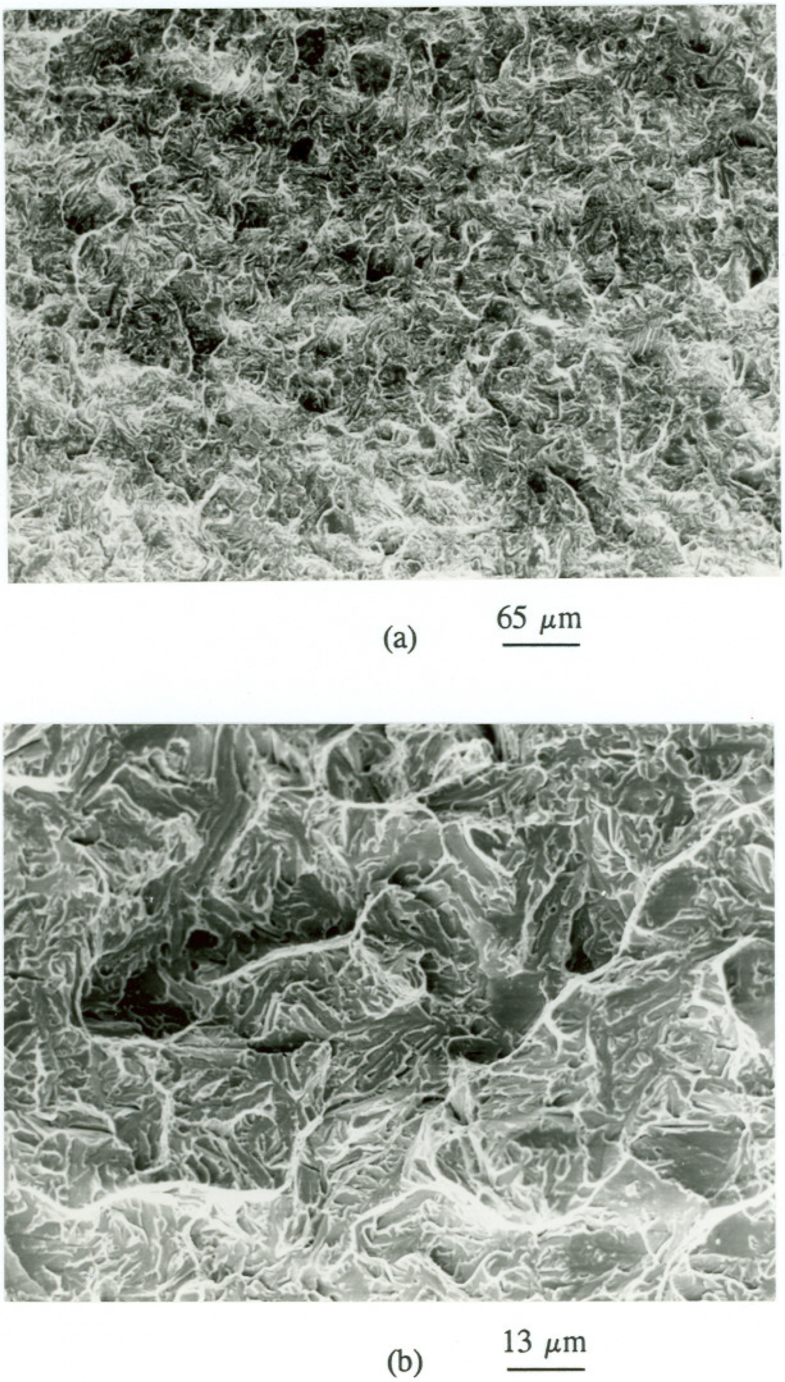

Figure 3.27. Fracture Surface of 280°C Austempered Specimen at (a) 150× and (b) 770×

(a) 130 μm

(b) 130 μm

Figure 3.28. Fracture Surfaces of (a) 280 and (b) 300°C Austempered Specimens.

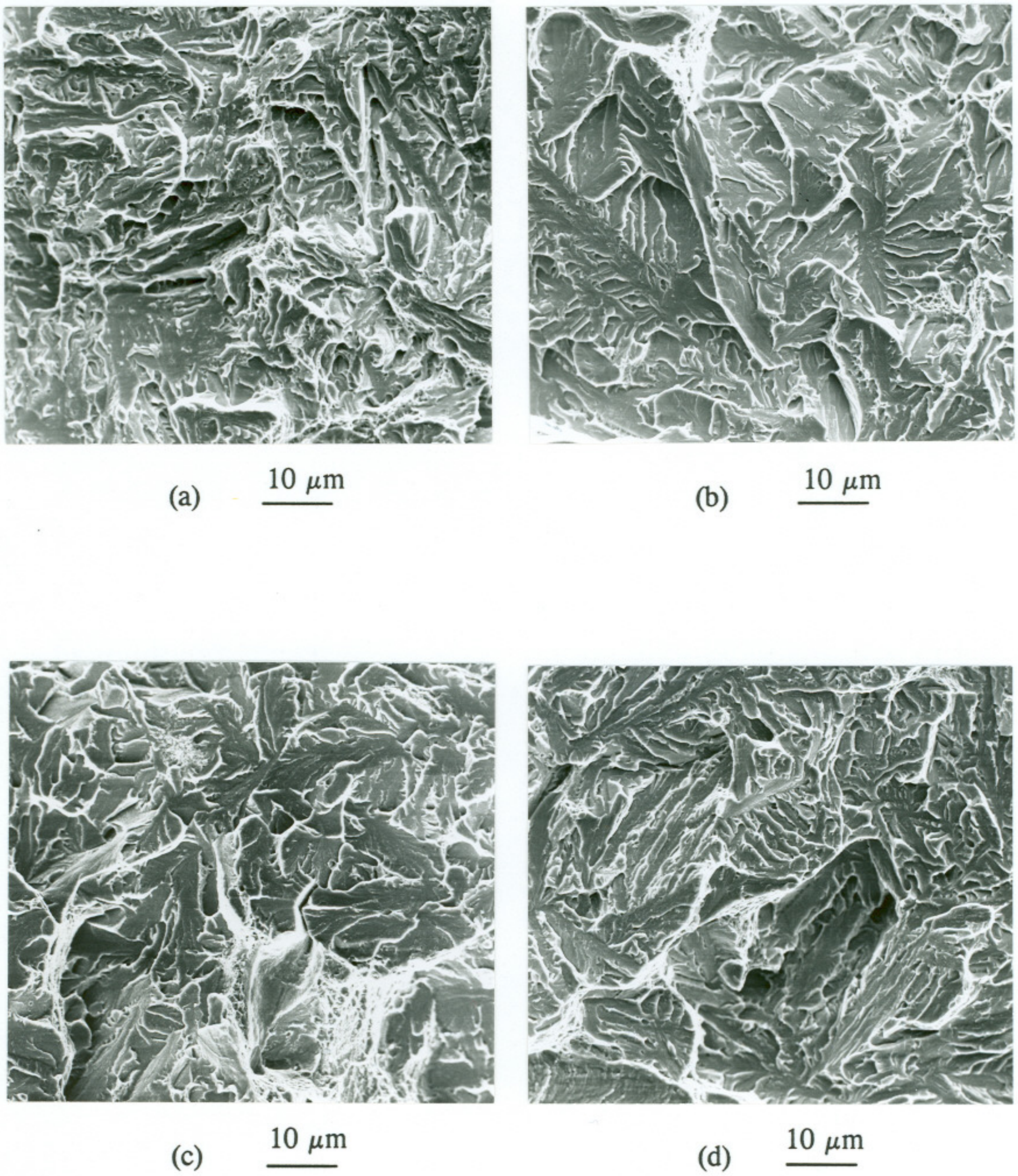

Figure 3.29. Fracture Surface Appearance Variation with Increasing Transformation Temperature. (a) 250 (b) 280 (c) 300 and (d) 320°C.

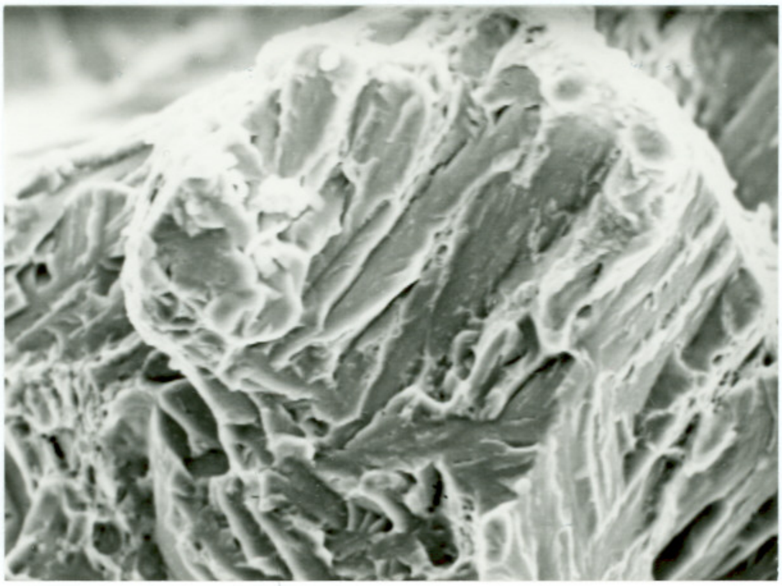

(a) 3.25 μm

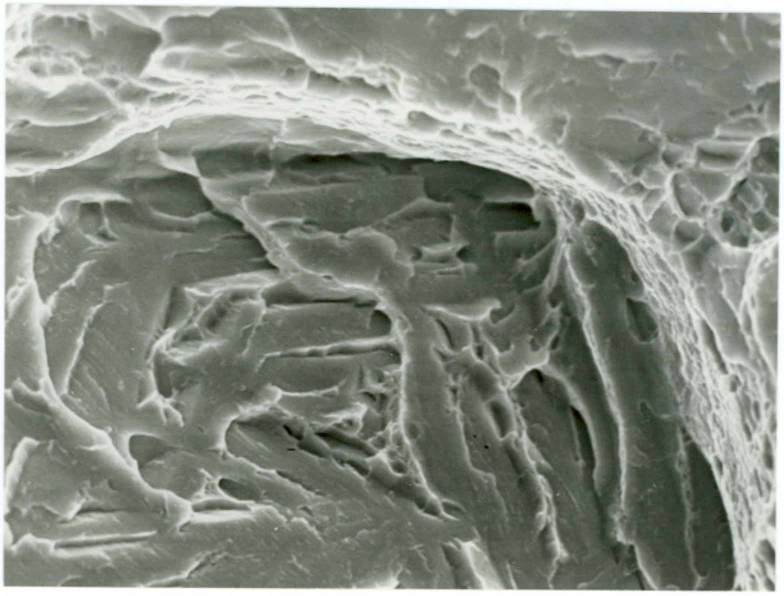

(b) 2.17 μm

Figure 3.30. Tear Ridges Surrounding Prior Austenite Grains.

CHAPTER 4

TRANSFORMATION KINETIC STUDY RESULTS

This work involved overall bainite transformation kinetics for the understanding of the microstructure and mechanical property developments. Viewing the distinction between phase transformation and structure-property relationship studies, separate introduction, mathematical derivation, results, and discussion sections on transformation kinetics are included in this chapter. The separate treatment was to present the development of isothermal transformation kinetics of this work more clearly. The effect of phase transformation study on structure and property control provided an obvious connection between this chapter and the others.

4.1. Introduction

Johnson and Mehl[145] and Avrami[146,157,158] developed the following equation independently about fifty years ago to describe isothermal transformation processes in steels:

$$X = 1 - \exp(-kt^n) \tag{4.1}$$

where X is volume fraction of the product phase, t is transformation time, k and n are material constants under a given transformation condition.

Equation (4.1) had two applications. First, the constants k and n could be extracted from experimental data and stored as the only values needed for reconstructing and representing the original data. Obviously, storing k and n pairs was much more economic in terms of storage space than storing the entire data set.[159]

Second, if k and n were known from a knowledge of steel composition and transformation temperature, volume fraction of the product phase could be predicted.

To date, equation (4.1) has not been used for the second purpose since relationships between steel composition, transformation temperature, and the constants have not been reported. Research studies for such relationships were few since it was believed that a knowledge of k and n alone did not, in general, give useful information about transformation mechanisms.[159] The studies that attempted the correlations did not yield applicable results but they collected evidence that indicated the existence of the correlations and inspired the present investigation.

Radcliffe and Rollason[160] studied overall transformation kinetics for the bainitic reaction in plain carbon steels and showed that the data were not consistent with the form of equation (4.1). They obtained n values ranging form 1.8 to 4.0; no correlation between n and reaction temperature (n-T) was available. Radcliffe and Rollason expected k to vary with transformation temperature following an Arrhenius relationship

$$\frac{1}{k} = C\exp\left(-\frac{Q}{RT}\right)$$

where Q is transformation activation energy, R is gas constant, and C is a constant. This equation predicted a decrease in k with increasing temperature whereas the observed k values showed an opposite trend.

Umemoto *et al*[161] found n values around 4.8 for a high chromium bearing steel. The temperature dependence of n was less than that in plain carbon steels. The observed k values by Okamoto and Oak[162] could be expressed as a second degree polynomial function of temperature but their n values did not reveal any sensible n-T relationship. Recent effort by Kang *et al*[16] showed that the different values of n might be indicative of some differences in transformation mode; again no *n*-T relationship was observed.

The values of *k* and *n* depend on transformation mode and reaction rate which in turn depend on transformation temperature; therefore, *k*-T and *n*-T relationships should exist. The reason that such relationships have not been observed is due to the over simplification involved in deriving of equation (4.1) by assuming transformation incubation time is negligible. Most nucleation and growth transformations involve an incubation time, usually designated as τ. This term divides the total transformation time into two sections: the incubation period and reaction period. The incubation period is from the instant of quenching to τ. The reaction rate is extremely slow and is generally assumed to be zero in this segment. The reaction period starts at τ and ends when all the parent phase has been transformed or when the maximum amount of product allowed by thermodynamics is reached. In the reaction period, transformation proceeds with appreciable rates. The overall reaction kinetics, such as the Johnson-Mehl-Avrami approach, is concerned with the relationship between the transformed amount and time during the reaction period. Hence, it should include the incubation time since this term modifies the length of the reaction time.

Equation (4.1), however, does not contain an incubation time; it represents only one special transformation case, i.e., when incubation is negligible. The equation approximates overall transformation kinetics for plain carbon steels and low alloy steels at the C curve nose temperatures well but may cause serious errors for these steels at other temperatures and for other alloy steels in general when significant incubation times are involved. The errors would then cause even larger errors to the extracted *k* and *n* values which in turn would confound any relationship between these parameters and transformation temperature.

The typical changes to the shape of a transformation curve due to neglecting the incubation time are depicted in Figure 4.1. The solid curve represents a transformation that starts at τ; the dashed curve, on the other hand, is one of many possible curves connecting the origin and transformation finish time. By neglecting incubation time, one changes a real transformation to an artificial reaction which may or may not represent the original transformation. When incubation time is short, neglecting it causes a small change in the shape of the transformation curve. As incubation time increases, neglecting it introduces increasingly significant changes to the shape of the transformation curve, i.e., equation (4.1) represents a totally different transformation situation. The obtained *k* and *n* parameters deviate more and more from their respective true values when incubation time increases. The consequence is that any *k*-T and *n*-T relationships will be confounded. This explanation applies to essentially all the previous phase transformation studies using the Johnson-Mehl-Avrami equation.

The present work modified equation (4.1) by incorporating the incubation time for a more accurate bainite transforation kinetic study. The modification reduced the errors in the assessment of *k* and *n*. As a result, a *n*-T relationship was revealed. A general trend of *k* as a function of the transformation temperature was also observed, but an accurate relationship could not be determined since *k* was on the order of 10^{-3} to 10^{-4} and was more vulnerable to experimental errors as compared to *n*.

The observed *n*-T relationship yielded a microstructure and transformation temperature correlation which could be used to determine austenite decomposition mode at a given temperature without metallographic analysis.

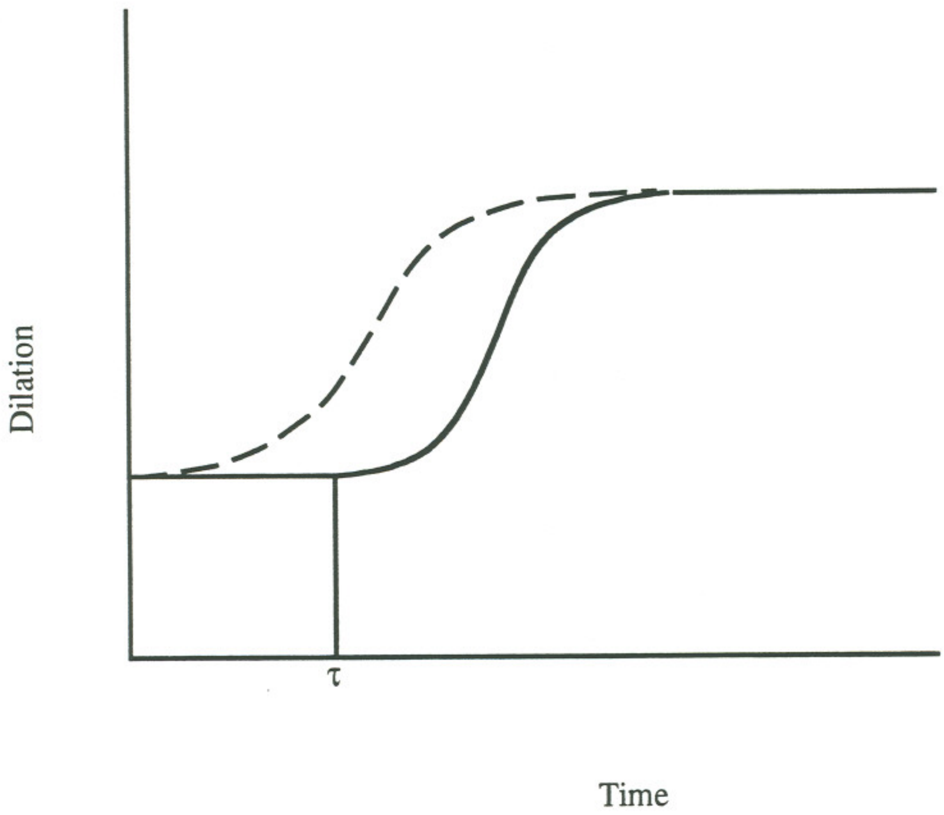

Figure 4.1. Effect of Ignoring Incubation Time on Transformation Curve Shape.

4.2. Transformation Kinetic Equation Derivation

Based on formal theory of transformation kinetics[147], the volume of a nucleus of the new phase formed at time t′ grows to the size $v_{t'}$ at time t (>t′), where

$$\begin{aligned} v_{t'} &= 0 && (t' < \tau) \\ v_{t'} &= \eta Y_1 Y_2 Y_3 (t - t')^3 && (t' > \tau) \end{aligned} \tag{4.2}$$

η is a shape factor, Y_i's are the principal growth velocities in three mutually perpendicular directions, and τ is incubation time. From t′ to t′+dt′, the volume of the new phase increases by

$$dV_v = v_{t'} V_o {}^V I dt' \tag{4.3}$$

where ${}^V I$ is nucleation rate per unit volume, V_o is the assembly volume, V_e is the extended volume including volume of the new phase which nucleates and grows in transformed regions as well as untransformed regions. The net volume increase of the new phase in untransformed regions is

$$dV = (1 - \frac{V}{V_o}) dV_e \tag{4.4}$$

Therefore,

$$\frac{dV}{V_o - V} = v_t {}^V I dt' \tag{4.5}$$

Integrating the left hand side from 0 to V and, correspondingly, the right hand side from 0 to t and setting X = V/V_o results in,

$$\ln (1 - X) = -\int_0^\tau 0 dt' - \int_\tau^t \eta Y_1 Y_2 Y_3 {}^V I (t - t')^3 dt' \tag{4.6}$$

The ability to integrate equation (4.6) depends on ${}^{v}I$. The easiest case is when ${}^{v}I$ is a constant, in which the integration gives

$$\ln(1 - X) = -\frac{1}{4}\eta\, Y_1\, Y_2\, Y_3{}^{v}I(t-\tau)^4 \tag{4.7}$$

To generalize, (4.7) becomes

$$X = 1 - \exp[-k(t - \tau)^n] \tag{4.8}$$

where k (= $1/4\eta Y_1 Y_2 Y_3{}^{v}I$) is the rate constant and n is commonly referred to as the curve shape constant.

The value of n depends on the nucleation site and rate.[147,157] For homogeneous nucleation and constant nucleation rate, as assumed in the above derivations, n equals 4. The value of n decreases if nucleation is heterogeneous and nucleation rate decreases as the transformation proceeds. When all the nucleation sites are saturated early in a transformation, n reduces to the lower limit value, 3. Therefore, for three dimensional transformations the value of n is usually between 3 and 4. Rarely but it is possible for n to be greater than 4, e.g., when number of nucleation sites increases with increasing volume fraction of the new phase.

In two dimensional transformations, the new phase grows in two directions; the integration of the term $(t-\tau)^2$ results in n values between 2 and 3. Similarly for one dimensional growth, n ranges from 1 to 2.

In experimental measurements, the method used to monitor the transformation processes also affects the range of n. If one dimensional detecting technique is used, the recorded transformation characteristic should be that of one dimensional, no matter what the original reaction dimensionality is; in particular, the measured n lies between 1 and 2.

Both equations (4.1) and (4.8) assume constant nucleation and growth rates; therefore they are valid only for linear growth and are approximately valid for the early stages of diffusion-controlled growth.[147] Previous investigations have established that bainite nucleation rate at one temperature is constant[159,163,164] and bainite growth rate under linear growth conditions is also constant.[39,163,165,166] Therefore, the equations apply to the linear growth section of bainite transformation. Since this section constitutes the main part of bainite transformation,[18] the result approximates that of the entire reaction period.

This work adopted an arbitrary 0.2 to 0.6 product volume fraction criterion and assumed that growth in this range was linear; the statements on the general features of equation (4.8) and reaction characteristics were based on this assumption.

4.3. Results

As described in Chapter 2, volume fraction of isothermal transformation product could be approximated using

$$X = \frac{\Delta L}{\Delta L_{MAX}} \tag{4.9}$$

The application of equation (4.9) on an isothermal transformation dilation data file yielded a volume fraction versus time relationship which could be plotted in a lnln[1/(1-X)] versus ln(t-τ) figure. Numerically n equaled the slope of the linear portion of the curve and k was the intersection of the extension of the linear portion with the vertical axis. Figure 4.2 shows a typical example in which the line was formed by unresolvable data points due to high sampling rate. The transformation temperature was 250°C, n was 1.22, and k was 7.64×10^{-4}.

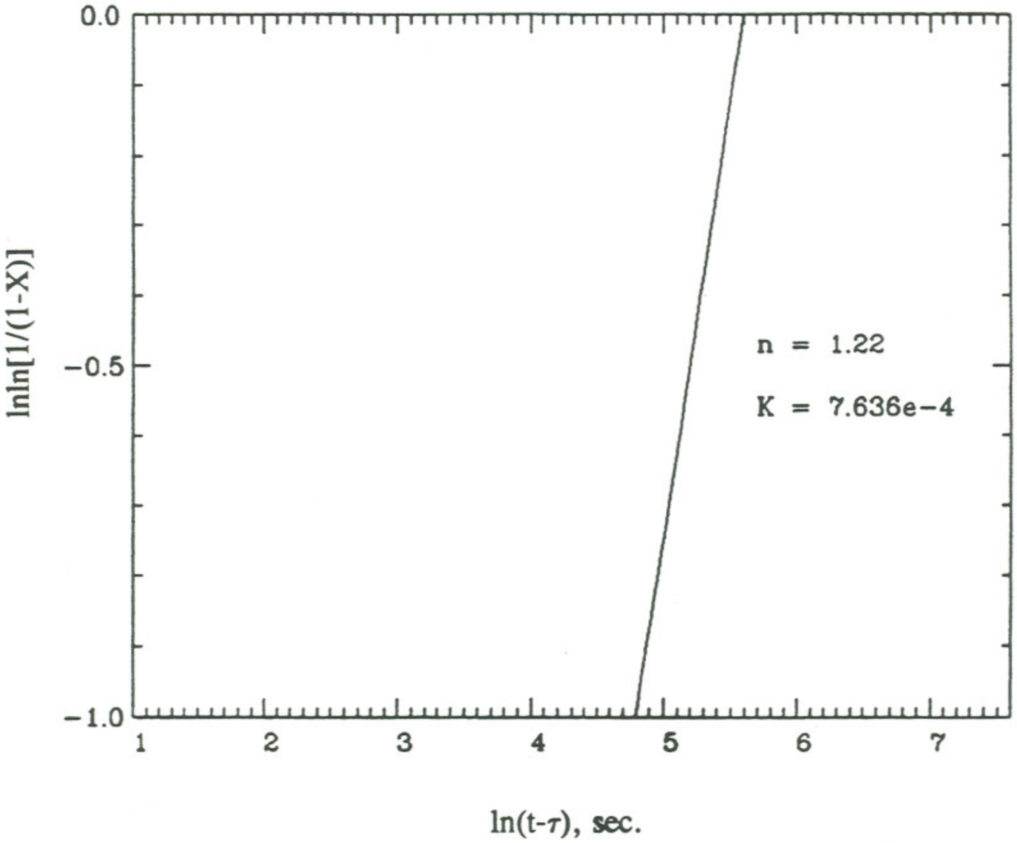

Figure 4.2. The lnln[1/(1-X)] versus ln(t-τ) Relationship of a High Carbon Low Alloy Steel. The Line Was Formed by Continuous Data Points due to High Sampling Rate.

The *n* values of isothermal heat treatments at temperatures ranging from 250 to 650°C are tabulated in Table 4.1 and plotted as a function of transformation temperature in Figure 4.3. Two points should be noted. First, the values are in the correct range, i.e., between 1 and 2, in accordance with the employment of the one dimensional detecting technique. Second, three lines with negative slopes could be drawn; the extent of each line closely corresponded to a particular product transformation temperature range. These lines were tentatively assigned as lower bainite, upper bainite, and pearlite transformation lines. The validity of these assignments had to be revealed by microscopic analysis.

Two lines with positive slopes could also be constructed connecting two adjacent mono-microstructure transformation temperature ranges. Following the above argument, these were the transition temperature ranges in which both high and low temperature products were transformed.

According to Figure 4.3, the temperature range for only lower bainite transformation was from 250 to 300°C, that for upper bainite reaction was between 375 and 500°C. Pearlite transformed at temperatures above 550°C. For any predictions the boundaries were the most difficult points; if the predictions were true at the boundaries, they would be true inside each range. Therefore, to verify the above structural predictions, only the microstructures transformed at the temperature range boundaries, namely 300, 375, 500, and 550°C needed to be analyzed. The microstructure formed at 350°C was also studied. Both upper and lower bainite were expected to be present.

Table 4.1. The n Values at Different Reaction Temperatures

Temperature, °C	n	Temperature, °C	n	Temperature, °C	n
250	1.22	330	1.45	450	1.36
280	1.14	340	1.53	500	1.27
300	1.07	350	1.60	550	1.70
310	1.18	375	1.67	600	1.34
320	1.26	400	1.61	650	1.27

Under optical microscope, lower bainite had a plate shape morphology, the aspect ratio decreased with increasing transformation temperature. At 300°C secondary plates could be seen growing from the primary plates, Figure 4.4a. In TEM, the microstructure assumed classical lower bainite morphology: carbides precipitated within ferrite plates at an angle about 60° from the long axis of the plate, Figure 4.4b.

Upper bainite formed at 375°C had a very different morphology than lower bainite, Figure 4.5. The structure nucleated at prior austenite grain boundaries, and the subunits grew into austenite grains in a parallel fashion. Most of the bainite sheaves grew more or less in equiaxed shape, although sharp needles could be seen occasionally. These needles might be the first or the first few subunits of a sheaf; their existence promoted other subunits to form and grow on their sides epitaxially.

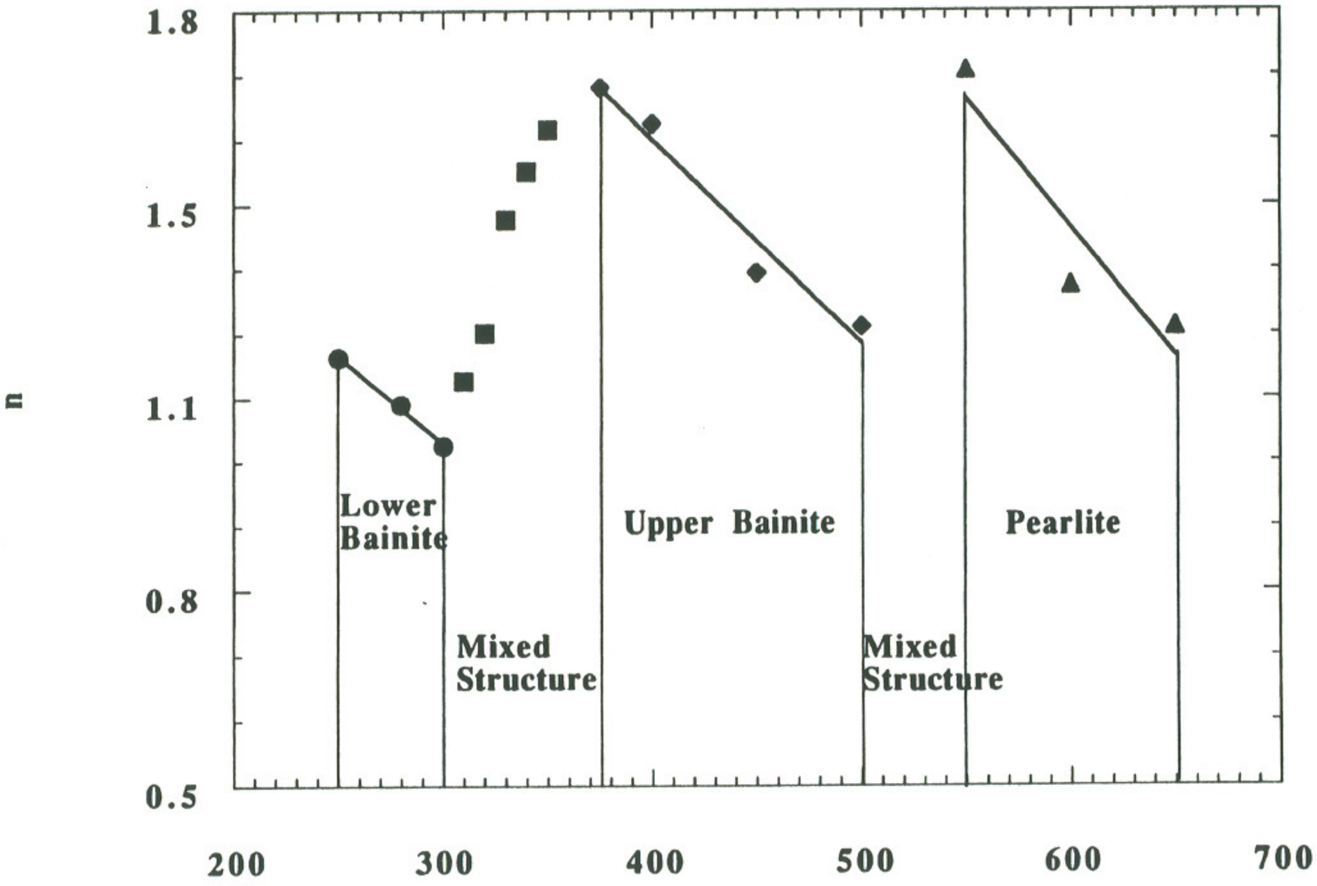

Figure 4.3. The *n* Lines of Different Reactions.

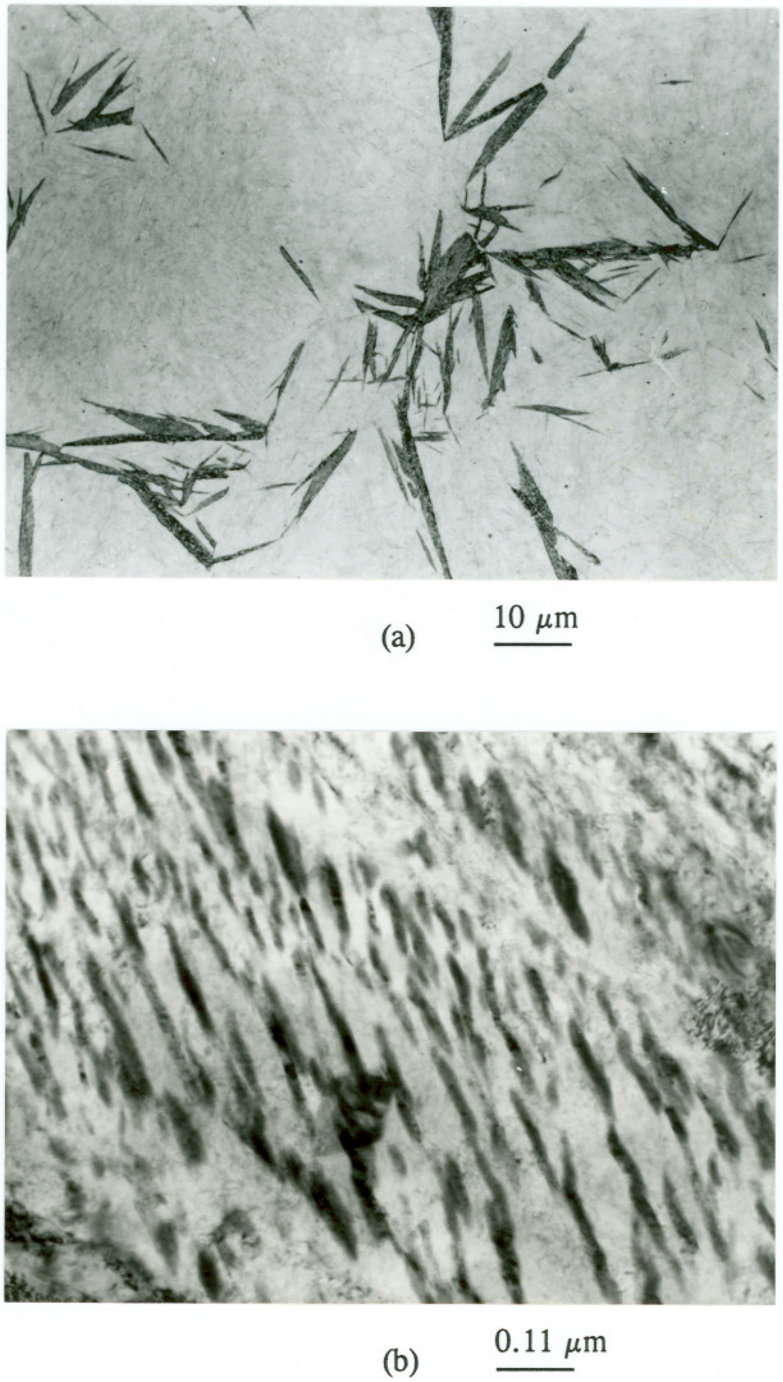

Figure 4.4. Lower Bainite Structure Formed at 300°C. (a) Optical and (b) TEM.

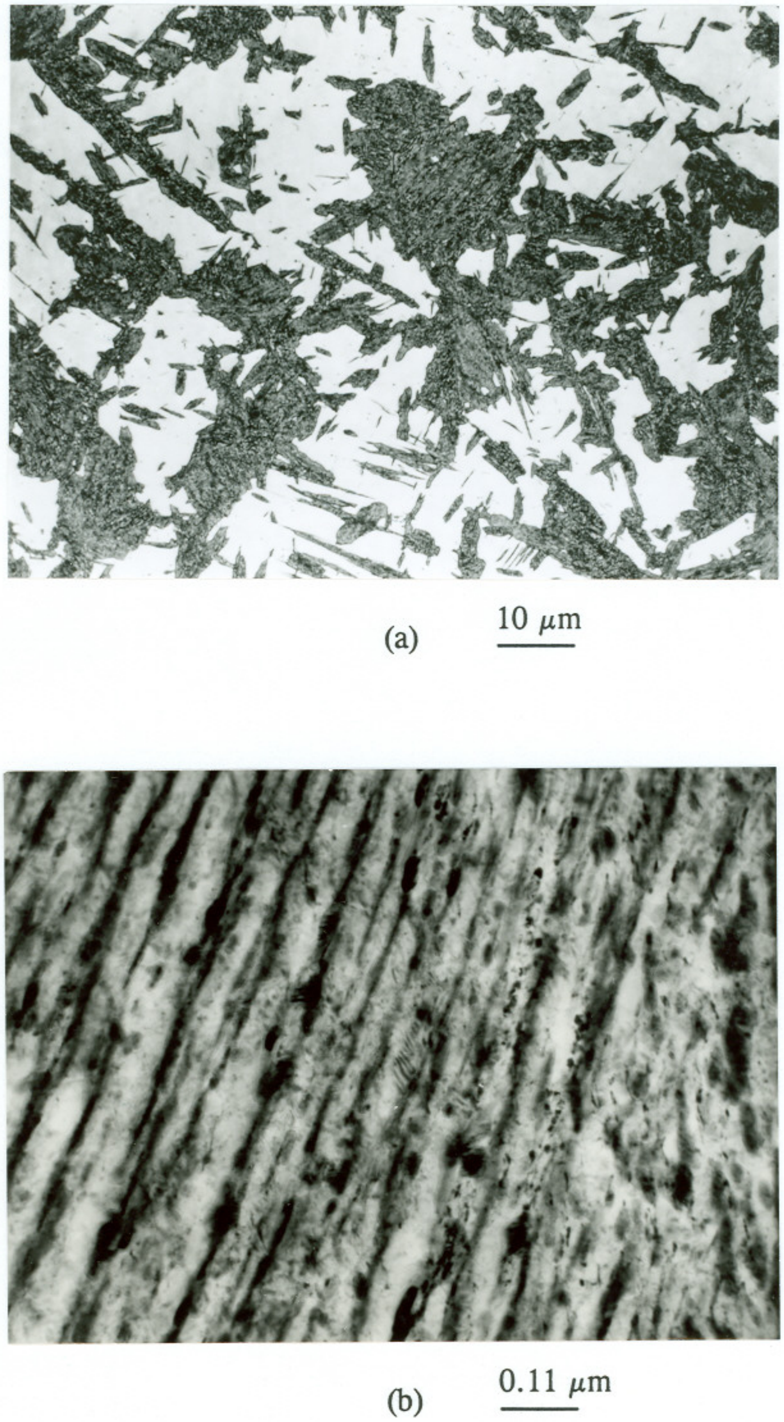
(a) 10 μm

(b) 0.11 μm

Figure 4.5. Upper Bainite Structure Formed at 375°C. (a) Optical and (b) TEM.

In TEM observations, upper bainite had a lath-like morphology, carbides precipitated between and within bainite laths, Figure 4.5b. The intralath carbides probably were formed and subsequently engulfed by growing ferrite. Both interlath and intralath carbides tended to grow parallel to the long axis of ferrite laths.

The striking morphological differences between the structures formed at 500 and 550°C under optical microscope clearly delineated these products Figure 4.6; the one formed at 500°C was upper bainite, the other was pearlite.

The transition from upper bainite transformation to lower bainite transformation took place in the temperature range of 300 to 375°C. In this range both upper and lower bainite existed. Figure 4.7 shows typical microstructures transformed at 350°C. At early transformation stages, upper bainite was formed, Figure 4.7a; after transformation completion, a mixture of upper bainite and lower bainite was obtained,Figure 4.7b. The observed transformation sequence could be explained as follows. The temperature 350°C was close to the upper limit of lower bainite transformation; the incubation time increased quickly with increasing reaction temperature. If the incubation time of lower bainite transformation was longer than that of upper bainite transformation, upper bainite reaction would precede the lower bainite reaction. Hence upper bainite prevailed at early stages, whereas lower bainite transformed after a certain degree of transformation.

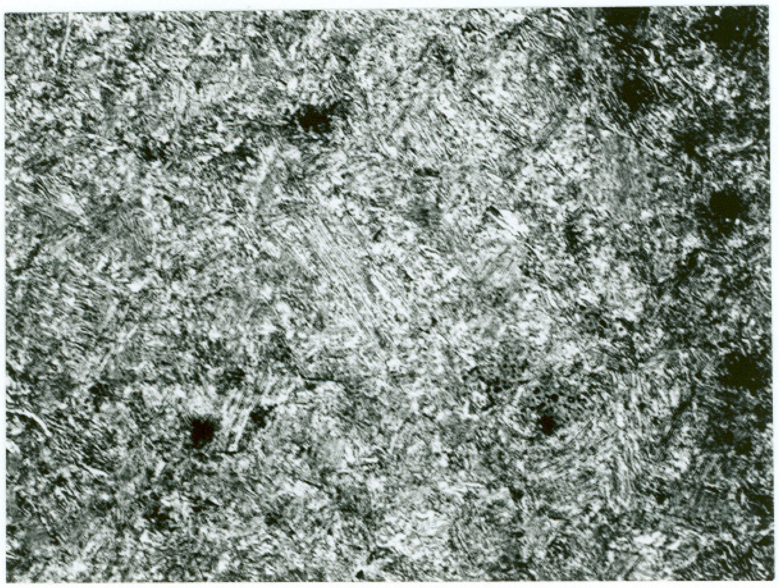

(a) 25 μm

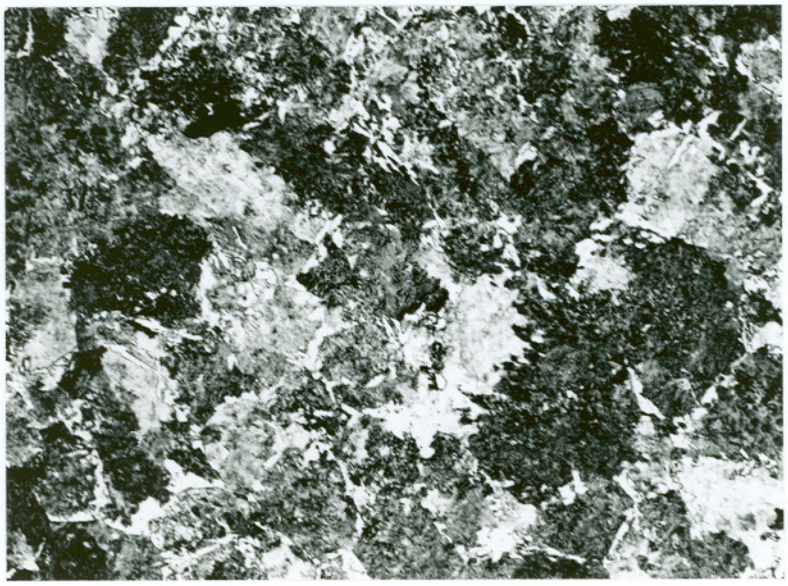

(b) 25 μm

Figure 4.6. Structures Formed at 500 and 550°C, respectively. (a) Upper Bainite and (b) Pearlite.

(a)

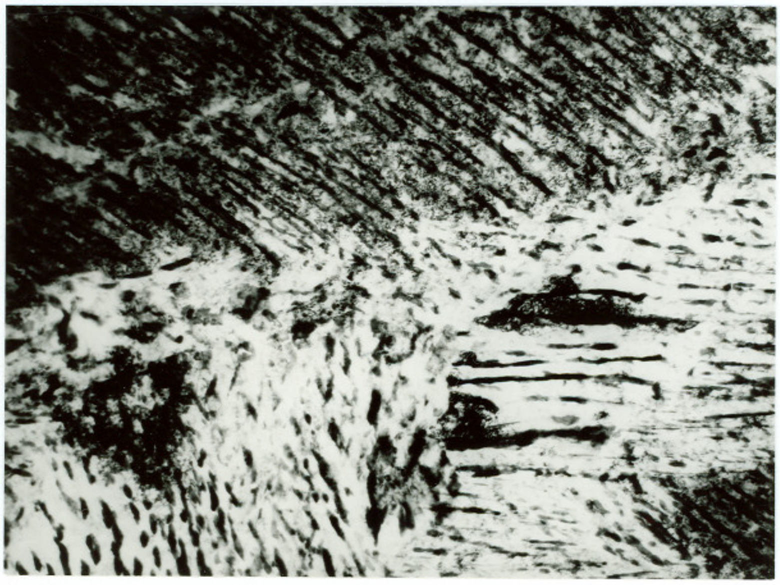

(b)

Figure 4.7. Microstructure Formed in Upper/Lower Bainite Transition Range. (a) Optical Structure of Upper Bainite and (b) TEM Structure of Mixture.

4.4. Discussion

A TTT diagram shows austenite decomposition rate at various temperatures. The transformation rate of austenite to pearlite, upper bainite, and lower bainite follows C curve shaped functions in a time-temperature space

$$R = C(T) \tag{4.10}$$

where R is reaction rate and T is transformation temperature. When two microstructures transform at similar temperature ranges and rates, their C curves tend to overlap. Overlapping pearlite and bainite C curves are common in carbon steels and low alloy steels since the temperatures and times at which pearlite and bainite reactions reach their respective maximum transformation rates are very close.

The pearlite and bainite C curves can be physically separated by the addition of alloying elements. Strong carbide forming elements such as titanium, vanadium, niobium, tungsten, and molybdenum effectively retard pearlite transformation, moving pearlite C curve up and pushing it to the right,[167] Figure 4.8a. These elements mildly retard bainite transformation and reduce the temperature at which bainite transformation has the maximum rate. Weak carbide forming elements, chromium and manganese, more effectively retard both pearlite and bainite transformations. Their effect on bainite transformation is more apparent, Figure 4.8b. Non-carbide forming elements, silicon and aluminum, increase austenite stability and effectively retard bainite transformation. They separate pearlite and bainite C curves mainly by increasing the temperature at which pearlite has the maximum transformation rate but decreasing that of bainite, Figure 4.8c. However, even though pearlite and bainite C curves can be separated by alloying element additions, upper bainite and lower bainite C curves often remain overlapping since no element is known to separate upper bainite and lower bainite C curves.

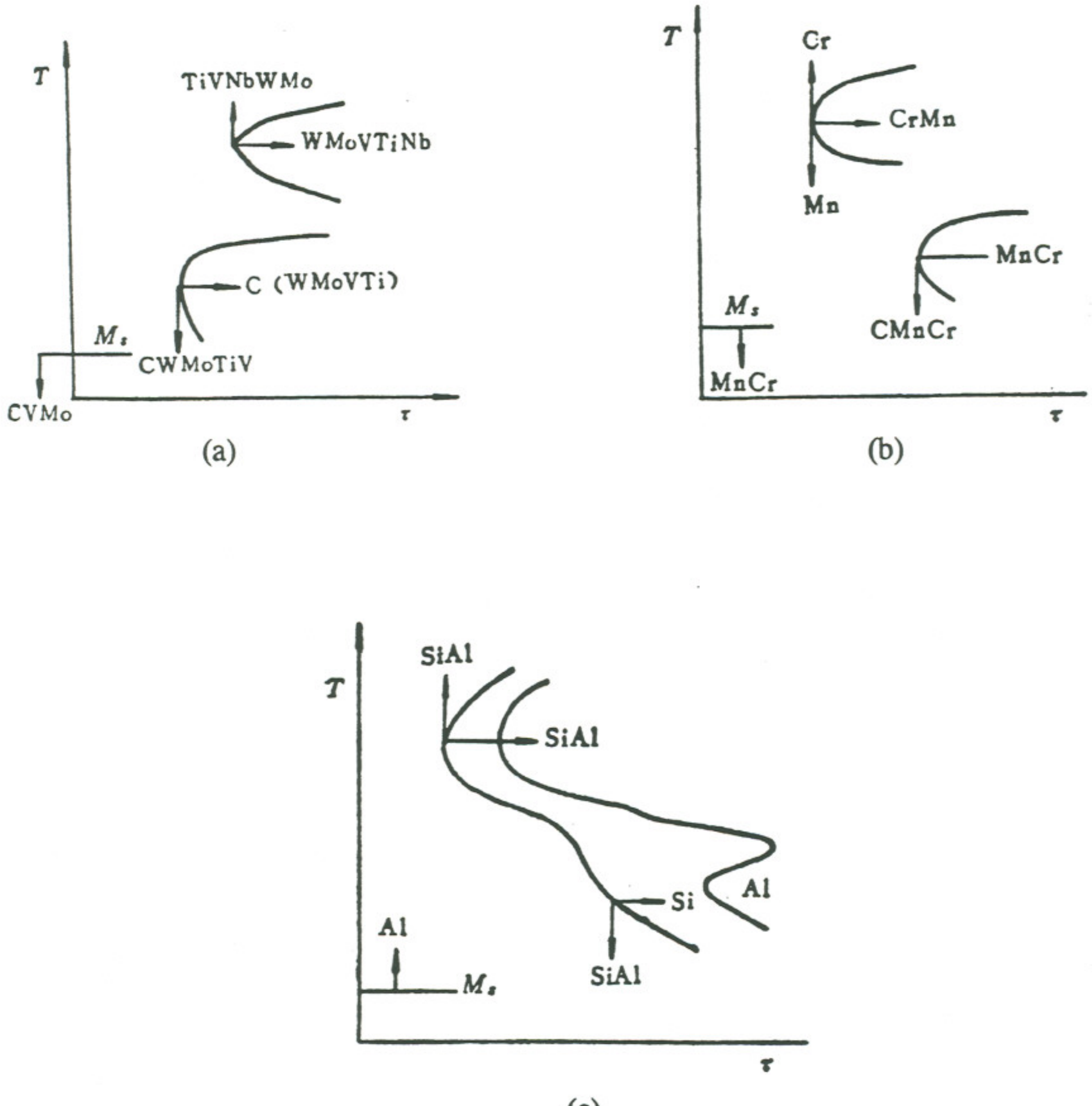

(a) (b) (c)

Figure 4.8. Effect of Alloying Element on C Curves of Pearlite and Bainite. (a) Strong Carbide Forming Elements, (b) Weak Carbide Forming Elements, and (c) Non-Carbide Forming Elements.

An alternative approach in phase transformation study is to determine the upper and lower transformation temperature limits for each product so that a complete C curve for each microstructure can be obtained even though the C curves overlap. By introducing a transformation rate sensitive parameter the rate-temperature relationship expressed in equation (4.10) is transformed to a parameter-temperature relation. If by this manipulation the upper and lower transformation temperature limits for each product can be determined, the problem is solved. This work selected the curve shape constant n as the reaction rate sensitive parameter, or

$$n = F(R)$$

Substituting equation (4.10) for R, results in

$$n = F[C(T)] \tag{4.11}$$

Function F separates the curves in a n versus temperature plot, Figure 4.3. Function C, on the other hand, helps the recognition of the lines in the plot. Since C curves in a T-t space have similar shapes, their transformation in a n-T space are also expected to have similar shapes. This argument leads to the recognition that each line in Figure 4.3 represents an austenite decomposition mode. The transformation temperature range for a product extends from the lowest to highest temperature covered by a line. For alloy steels which may have a separate pearlite C curve from the overlapping upper and lower bainite C curves, the argument also holds true; separate n lines for lower bainite and upper bainite can be obtained in a n versus temperature plot. The transformation temperature ranges for each reaction can be determined in a similar manner.

Equation (4.8) was also tested on Radcliffe and Rollason's data,[160] which was obtained using electric resistivity method on thin wire specimens. The calculated n

was between 1 and 2 for this perfect one dimensional case. The relationship between *n* and temperature is clearly shown in Figure 4.9 in which the single product line stretching from 300 to 380°C was due to lower bainite transformation as could be seen from the TTT diagram in the original article.

The confirmation of the microstructure predictions based on the *n*-T relationship produced the discovery of a third application of equation (4.8), or the development of a non-metallographic microstructure identification technique which was quick, accurate, and convenient. The technique determined transformation temperature ranges for each microstructure without tedious metallographic analysis, but using the same data needed for TTT diagram construction. The technique would be very useful in TTT diagram determination for plain carbon steels and low alloy steels in which the C curves of different products always overlapped. The separation of the C curves was difficult, if not impossible, using metallographic analysis but was fairly easy with the new technique which could determine the upper and lower temperature limits for each transformation product. An immediate application of this feature of the technique was the measurement of bainite transformation start temperature, B_s.

Considering the morphological similarity between pearlite and upper bainite at temperatures close to B_s, one could appreciate the complexity involved in the detection of B_s metallographically. Using Figure 4.3, on the other hand, B_s was readily obtained as the temperature at which upper bainite started to form, e.g., 550°C for the current steel. This temperature agreed well with the calculated value, 533°C, using the equation developed by Steven and Haynes[168]

$$B_s\,(^{\circ}C) = 830 - 270C - 90Mn - 37Ni - 70Cr - 83Mo \tag{4.12}$$

The discrepancy could be due to the large temperature steps used in the development of Figure 4.3 or the chemical mismatch since the composition of the current steel was outside the composition range on which equation (4.12) was developed.

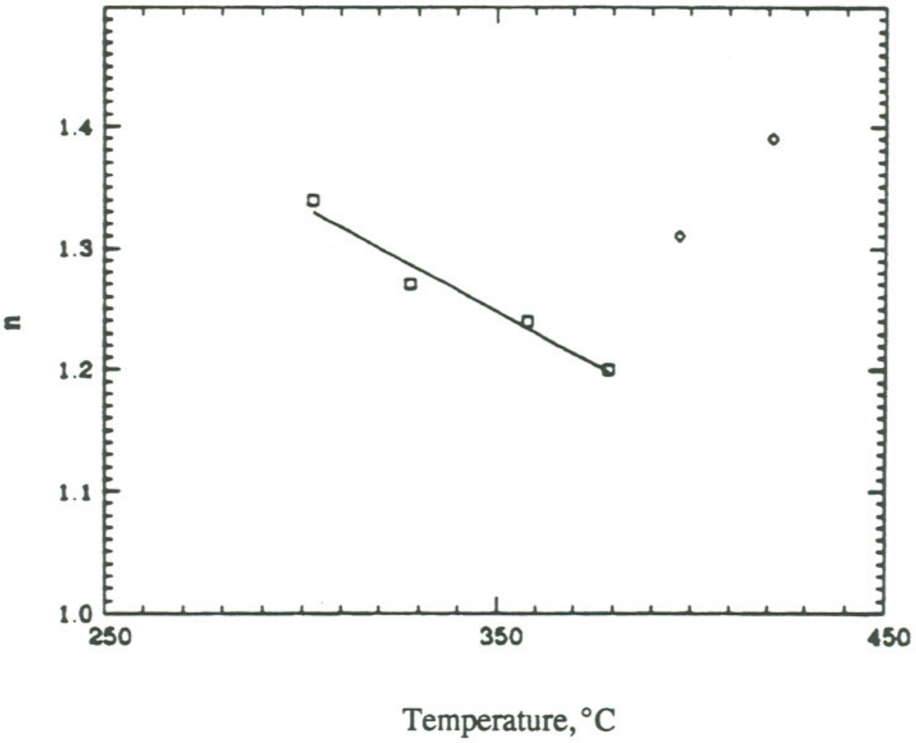

Figure 4.9. The n-T Relationship in a 0.65%C Plain Carbon Steel.

The evolution of the upper temperature limit for lower bainite transformation, or the equilibrium temperature between austenite and lower bainite, leads to the postulation of lower bainite transformation start temperature, B_{Ls}. Correspondingly, the conventional bainite transformation start temperature B_s should be denoted as upper bainite transformation start temperature, B_{Us}.

An immediate application of the B_{Ls} is the calculation of lower bainite C curve using Zener's model

$$t = \frac{K \exp(\frac{Q}{RT})}{(T_E - T)^3} \tag{4.12}$$

where K is a constant, Q is transformation activation energy, R is gas constant, T is absolute temperature, and T_E is equilibrium temperature. Depending on the value of K, t can be either incubation time or transformation finish time.

The temperature T_E is the highest temperature of a transformation; it is the reference temperature base on which the C curve of one transformation is calculated. In the past, lower bainite C curve was calculated as part of the pearlite C curve[169] or upper bainite C curve[170] even though compelling evidence in the literature showed that the products nucleated or grew by different mechanisms.[33,44,163,171] The establishment of lower bainite transformation start temperature B_{Ls} not only strongly supported the concept that upper and lower bainite grew by different mechanisms[33,44,163,171] but also made separate kinetic study of these two products possible.

By incorporating the temperature ranges determined for each product the TTT diagram of the studied steel could be re-plotted to show the transformation characteristics of each reaction, Figure 4.10. For comparison purposes, the one reported in Chapter 3 was also included.

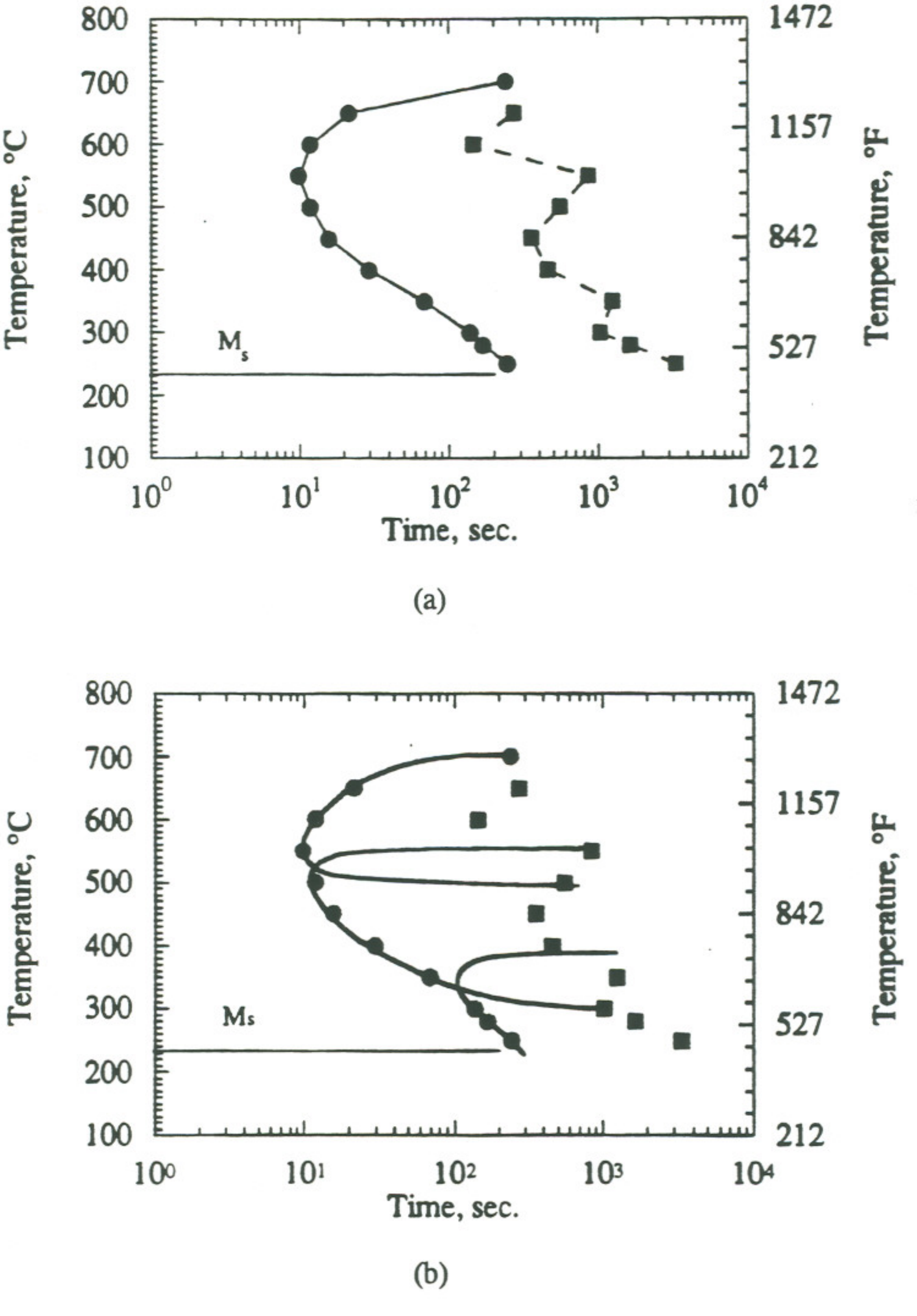

Figure 4.10. TTT Diagram of the Studied Steel. (a) Overlapping C curves (b) Upper and Lower Transforation Temperature Limit Determined.

The single product formation lines in Figure 4.3 were formed by increasing *n* values with decreasing reaction temperature in each respective temperature range. This trend could be explained in two ways. First, as the transformation temperature was decreased, nucleation sites for a product increased.[157] Hence, *n* increased. Second, the decrease in transformation temperature reduced the reaction rate which caused an increase in *n* as shown below.

From equation (4.8)

$$n = \frac{\ln\ln(\frac{1}{1-X_2}) - \ln\ln(\frac{1}{1-X_1})}{\ln(t_2-\tau) - \ln(t_1-\tau)} \tag{4.13}$$

where t_1 and t_2 are the times for achieving the arbitrary volume fractions X_1 and X_2 in the linear growth region. The denominator of equation (4.13) could be written as

$$\ln(1+\frac{\Delta t}{t_1-\tau}) \tag{4.14}$$

where $\Delta t = t_2 - t_1$. With fixed X_1 and X_2, the numerator of equation (4.13) was constant. The terms τ, t_1, and $t_1-\tau$ increased more than Δt with decreasing temperature; so the value of equation (4.14), or the denominator in equation (4.13) decreased. Hence, *n* increased with decreasing transformation temperature. Since increasing τ, t_1, and $t_1-\tau$ meant decreasing transformation rate, the effects of reducing reaction temperature were to reduce transformation rate and to increase the corresponding *n* of the reaction.

The values of equation (4.14) for lower bainite transformation at 250 and 280°C as functions of bainite volume fraction are shown in Figure 4.11a. As expected, the slower reaction at 250°C always had a smaller value. The difference in

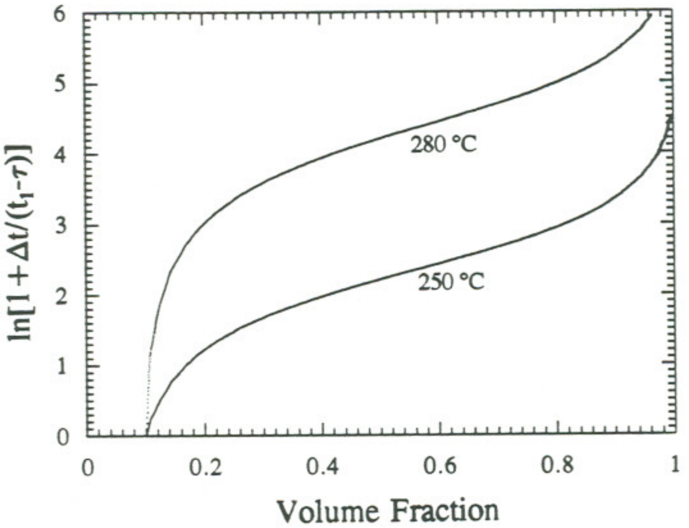

(a)

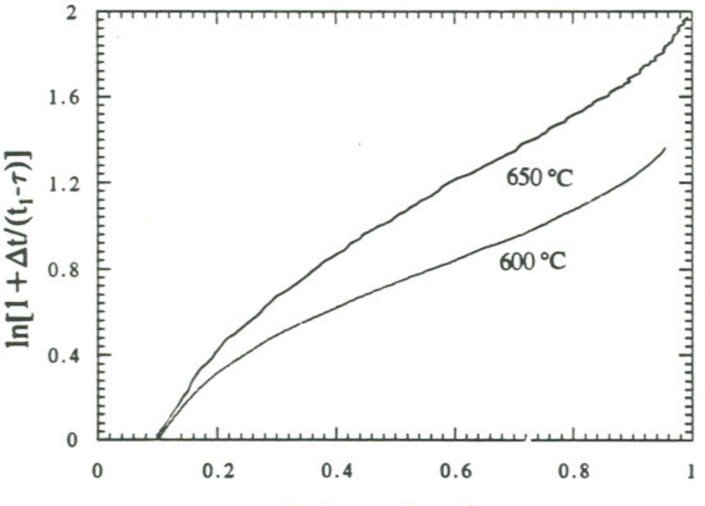

(b)

Figure 4.11. The Effect of Transformation Temperature on $\ln[1+\Delta t/(t_1-\tau)]$. (a) Low Bainite Range (b) Pearlite Range.

these values could explain the increase of *n* as temperature was reduced from 280 to 250°C.

Assuming $X_1 = 0.3$ and $X_2 = 0.7$, the values of $t_1 - \tau$, Δt, and $\ln[1 + \Delta t/(t_1-\tau)]$ of the transformations at 250 and 280 °C are listed in Table 4.2. The relative changes, δ, were also included as referenced to the 280°C transformation, where

$$\delta = \frac{|P_{280} - P_{250}|}{P_{280}}$$

where *P* was the property under consideration at the indicated temperature.

Table 4.2. Lower Bainite Transformation Rate Related Parameters.

Temperature °C	$t_1-\tau$ sec.	Δt sec.	$\ln[1+\Delta t/(t_1-\tau)]$
280	72	133	1.05
250	154	261	0.99
δ	1.13	0.96	0.06

Both $t_1 - \tau$ and Δt increased with decreasing temperature. The first term increased more than the second, leading to a small change in $\ln[1 + \Delta t/(t_1-\tau)]$. The effect of changing $\ln[1 + \Delta t/(t_1-\tau)]$ on *n* could be studied by re-writing (4.13) as

$$(1+\beta)\, n = \frac{\Delta \ln\ln\left(\frac{1}{1-X}\right)}{(1+\alpha)\, \Delta \ln\left(1+\frac{\Delta t}{t_1-\tau}\right)}$$

where α and β represent the relative change in the denominator and n, respectively. The numerator was 1.217. The values of $\ln[1+\Delta t/(t_1-\tau)]$ and n were set to that of the 280°C transformation, equaled to 1.051 and 1.16, respectively. Rearranging for β led to

$$\beta = \frac{0.998}{1+\alpha} - 1$$

The values of β are tabulated in Table 4.3 as α decreases by 0.01 to 0.05. A reverse linear correlation between α and β seems to exist. Hence the decrease in $\ln[1+\Delta t/(t_1-\tau)]$ seems to be the primary reason for the increase in n when transformation temperature is decreased. For example, by reducing temperature from 280 to 250°C, α decreases by 6%, while n increases by 6.5%. The small difference could be due to nucleation rate change but it was more likely to be caused by experimental error.

Table 4.3. Effect of Changing α on β.

α	β
-0.01	0.008
-0.02	0.018
-0.03	0.029
-0.04	0.039
-0.05	0.050
-0.06	0.062

Equation (4.12) was also evaluated at 600 and 650°C, Figure 4.11b. The correct order was obtained, i.e., the value was low at the lower temperature. However, the physical meaning was not clear since the temperatures were above the pearlite C curve nose temperature; transformation rate should increase as the transformation temperature was decreased.

In a single product transformation temperature range, reaction rate decreased as temperature was decreased. Correspondingly, n increased to a maximum at the boundary of the temperature range. Further decrease in temperature into the mixed mode transformation range induced the reaction of a low temperature product which gradually dominated the overall transformation rate as temperature was further decreased. Since the low temperature transformation process may have a higher reaction rate than the high temperature product at the same temperature, the total reaction rate increased leading to a decrease in n. When the temperature at which single low temperature transformation prevailed, the reaction rate was the highest; n decreased to a minimum.

The measured k values fluctuated around the curve

$$k = 0.000247 \exp(0.00544\, T)$$

Similar periodic variations revealing transformation mode change as that shown by n-T relationship was not observed. Considering the magnitude of k, the experimental errors involved in obtaining n and k, and the dependence of k on n, the k versus transformation mode correlation might be obscured. The fluctuation of the k values around the above curve instead of falling on any particular k-T expression may be taken as the evidence of the existence of a k-microstructure relationship.

The activation energies for upper and lower bainite transformations were determined using the Arrhenius equation of the form[44,163,171,172]

$$Q_X = -R\left[\frac{\partial \ln(\frac{\partial x}{\partial t})}{\partial(\frac{1}{T})}\right]_X \tag{4.15}$$

where Q_X and $(\partial x/\partial t)_X$ were the activation energy and reaction rate, respectively, when volume fraction of the product was X. Activation energy equaled the slopes of the lines in a $\ln(\partial x/\partial t)$ versus 1/T plot multiplied by -R. Figure 4.12 shows an example at 50% bainite transformation where the activation energy for upper and lower bainite transformations are 49 kJ and 35 kJ, respectively. These values, especially that for upper bainite, are relatively low compared with those measured for other plain carbon or low alloy steels of the same carbon content.[163] When plotted on the published activation energy versus carbon content curve by Hawkins and Barford[163], Figure 4.13, the activation energy values of the current steel are located around the lower bainite activation energy line. As observed by previous investigators[163,173] the measured activation energy for upper and lower bainite transformation was below that for carbon diffusion in austenite and ferrite. Therefore, carbon diffusion in austenite or ferrite could not be the bainite transformation rate controlling process.

The Arrhenius equation (4.15) should apply to transformation data obtained at temperatures below the corresponding C curve nose temperature.[172] However, in the determination of the activation energy of upper bainite transformation, the correlation coefficient was greatly increased if the data point at 500°C was excluded even though this temperature was below the upper bainite C curve nose temperature. Ambiguity also existed in whether the data point at 350°C belonged to upper bainite transformation. The temptation of including transformation rate at 350°C in the

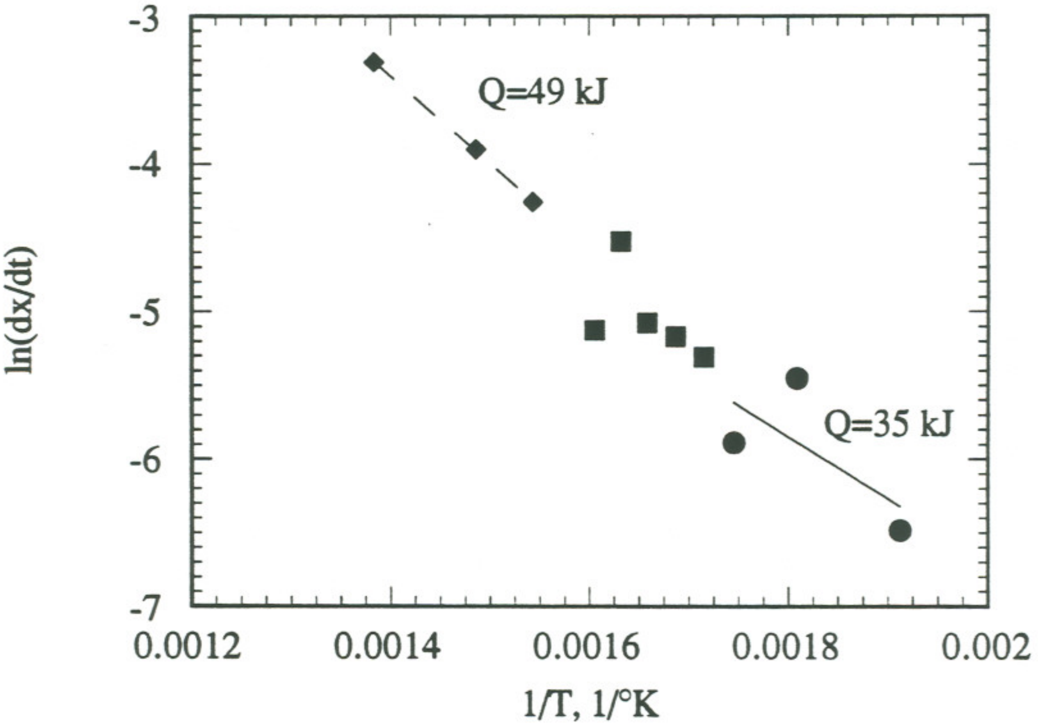

Figure 4.12. Temperature Dependence of the Overall Reaction Rate at 50% Transformation.

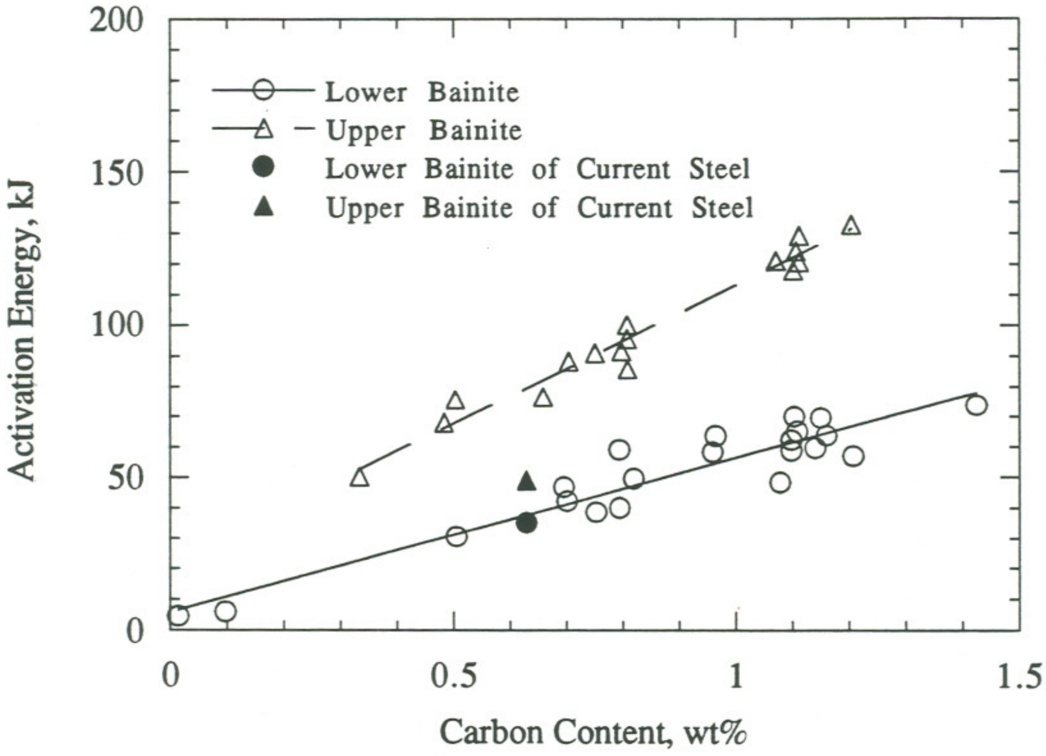

Figure 4.13. Activation Energy for Bainite Transformation as a Function of Carbon Content (After Hawkins and Barford).

upper bainite category was strong since this classification would increase the calculated activation energy to the upper line in Figure 4.13, i.e., the measured energy terms of this work would agree better with those of previous studies. The above observation showed that the temperature range for upper bainite transformation determined using the activation energy method deviated from that obtained using metallographic method and *n*-T correlation.

Activation energies for upper and lower bainite transformations at different bainite volume fractions are tabulated in Table 4.4 and plotted in Figure 4.14. At volume fraction, up to 0.1, upper and lower bainite transformations had virtually the same activation energy. Since nucleation was the dominating process at early stages of bainite transformation, previous investigators[44,163,171] have suggested that the same nucleation mechanism is operative for both upper and lower bainite transformation.

Table 4.4. Activation Energy for Upper and Lower Bainite Transformation.

Bainite Transformation Activation Energy, J		
Bainite Volume Fraction	Lower Bainite	Upper Bainite
0.1	55928	55815
0.2	45864	56276
0.3	44253	61847
0.4	40640	63088
0.5	34948	49086
0.6	33359	55026

As bainite volume fraction was increased, activation energy for the transformation processes decreased according to the correlations

$$\begin{aligned} Q_{LB} &= 57417 - 42613X \\ Q_{UB} &= 59284 - \ \ 6935X \end{aligned}$$

Barford[171] assumed that bainite transformation in hypereutecoid steels in the range $0.1 < X < 0.6$ took place solely by unimpeded growth at constant rate. Should this assumption apply to the current steel, then upper bainite transformation maintained a relatively constant activation energy during growth, whereas lower bainite transformation reduced its activation energy as transformation proceeded.

The observations of previous investigations and the present study show that upper bainite transforms by a sympathetic nucleation and growth process. The first plates usually nucleate at a prior austenite grain boundary. Other subunits nucleate on the side of existing bainite plates and all the subunits grow in a parallel fashion. Figure 4.15a presents an upper bainite sheaf transformed at 400°C. In the temperature range in which upper bainite transforms, nucleation sites are limited[146] due to the relatively low transformation driving force. Transformation induced strain in the vicinity of existing bainite plates promotes the nucleation of new subunits but the growth of these new subunits inside the higher carbon content layer surrounding the pre-existing plates is difficult. The constant activation energy for upper bainite transformation may suggest the balancing of the above two factors.

The lower bainite plates, on the other hand, nucleate inside austenite grains as well as on austenite grain boundaries. In the early stages, bainite plates form in clusters instead of nucleating randomly, signifying that nucleation of lower bainite is also a synergistic process, Figure 4.15b. However, the plates tend to grow in different directions which means either these directions are the easiest nucleation and

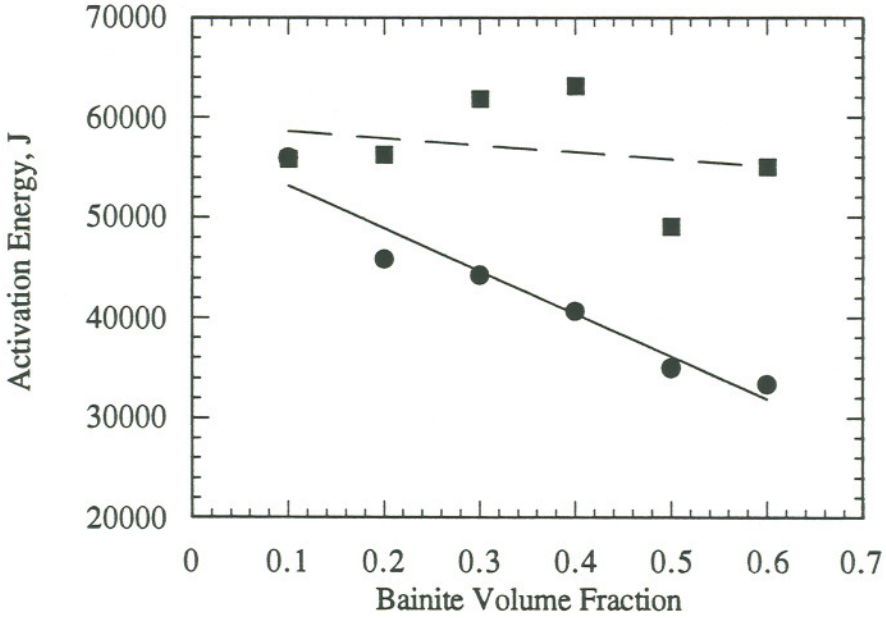

Figure 4.14. Bainite Transformation Activation Energy as Functions of Bainite Volume Fraction.

As bainite volume fraction was increased, activation energy for the transformation processes decreased according to the correlations

$$Q_{LB} = 57417 - 42613X$$
$$Q_{UB} = 59284 - 6935X$$

Barford[171] assumed that bainite transformation in hypereutecoid steels in the range $0.1 < X < 0.6$ took place solely by unimpeded growth at constant rate. Should this assumption apply to the current steel, then upper bainite transformation maintained a relatively constant activation energy during growth, whereas lower bainite transformation reduced its activation energy as transformation proceeded.

The observations of previous investigations and the present study show that upper bainite transforms by a sympathetic nucleation and growth process. The first plates usually nucleate at a prior austenite grain boundary. Other subunits nucleate on the side of existing bainite plates and all the subunits grow in a parallel fashion. Figure 4.15a presents an upper bainite sheaf transformed at 400°C. In the temperature range in which upper bainite transforms, nucleation sites are limited[146] due to the relatively low transformation driving force. Transformation induced strain in the vicinity of existing bainite plates promotes the nucleation of new subunits but the growth of these new subunits inside the higher carbon content layer surrounding the pre-existing plates is difficult. The constant activation energy for upper bainite transformation may suggest the balancing of the above two factors.

The lower bainite plates, on the other hand, nucleate inside austenite grains as well as on austenite grain boundaries. In the early stages, bainite plates form in clusters instead of nucleating randomly, signifying that nucleation of lower bainite is also a synergistic process, Figure 4.15b. However, the plates tend to grow in different directions which means either these directions are the easiest nucleation and growth directions or sympathetic nucleation of lower bainite at early transformation stages is not as important as it is in upper bainite transformation. As transformation proceeds, more smaller parallel bainite plates are seen to fill the space between existing larger plates, Figures 4.15c and d. If parallel growth requires less energy than multidirectional growth, the change from the latter to the former way of growth may qualitatively explain the decrease in transformation activation energy. However, the relatively large variation in transformation activation energy may not be accounted for quantitatively solely by the change in growth directions. Detailed analysis is not available; further investigation is necessary.

In summary, bainite transformation kinetics was studied using a modified Johnson-Mehl-Avrami equation which incorporated transformation incubation time. A correlation between the curve shape constant and transformation temperature was observed. Further analysis of this correlation revealed a relationship between austenite decomposition mode and transformation temperature. This development led to the discovery of the third application of the Johnson-Mehl-Avrami equation, i.e., a non-metallographic microstructure characterization technique. The transformation temperature ranges for pearlite, upper bainite, and lower bainite were determined using this technique and were verified metallographically. The significance of the evolution of the lower bainite transformation start temperature was that the transformation C curves of each product could be calculated separately and more accurately.

The activation energy measurement for upper and lower bainite yielded relatively low values compared to previous investigations. Contrary to the reported constant activation energy for bainite growth in other studies, the activation energy of bainite growth in the current steel was found to decrease with increasing bainite volume fraction. The different activation energy levels for the growth of upper and lower bainite and the different response of the energy terms to upper and lower bainite transformations were taken as evidence supporting the proposal that these two variants grow by different mechanisms.

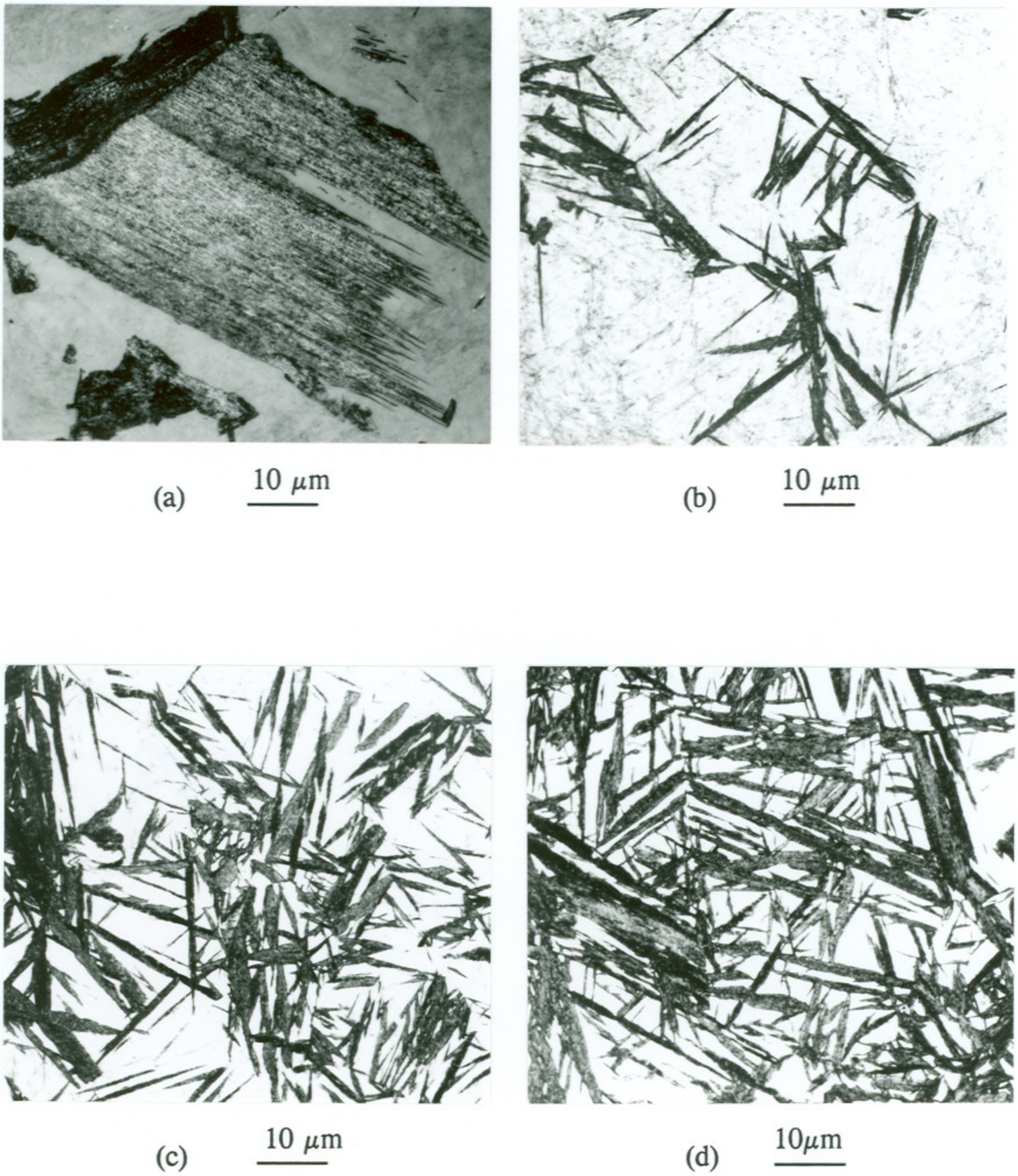

(a) (b)

(c) (d)

Figure 4.15. Early Stages of Bainite Transformation. (a) Upper Bainite Transformed at 400°C. Lower Bainite Transformed at 280 °C for (b) 5 minutes (c) 7 minutes and (d) 9 minutes.

CHAPTER 5

DISCUSSION

The thickness of the fracture toughness specimens did not satisfy the requirement

$$B \geq 2.5\left(\frac{K_{IC}}{\sigma_{ys}}\right)^2 \tag{5.1}$$

Hence, the measured fracture toughness did not qualify for valid K_{IC}. Nonetheless, the fracture surface was largely composed of square fracture[134] with tear lips occupying less that 10% of the fracture surface. According to Tetelman and McEvily,[174] when plastic zone size is less than about half of the specimen thickness, the deformation was predominantly plane strain. Based on Irwin's plastic zone size approximation[134] and the data listed in Tables 3.9, 3.10, and 3.11, this latter condition was satisfied; therefore, the stress state of the specimens during fracture toughness testing might be regarded as plane strain. It is noted that the required specimen thickness differs by four times according to equation (5.1) and Tetelman and McEvily's criterion. The stress state of specimens with thickness between the two calculated values could be in the transient region, close to plane strain. Further study of the stress state is difficult. Experimental determination of the stress state was also impossible since specimens of only one thickness were available. Hence, the exact stress state at the crack tip is not known.

5.1. Fracture Mechanics

During its course of evolution, fracture mechanics developed several branches, each dealt with a certain class of problems. For example, the crack growth resistance, or R-curve concept,[175] was introduced in 1954 for the determination of the onset of unstable fracture propagation using an energy approach. Irwin and Kies[175] concluded "that the strain energy release rate and the fracturing work rate must be equal at onset of instability, and they are unlikely to differ widely in magnitude as fracturing continues." This concept applied to the fracture of thin sheet panels where plane stress state prevailed and where "the fracture process of a cracked thin metal sheet is not usually comprised of a single sudden explosive-type change from initial crack length to total failure ... as the load increases considerable slow stable crack growth takes place prior to catastrophic failure."[176] However, "several laboratories carried out expensive programs in wide panel testing, attempting to arrive at the rather elusive constant K_c-value. An apparently constant value was oftentimes obtained with panels up to 48 in. wide, but experimental difficulties in defining the instability event eroded confidence;"[177] the R-curve approach was not accepted generally as a useful tool for materials evaluation although R-curve principles were fairly well established. The method could be extended to plane strain situations, in which the crack growth resistance was a constant as the crack propagated; very little stable crack growth took place before instability.

The plain strain stress intensity method became popular a little later. In 1959, in response to a request for assistance from the U.S. Secretary of Defense, ASTM formed a special technical committee to study the brittle fracture of high strength materials that were being used in various missile and rocket motor cases. Based on the available technical information, the committee adopted the concept of characterizing the fracture behavior of materials by using the crack-tip stress field parameters rather than by using the energy criterion. The result of the effort of the committee was the well developed stress intensity factor method as recorded in the book *Fracture Toughness Testing and Its Applications ASTM STP 381* and the five reports collected in *Fracture Mechanics Retrospective*. The fracture toughness testing method was largely based on linear elastic fracture mechanics and was applicable to thick, high strength materials in which plane strain state existed. It defined the instability of specimens of various shapes as the point at which the stress intensity factor ahead of sharp notches and cracks embedded in the body achieved a critical value K_{IC}. Fracture toughness was found to depend on specimen geometry and testing conditions[142,178] but if the thickness was adequate for a plane strain state ahead of the crack, toughness became a material property.

In engineering materials in which linear elastic fracture mechanics is approximately valid, e.g., when fracture is stress controlled, the energy approach and fracture toughness method have proved equivalent.[174] Fracture toughness is related to the elastic energy release rate by

$$K_C = \sqrt{EG_C}$$

This equation provides the basis for the development of the following model describing the fracture toughness of lower bainite in ultrahigh strength steels.

Applying the R-curve concept,[134] the crack growth resistance of a material can be obtained. Figure 5.1 shows the elastic energy release rate and crack resistance as functions of the initial crack length and crack extensions. In Figure 5.1, to the right of the origin is the crack extension Δa and to the left the initial crack size a_i. The dashed straight lines with positive slopes represent the elastic energy release rate G at different applied nominal stress, the parabola curve and the horizontal line show the crack resistance of a steel under plane stress and plane strain states, respectively. The increase in crack resistance with increasing crack extensions under plane stress is due

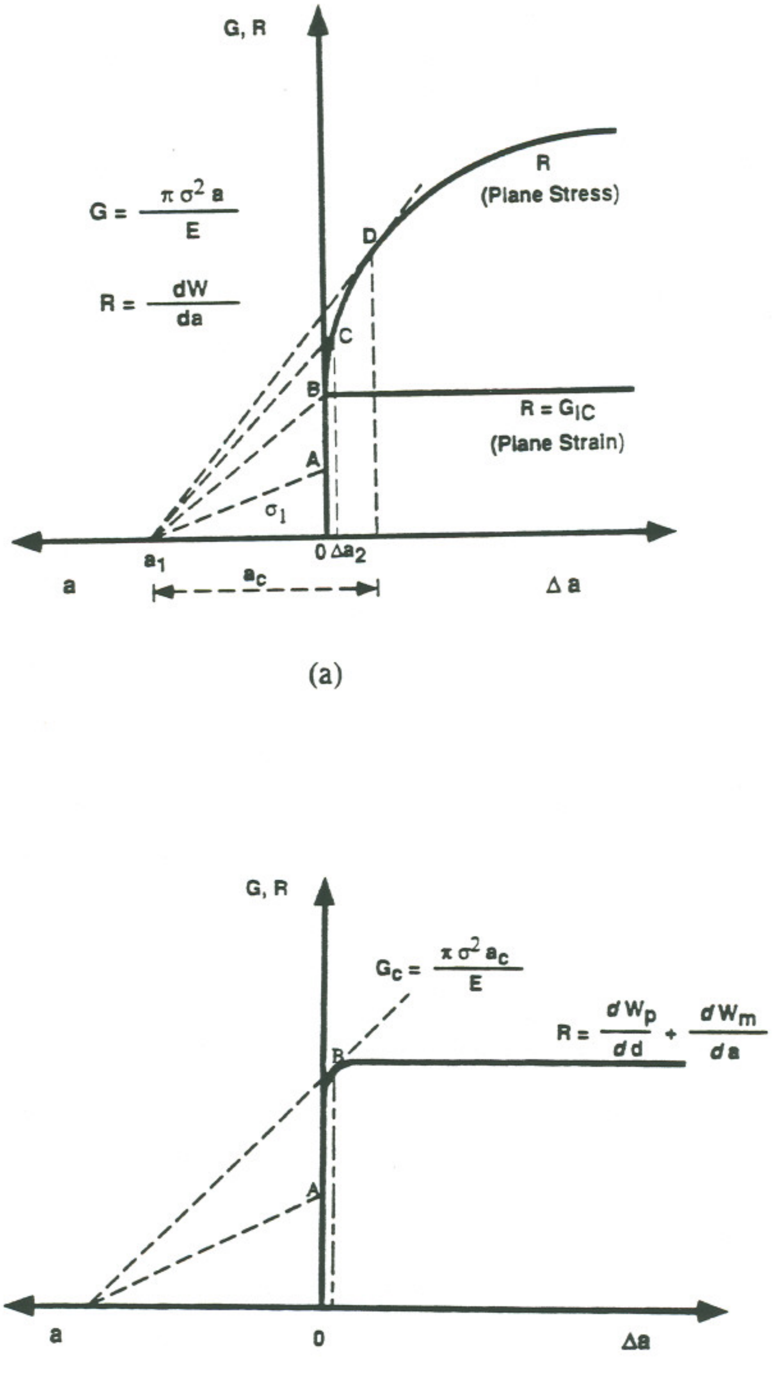

(a)

(b)

Figure 5.1. Crack Resistance Curve (R-Curve) (a) under plane stress and plane strain conditions and (b) in the present specimens.

to the development of crack tip plastic zone,[179] while the constant crack resistance in plane strain state comes from the energy absorption by microstructure upon fracture. Since instability occurs only when the released elastic energy equals the energy needed for the creation of new surfaces[178] and the local plastic deformation associated with the fracture of metals,[180,181] at the onset of fracture an additional infinitesimal crack extension has to raise G to R, or

$$\frac{\partial G}{\partial a} = \frac{\partial R}{\partial a}; \qquad G = R \tag{5.2}$$

The stress states in the present specimens are close to plane strain condition; the associated R-curve is shown in Figure 5.1b in which a very small transition zone exists. With a crack size a_0 and applied stress σ_1, the energy release rate G, represented by A, is less than R; crack cannot propagate. Increasing the applied stress to σ_c, raises G to R with a negligible crack extension, point B. The requirements expressed in equation (5.2) are satisfied, hence, fracture takes place. At the onset of fracture,

$$G_c = \frac{\pi \sigma_c^2 a}{E} \tag{5.3}$$

The critical nominal stress can be obtained as

$$\sigma_c = \sqrt{\frac{EG}{\pi a}}$$

A finite element analysis of the current specimen geometry has shown that the local stress at the crack tip is 16.7 times that of the nominal stress. Hence, the local fracture stress is

$$\sigma_f = 16.7\sqrt{\frac{EG}{\pi a}} \tag{5.4}$$

According to Ritchie *et al*[182], the local normal stress must exceed the fracture stress over a characteristic distance or process zone, r^*, for fracture to occur

$$\sigma_{yy} \geq \sigma_f; \qquad r \geq r* \tag{5.5}$$

where the normal stress ahead of the macroscopic crack follows

$$\sigma_{yy} = \frac{K}{\sqrt{2\pi r}} \tag{5.6}$$

Substituting equations (5.4) and (5.5) into (5.6), leads to

$$K_{IC} = 16.7\sqrt{\frac{2EGr^*}{a}} \tag{5.7}$$

The crack resistance R is a measure of the energy absorbed during fracture; it is evaluated as the energy dissipated at an infinitesimal increment of the crack

$$R = \frac{dW_p}{da} + \frac{dW_M}{da}$$

where W_p is the energy spent in developing a plastic zone and W_M is the energy absorbed by the microstructure. In plane strain states, the plastic zone and energy absorbed in it are negligible; the crack resistance mainly arises from microstructure contributions

$$R \approx \frac{dW_M}{da} \tag{5.8}$$

The energy dissipated due to the extension of a crack by *da* is

$$dW_M = \frac{da}{d}\gamma_d + \frac{da}{w}\gamma_l \qquad (5.9)$$

where d is prior austenite grain diameter, γ_d is the energy needed to rupture an austenite grain boundary, w is bainite lath width, and γ_l is the energy spent in cleaving a bainite lath and tearing a bainite lath boundary. The contribution from bainite packet boundary is included in that of bainite lath boundary and is not treated separately as discussed in Chapter 3. For steels in which the contribution from bainite packet boundary is significant, a separate term can be added. From equations (5.8) and (5.9), it follows

$$R = \frac{\gamma_d}{d} + \frac{\gamma_l}{w} \qquad (5.10)$$

Substituting (5.10) in the place of G in (5.7) results in

$$K_{IC} = 16.7\sqrt{\frac{2E\left(\frac{r^*}{d}\gamma_d + \frac{r^*}{w}\gamma_l\right)}{a}} \qquad (5.11)$$

This equation states that fracture toughness increases with increasing crack resistance and characteristic distance but decreases with coarsening of microstructure and increasing initial crack length. The effect of heat treatment on toughness arises from the change of microstructural features such as austenite grain size and bainite lath width as well as the resistance of grain boundary and lath boundary to crack propagation. These effects are discussed in the following sections.

5.2. Effect of Austenitizing Temperature

The most obvious effect of austenitizing temperature on microstructural parameters are to increase prior austenite grain size and the characteristic distance. Since these two changes are proportional, i.e., the characteristic distance is some multiple of grain size, and their effects on toughness are opposite and equivalent, the net effect of changing austenitizing temperature on toughness is small, if only these two dimensions are considered.

The significant contribution to toughness comes from the relative change of the characteristic distance to bainite lath width, i.e., the ratio r^*/w, according to equation (5.11). As has been observed[69,183] martensite and bainite lath widths change only slightly with increasing austenite grain size; the ratio and, therefore, toughness increase with increasing austenitizing temperature. A physical interpretation of this phenomenon is that as the austenite grain size increases, the characteristic distance increases. More bainite laths are encompassed in the process zone. Since the energy spent in cleaving bainite lath and tearing bainite lath boundaries constitutes a major fraction of the total fracture energy, more lath boundaries in the process zone necessarily require more fracture energy.

It should be clear that fracture toughness is determined by the number of bainite laths in the process zone and not in the cleavage plane across the whole fracture surface since stress controlled fracture is a phenomenon local to a small region near the crack tip. As soon as a crack nucleates and propagates over the characteristic distance, the whole structure fails without further supplements of external energy[183].

The evaluation of fracture toughness using equation (5.11) is not possible since experimental measurement of the energy required to rupture a prior austenite grain boundary and to cleave a bainite lath and tear its boundary is difficult. At present, equation (5.11) can be qualitatively used to explain the change of toughness with various microstructural changes. For example, the relative increase in fracture toughness due to prior austenite grain growth can be calculated as

$$\delta = \frac{K'_{IC} - K_{IC}}{K_{IC}} = \frac{\sqrt{\frac{r^{*'}}{d'}\gamma_d + \frac{r^{*'}}{w'}\gamma_l} - \sqrt{\frac{r^*}{d}\gamma_d + \frac{r^*}{w}\gamma_l}}{\sqrt{\frac{r^*}{d}\gamma_d + \frac{r^*}{w}\gamma_l}} \qquad (5.12)$$

where K'_{IC} is the fracture toughness associated with the larger grain size d', characteristic distance $r^{*'}$, and bainite lath width w' and K_{IC} is the fracture toughness of the reference structure with grain size d, characteristic distance r^*, and lath width w. Setting $r^{*'} = 2d'$ and $r^* = 2d$, according to RKR model[182], and assuming γ_d is 50 times γ_l, equation (5.12) reduces to

$$\delta = \frac{\sqrt{100 + \frac{2d'}{w'}} - \sqrt{100 + \frac{2d}{w}}}{\sqrt{100 + \frac{2d}{w}}} \qquad (5.13)$$

Plugging in the austenite grain sizes of 25 and 20 μm for 950 and 900°C austenitization, respectively, and bainite lath width of 0.88 and 0.99 μm for 280°C austempering after austenitization at the temperatures, δ equals 0.06, which compares favorably with the observed 4.6% toughness improvement. The agreement, however, may be regarded as fortuitous, since the value of δ depends heavily on the choice of the ratio of γ_d/γ_l. For a match between the calculated δ value and the observed toughness improvement associated with increasing austenitizing temperature from 900 to 1000°C, the value of γ_d/γ_l has to be between 15 to 20.

Higher austenitizing temperature promotes homogenous alloying element distribution, reduces impurity segregation along prior austenite grain boundaries, and increases misorientation among prior austenite grains. These changes increase γ_d, the energy required to rupture prior austenite grain boundaries. On the other hand, the variation of austenitizing temperature is expected to bring only minor changes to bainite submicrostructure; γ_l should not change much, i.e., the ratio γ_d/γ_l should increase with increasing austenitizing temperature. Therefore, the necessity of reducing the ratio γ_d/γ_l as the austenitizing temperature is increased may largely arise from the experimental errors associated with grain size and lath width measurements; it may also come from other sources such as the assumption that $r^* = 2d$ for all austenitizing conditions.

The characteristic distance equals the inter-spacing of the microstructural feature that controls the fracture process. This microstructural feature could be martensite or bainite packet boundary or carbide but is usually prior austenite grain boundary. When austenite grains grow over a certain size, austenite grain boundary may render the fracture controlling effect to carbide or bainite packet boundary; the inter-spacing of the new fracture controlling substructure becomes the characteristic distance. The relation $r^* = 2d$ may not hold anymore. If the effect of these fundamental changes could be formulated, more realistic values of the ratio of γ_d/γ_l can be assumed and more close predictions of fracture toughness variations can be obtained. The fact that fracture toughness does not continuously increase with austenitizing temperature beyond the grain growth temperature could be interpreted as a support of the above argument. If the fracture process controlling power is assumed to shift from prior austenite grain boundary to another microstructural feature, the inter-spacing of which is less sensitive to the increase in austenitizing temperature than austenite grain size, further increasing in austenitizing temperature will reduce toughness due to the decrease in fracture stress.

5.3. Effect of Bainite Transformation Temperature

At a constant austenitizing temperature, an increase in bainite lath width with increasing bainite transformation temperature was observed; the improved toughness could not be explained through the number of bainite laths inside the process zone but was proposed to result from an increase in the energy required to cleave a bainite lath and to tear a lath boundary.

The bainitic ferrite was assumed to transform with a carbon supersaturation which was relieved by carbide precipitation and carbon diffusion into the surrounding austenite. Experimental measurement of carbon content in freshly transformed ferrite was difficult; carbon supersaturation in bainite remained as a point of argument.[5] In the current steel, however, carbon supersaturation in bainitic ferrite was evident since carbide volume fraction increased with increasing transformation temperature, i.e., given an opportunity, more carbon could be relieved from bainitic ferrite in the form of carbide. Since carbon supersaturation in bcc structure caused a higher tendency of cleavage and a lower fracture energy, a reduction in carbon supersaturation would lead to increases in bainite lath cleavage energy and fracture toughness.

The difference in transformation behaviors between the current steel and other steels is noted. These differences can be used to explain the different mechanical behaviors in the steels. Commonly, it is expected that with decreasing transformation temperature the carbides become finer, more numerous and more evenly dispersed.[62] These changes would increase strength and reduce the tendency of crack forming at carbide/ferrite interface and therefore, increase fracture toughness without losing strength. In the present steel, on the other hand, carbide length and volume fraction increased with bainite transformation temperature, while carbide width remained constant. Since carbide width, rather than its length, determines the microcrack nucleation tendency, carbide length change does not affect fracture process; carbon content in bainitic ferrite controls toughness. This explains the relationship between toughness and bainite transformation temperature. Considering the magnitude of the effect of austenitizing temperature and bainite transformation temperature on fracture toughness, bainitic carbide width and volume fraction seem to be the primary toughness controlling microstructural features. This is why bainite transformation temperate shows a stronger effect on toughness that austenitizing temperature.

Similar to the treatment used in the previous section, the relative toughness improvement can be calculated as

$$\delta' = \frac{K''_{IC} - K_{IC}}{K_{IC}} = \frac{\sqrt{\frac{r*}{d}\gamma_d + \frac{r*}{w'}\gamma_l'} - \sqrt{\frac{r*}{d}\gamma_d + \frac{r*}{w}\gamma_l}}{\sqrt{\frac{r*}{d}\gamma_d + \frac{r*}{w}\gamma_l}} \tag{5.14}$$

If $r* = 2d$, $\gamma_d = 20\gamma_l$, equation (5.14) reduces to

$$\delta' = \frac{\sqrt{40\gamma_l + \frac{2d}{w'}\gamma_l'} - \sqrt{40\gamma_l + \frac{2d}{w}\gamma_l}}{\sqrt{40\gamma_l + \frac{2d}{w}\gamma_l}} \tag{5.15}$$

Setting $\gamma_l' = \alpha\gamma_l$,

$$\delta' = \frac{\sqrt{40 + \frac{2\alpha d}{w'}} - \sqrt{40 + \frac{2d}{w}}}{\sqrt{40 + \frac{2d}{w}}} \tag{5.16}$$

If $\alpha = 1.5$, i.e., bainite lath cleavage energy and lath boundary tearing energy increase by 50%, fracture toughness increases by 17%. Raising bainite transformation temperature from 250 to 280°C improves toughness by about 30%;

this requires an increase in γ_1 by about 100%. Although macroscopic and microscopic fracture surface roughness does increase with increasing bainite transformation temperature, it is doubtful whether fracture energy would change by as much as 100% due to the reduction of carbon supersaturation in bainitic ferrite. The discrepancy comes, again, from experimental errors and the choice of γ_d/γ_1 ratio. Further theoretical elaboration of the above model and experimental exploration of the microstructural changes and the associated energy term changes are needed.

The negative effect of prior austenite grain coarsening on fracture toughness was attributed to the corresponding reduction of fracture stress σ_c.[79] The effect of increasing bainite lath width was to decrease the number of laths in the process zone. Both these effects could be considered through the effect of austenitizing and bainite transformation temperatures on fracture toughness and yield strength.

According to Hahn and Rosenfield[184] fracture stress depends on fracture toughness and yield strength

$$\sigma_f = f\,(\sigma_{ys}, K_{IC})$$

The derivative of fracture stress is

$$d\sigma_f = \frac{\partial \sigma_f}{\partial \sigma_{ys}} d\sigma_{ys} + \frac{\partial \sigma_f}{\partial K_{IC}} dK_{IC} \tag{5.17}$$

Since yield strength and fracture toughness are functions of austenitizing temperature (AT) and bainite transformation temperature (BT), it follows:

$$\begin{aligned} d\sigma_{ys} &= \frac{\partial \sigma_{ys}}{\partial AT} dAT + \frac{\partial \sigma_{ys}}{\partial BT} dBT \\ dK_{IC} &= \frac{\partial K_{IC}}{\partial AT} dAT + \frac{\partial K_{IC}}{\partial BT} dBT \end{aligned} \tag{5.18}$$

Substituting equation (5.18) into (5.17) and regrouping for *AT* and *BT* lead to

$$d\sigma_f = \left(\frac{\partial \sigma_f}{\partial \sigma_{ys}} \frac{\partial \sigma_{ys}}{\partial AT} + \frac{\partial \sigma_f}{\partial K_{IC}} \frac{\partial K_{IC}}{\partial AT} \right) dAT + \left(\frac{\partial \sigma_f}{\partial \sigma_{ys}} \frac{\partial \sigma_{ys}}{\partial BT} + \frac{\partial \sigma_f}{\partial K_{IC}} \frac{\partial K_{IC}}{\partial BT} \right) dBT \qquad (5.19)$$

Applying the plastic constraint factor concept[185] and noting Hahn and Rosenfield's empirical correlation between the plastic constraint factor, and toughness and yield strength,[184] fracture stress can be written as

$$\sigma_f = \sigma_{ys} + 2K_{IC}$$

where the coefficient 2 has a unit of inch.$^{-1/2}$ Plugging this relation into equation (5.19) gives

$$d\sigma_f = \left(\frac{\partial \sigma_{ys}}{\partial AT} + 2\frac{\partial K_{IC}}{\partial AT} \right) dAT + \left(\frac{\partial \sigma_{ys}}{\partial BT} + 2\frac{\partial K_{IC}}{\partial BT} \right) dBT \qquad (5.20)$$

Substituting the experimental results of the present investigation into equation (5.20) leads to

$$d\sigma_f = -0.83\, dAT - 1.84\, dBT \qquad (5.21)$$

Hence, increasing austenitizing temperature and bainite transformation temperature suppresses fracture stress as has been reported by previous investigators.[69,79]

Based on the effect of austenitizing temperature and bainite transformation temperature on the microstructural parameters and the energy terms, equation (5.11) and (5.21) could be used to explain some discrepancies of fracture behavior of different steels. Reducing bainite transformation temperature has been reported to increase fracture toughness in low carbon steels[87] due to structure refinement. In the current high carbon low alloy steel, on the other hand, the energy for bainite lath cleavage and lath boundary tearing is the controlling parameter; bainite transformation temperature affects toughness mainly through its effect on the energy term γ_l. At higher bainite transformation temperatures, carbide volume fraction increases. The increase in bainite fracture energy due to the reduced carbon supersaturation in bainitic ferrite outweighs the decrease in fracture stress.

Raising the austenitizing temperature increases the characteristic distance and decreases fracture stress; the first effect enhances toughness, while the second reduces it. The latter effect, however, is usually negligible. Under this condition, fracture toughness increases with austenitizing temperature. However, if austenite grains over-grow and pass the fracture controlling effect to another substructure, the only effect of increasing austenitizing temperature is to reduce the fracture stress and, hence, to decrease fracture toughness.

5.4. Effect of Tempering on Fracture Toughness

In light of the above development, the effect of tempering on fracture toughness can be understood in terms of further reduction of carbon supersaturation in ferrite by carbide growth and tempering of the as-transformed martensite. The assumption that tempering at temperatures below the bainite transformation temperature would increase carbide volume fraction and reduce carbon supersaturation in ferrite is doubtful. However, judging from the fact that, in the temperature range between 250 and 300°C, detectable bainite transformation proceeds for less than one hour and increased transformation temperatures lead to an increase in carbide volume fraction, it is conceivable that tempering at 200°C for two hours would allow some carbon atoms to diffuse out of ferrite. Hence, part of the effect of tempering on toughness could be attributed to the reduction of carbon content in ferrite.

The main effect of tempering comes from the tempering of martensite. Bainite transformation is usually incomplete. The residual austenite transforms to high carbon martensite during subsequent cooling. As transformation temperature is increased, volume fraction of residual austenite and, therefore, that of martensite increases. Since untempered martensite reduces fracture toughness, tempering of the as-transformed structure formed at high temperature should exhibit a more pronounced effect. However, because lower bainitic ferrite transformed at high temperature contains less carbon, the effect of tempering on bainite becomes less appreciable. The balance of the effects of tempering on martensite and bainite results in about the same relative toughness improvement for the structures formed at different temperatures, Table 3.6.

The statement that the main effect of tempering comes from the tempering of martensite implies that the common characteristics of tempering of martensite would prevail during the tempering of bainite/martensite duplex structures. One of the concerns is martensite temper embrittlement. Low temperature temper embrittlement occurs in the range of 250 to 350°C, while high temperature temper embrittlement develops between 400 to 550°C. To avoid these types of embrittlement, duplex structures should be tempered at temperatures most suitable for the tempering of martensite in the same steel.

The effect of austenitizing temperature on the effectiveness of tempering on the present steel is surprising. In alloy steels in which residual alloy carbides exist, toughness is controlled by the residual carbides. Tempering does not improve toughness. Using high austenitizing temperatures would dissolve the carbides. When toughness is controlled by other substructural features than residual carbides, tempering treatment may lead to toughness improvements. In the current low alloy steel, residual carbides were not expected but the fact that tempering of bainite was effective if austenitizing temperature was above 900°C and the decrease in M_s temperature with increasing austenitizing temperature indicated the existence of residual carbides when austenitizing temperatures was below 900°C.

5.5. Fracture Toughness of Duplex Structures

In many steels, duplex martensite/bainite rather than each of the structures alone were reported to have higher hardness and toughness due to ferrite grain sub-division.[81] Accordingly, bainite transformation time was selected as a heat treatment parameter in this investigation to vary bainite volume fraction and to partition austenite grains to different degrees. At temperatures above M_s, bainite transformed first and divided austenite grains to limit martensite grain size. At temperatures lower than M_s, martensite plates formed initially and reduced bainite grain size. If ferrite grain refinement was the toughness controlling factor, both martensite and bainite grain size reduction would improve toughness. However, no toughness improvement due to grain refinement by sub-dividing austenite grains and by decreasing bainite transformation temperature was observed, hence, ferrite grain size was not an effective toughness controlling factor. In fact, the increase in toughness with increasing bainite transformation temperature suggested that other substructural changes, such as increase in carbide volume fraction, available at higher temperatures would be more beneficial.

In the light of the microstructure characterization reported in Chapters 3 and 4 and the toughening mechanisms of bainite discussed in the previous sections, the fracture toughness ranking of the nine heat treating conditions used in the factorial analysis could be understood. Figure 5.2 reproduces part of the TTT diagram with the nine heat treating conditions superimposed. For convenience, the following discussion compares toughness of structures formed at constant temperatures, since this is the variable that affected toughness most.

Lower bainite formed at higher temperatures possessed higher toughness. If martensite plates were present as second phase particles in lower bainite matrix, toughness would decrease since martensite seemed to increase intergranular fracture tendency. The heat treatments *F, C,* and *I* transformed bainite at 280°C. Condition *F* had the lowest toughness due to the presence of martensite. Both *C* and *I* produced much higher toughness, that by *C* was 23% higher than that by *I* since the former condition included austenitization at a higher temperature, Table 3.3, and invoked an additional toughening through tempering.

Heat treatments *H*, *E*, and *B* resulted in martensite/bainite duplex structures, in which the lower bainite was also formed above M_s. Both *H* and *E* had martensite matrix and bainite second phase structures. Toughness of *H* was slightly higher than that of *E* due to the higher austenitizing temperature applied. Condition *B*, on the other hand, produced bainite matrix and 12% martensite. Consequently, the toughness increased by 28% and 14%, respectively from that of *E* and *H*. Prolonged transformation might remove most of the martensite and improve toughness. However, comparing with the toughness obtained in similar conditions through the systematic analysis and assuming a 17% tempering effect, toughness of condition *B* was very close to the maximum toughness attainable using 950°C austenitizing and 250°C austempering condition.

Tempered martensite structure in the steel was relatively brittle and had a tendency to fail intergranularly. The duplex structure of martensite and bainite, with the bainite formed below M_s temperature, was even more brittle. The presence of the bainite particles seemed to increase the intergranular fracture tendency. Condition *A*

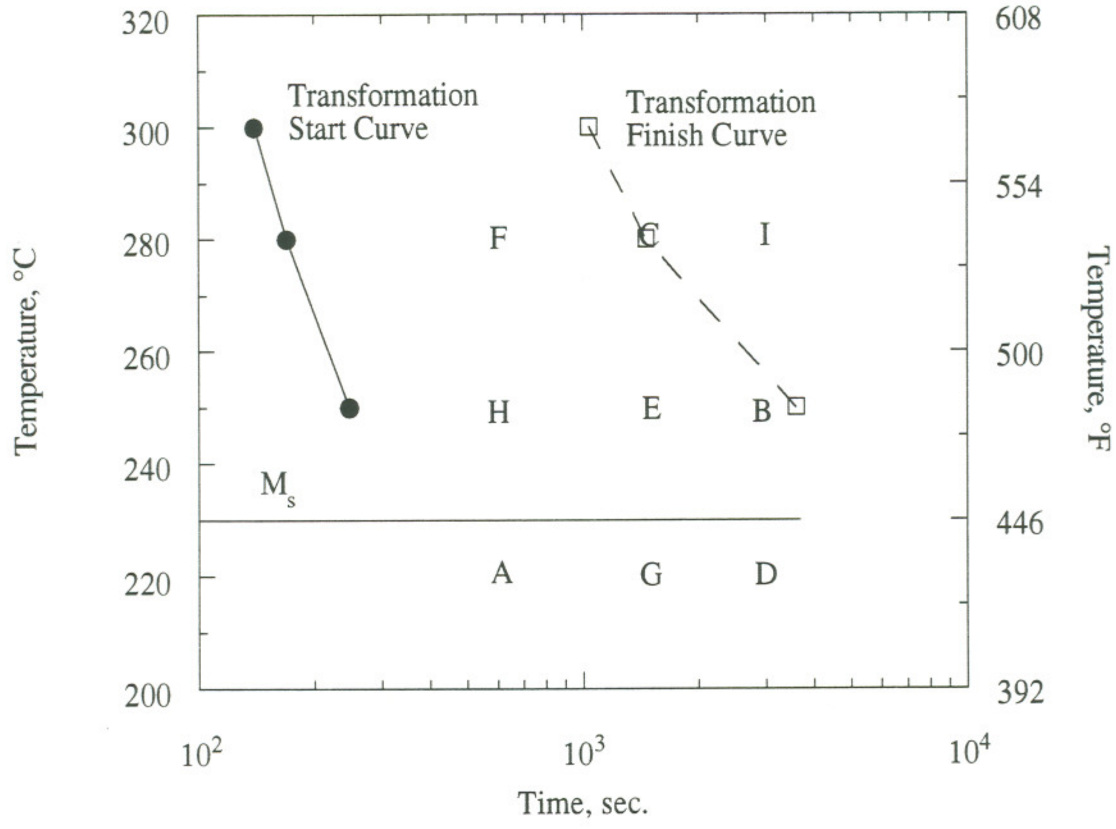

Figure 5.2. The Factorial Heat Treating Conditions with Respect to TTT Diagram.

produced less bainite than conditions *G* and *D*; its toughness approached that of tempered martensite in the steel. Conditions *G* and *D*, on the other hand, differed in bainite volume fraction and intergranular fracture tendency but had similar toughness.

5.6. Heat Treatment Recommendations

Both experimental results and theoretical analysis indicated that fracture toughness increased with increasing austenitizing temperature and bainite transformation temperature. Experimental evidences also showed that an additional toughness improvement was attainable if the austenitizing temperature was higher than 900°C. However, the long term operation temperature of most industrial furnaces is 900°C, which might be raised to about 950°C when protective atmospheres are involved. This limits the use of austenitizing temperatures higher than 950°C in industrial practice. To meet high strength requirements, on the other hand, bainite transformation temperature could not be increased beyond 300°C. These limiting temperatures form a simple austempering treatment, i.e., austenitizing at 950°C followed by austempering at 300°C.

Bainite transformation finish time was shortened with increasing austempering temperature below the C curve nose temperature. This meant that the heat treatment time could be reduced with higher transformation temperatures. Hence, this simple austempering treatment design featured a great production cost reduction while offering a competitive strength and toughness combination. Based on the empirical equations (3.4) and (3.6) the fracture toughness and hardness were about 50 $\mathrm{ksi}\sqrt{\mathrm{in}}$ and HRC 53, respectively for the as-austempered condition.

A more comprehensive tool for heat treatment design to target toughness and hardness requirements for a certain application is the toughness map which is produced by superimposing the toughness and hardness obtained at each austempering temperature onto a corresponding TTT diagram, Figure 5.3. The toughness map shown in Figure 5.3 not only tells fracture toughness and hardness attainable at each austempering temperature but also indicates the resulting microstructure.

When higher fracture toughness is more desirable, a 200°C tempering treatment can be added. This would produce a fracture toughness, according to equation (3.2), of 58 $\mathrm{ksi}\sqrt{\mathrm{in}}$ and a hardness of HRC 53 to 54 since low temperature tempering either maintains the hardness or slightly increases it. Simply assuming that tempering would improve toughness by 17% from the as-austempered value also leads to a toughness of 58 $\mathrm{ksi}\sqrt{\mathrm{in}}$.

It should be pointed out that adding a tempering treatment does not necessarily increase production time significantly. As has been discussed earlier, the effect of tempering arises mainly from the tempering of martensite that forms inevitably due to the incomplete transformation nature of bainite. Further reduction of carbon supersaturation only produces a secondary effect. A short tempering, e.g., one hour or half an hour tempering, may result in the similar effect as a two hour treatment. If this is true, then a short austempering of just long enough duration for detectable bainite transformation to finish and a short tempering treatment can be an attractive alternative for low production cost and superior mechanical property combination.

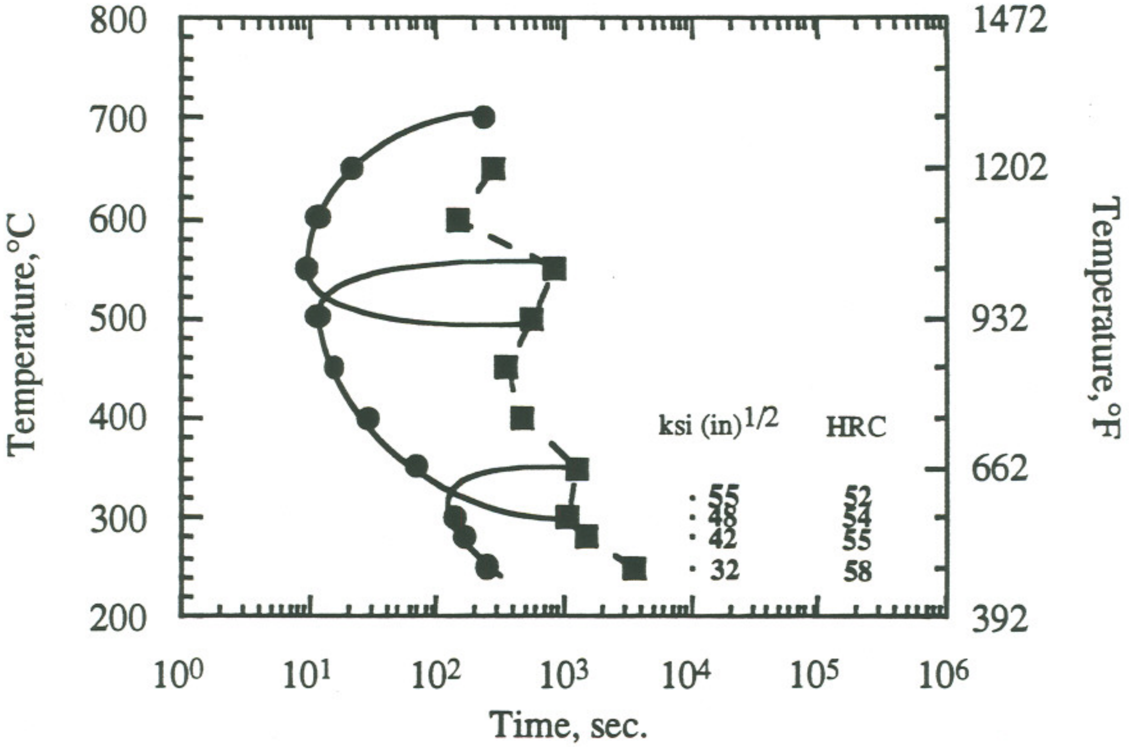

Figure 5.3. Fracture Toughness Map of the Studied Steel.

CHAPTER 6

SUMMARY AND CONCLUSION

Ultra high strength low alloy steels were developed to substitute for more expensive high alloy steels and to save strategic alloying elements. Although more economic, the low alloy steels do not possess adequate fracture toughness at high strength levels. Therefore, their replacement is limited. Numerous investigations have been conducted to improve fracture toughness of high strength low alloy steels. To date, large amounts of experimental data have been accumulated, many theories have been formulated, and considerable toughness improvement has been achieved in different alloys. However, the problem is far from completely solved.

The literature survey reveals the complexity of the problem. The mechanical properties of a material are affected by many variables. The most easily controlled are the parameters used in the steel making processes and the subsequent thermal-mechanical treatments. As far as machinery industry is concerned, the most important property controlling variables are the heat treatment route and parameters.

For high strength applications, the most widely used heat treatments are quenching and tempering, and austempering. The first treatment produces martensite while the latter bainite. In many steels bainite or bainite/martensite duplex structures have been found to be tougher than martensite. However, a systematic investigation of bainite toughening mechanism is lacking.

This work studied the fracture toughness of bainite as functions of heat treatment parameter and microstructural features using a factorial analysis and a systematic analysis. The significant conclusions are

1. Fracture toughness of the lower bainite increased with bainite transformation temperature into the upper/lower bainite transition temperature region.
2. Fracture toughness increased with austenitizing temperature until the grain growth temperature was reached.
3. Tempering increased fracture toughness by about 20% if the austenitizing temperature used in the austempering treatment was above 900°C but imposed no effect if the austenitizing temperature was below or at 900°C.
4. The fracture toughness and hardness of as-austempered structure were calculated by

$$K_{IC} = 0.05AT + 0.33BT - 97$$

and

$$HRC = -0.013AT - 0.09BT + 92.75$$

5. The fracture toughness and hardness of austempered and low temperature tempered structure, on the other hand, could be estimated as functions of the heat treatment parameters using

$$\begin{aligned} K_{IC} &= 0.27BT - 30.67 \\ K_{IC} &= 0.10AT - 53.67 \\ K_{IC} &= 0.05Bt + 35.06 \end{aligned}$$

and

$$\begin{aligned} HRC &= 0.003AT + 54 \\ HRC &= -0.067BT + 74 \\ HRC &= -0.071Bt + 59 \end{aligned}$$

6. Two heat treatments were recommended. One aimed at reducing production costs through shortening heat treatment time. The other emphasized further improvement in toughness through tempering.

7. Fracture toughness of bainite depended on prior austenite grain size, characteristic distance, bainite lath width, the energy required to rupture an austenite grain boundary, and the energy needed to cleave a bainite lath and to tear its boundary. Toughness was expressed as a function of these microstructural parameters by

$$K_{IC} = 16.7\sqrt{\frac{2E(\frac{r*}{d}\gamma_d + \frac{r*}{w}\gamma_l)}{a}}$$

8. Constant fine carbide width and increasing carbide volume fraction with increasing bainite transformation temperature were identified as the main toughening mechanisms in the present steel. The contributions of these variables evolved through the term γ_l.

9. A relationship between the curve shape constant and transformation temperature existed. This relationship led to the observation of a correlation between transformation mode and the transformation temperature, which could be used to identify microstructure using isothermal transformation kinetics rather than the tedious, metallographic methods. The technique also accurately and efficiently determined the isothermal transformation temperature ranges for pearlite, upper, and lower bainite.

10. The evolution of the upper limit of lower bainite transformation temperature led to the proposal of the existence of a lower bainite transformation start temperature. Correspondingly, this investigation suggested that the bainite

transformation start temperature be replaced by 'upper bainite transformation start temperature' for clarity.

This study revealed a relationship between bainite microstructure and fracture toughness. For a further understanding of toughness development and a quantitative toughness evaluation, the energy spent in rupturing a prior austenite grain boundary, cleaving a bainite lath, and tearing the lath boundary need to be assessed experimentally or analytically. Future study should also concentrate on finding the mechanism for the width of cementite carbide to remain fine and constant when bainite transformation temperature is increased. If this mechanism can be implemented to other steels, alloy addition for carbide suppression will not be necessary for high fracture toughness. The reduction of carbon supersaturation in bcc solid solution due to fine carbide precipitation may result in higher toughness than supersaturated, carbide free bainite.

An interesting observation that needs to be confirmed is the inconsistency of the orientation relationship between carbides and bainitic ferrite in the studied steel. A unique orientation relationship was determined for each indexed diffraction pattern. In no case did the same orientation relationship prevail in two bainite plates; Bagaryatski relationship was never satisfied. This observation suggested that orientation relationship was random, it also implied that bainite transformation mechanism was different from that of martensite transformation.

Different unit systems were used in this work. These units can be converted into the international system of units as

$$1 \text{ ksi} = 6.895 \text{ MPa}$$

$$1 \text{ ksi}\sqrt{\text{in}} = 1.098 \text{ MPa}\sqrt{\text{m}}$$

$$1 \text{ cal} = 4.18 \text{ J}$$

REFERENCE

1. Aaronson, H.I., in: *THE MECHANISM OF PHASE TRANSFORMATION IN CRYSTALLINE SOLIDS*, Institute of Metals, London, **1969**, pp. 270.

2. Hillert, M., The Formation of Pearlite, in: *DECOMPOSITION OF AUSTENITE BY DIFFUSIONAL PROCESSES*, Zackay, V.F. and Aaronson, H.I. eds. Interscience, New York, **1962**, pp. 197-237.

3. Bhadeshia, J.K.D.H., *BAINITE IN STEELS*, The Institute of Materials, Cambridge, England, 1992,

4. Davenport, E.S. and Bain, E.C., Transformation of Austenite at Constant Subcritical Temperatures, Trans. AIME, 1930, **90**, pp. 117-154.

5. Hehemann, R.F., Kinsman, K.R., and Aaronson, H.I., A Debate on the Bainite Reaction, Metall. Trans., 1972, **3**, pp. 1077-1094.

6. Ko, T. and Cottrell, S.A., The Formation of Bainite, J. Iron Steel Inst., 1952, **172**, pp. 307-313.

7. Bhadeshia, H.K.D.H. and Waugh, A.R., Bainite: an Atom-probe Study of the Incomplete Reaction Phenomenon, Acta Metall., 1982, **30**, pp. 775-784.

8. Mehl, R.F., in: *HARDENABILITY OF ALLOY STEELS*, ASM, Cleveland, OH, **1939**, pp. 1-54.

9. Aaronson, H.I. and Wells, C., Trans. AIME, 1956, **206**, pp. 1216-1223.

10. Bhadeshia, H.K.D.H., Bainite in Steels, Metall. Trans., 1990, **21A**, pp. 767-797.

11. Davenport, A.T., *THE CRYSTALLOGRAPHY OF UPPER BAINITE*, Republic Steel Research Report on Project 12051, 1974, pp. 1-35.

12. Kurdjumov, G.V. and Sach, G., Z. Phys., 1930, **64**, pp. 325.

13. Nishiyama, Z., Sci. Rep. Tohoku Univ., 1934, **23**, pp. 325.

14. Pitsch, W., Acta Metall., 1962, **10**, pp. 897.

15. Shackleton, D.N. and Kelly, P.M., in: *THE PHYSICAL PROPERTIES OF MARTENSITE AND BAINITE*, The Iron and Steel Institute, London, **1965**, pp. 126-134.

16. Shackleton, D.N. and Kelly, P.M., Acta Metall., 1967, **15**, pp. 979-992.

17. Bagaryatski, Y.A., Dokl. Akad. Nauk. SSSR, 1950, **73**, pp. 1161.

18. Houillier, R.L, Begin, G., and Dube, Metall. Trans., 1971, **9A**, pp. 2645-2653.

19. Schissler, J.M., Arnould, J., and Metauer, G., Mem. Sci. Rev. Metallurgie, 1975, **6**, pp. 779-793.

20. Sandvik, B.P.J., The Bainite Reaction in Fe-Si-C Alloys II: The Secondary Stage, Metall. Trans., 1982, **13A**, pp. 789-800.

21. Bhadeshia, H.K.D.H., Acta Metall., 1980, **28**, pp. 1103-1114.

22. Greninger, A.B. and Troiano, A.R., Trans. AIME, 1940, **140**, pp. 311.

23. Vilella, J.R., Trans. AIME, 1940, **140**, pp. 332.

24. Austin, A.E. and Schwartz, C.M., Proc. of ASTM, 1952, **52**, pp. 592-596.

25. Matas, S.J. and Hehemann, R.F., Trans. AIME, 1961, **221**, pp. 179-185.

26. Deliry, J., Mem. Sci. Rev. Metallurgie, 1965, **62**, pp. 527-550.

27. Pomey, J., Mem. Sci. Rev. Metallurgie, 1966, **63**, pp. 507-532.

28. Oblak, J.M. and Hehemann, R.F., in: *TRANSFORMATION AND HARDENABILITY IN STEELS*, Climax Molybdenum Company, Ann Arbor, MI, **1967**, pp. 15-30.

29. Hehemann, R.F., in: *PHASE TRANSFORMATIONS*, ASM, Metals Park, OH, **1970**, pp. 397-432.

30. Lai, G.Y., Metall. Trans., 1975, **6A**, pp. 1469.

31. Huang, D.H. and Thomas, G., Metall. Trans., 1977, **8A**, pp. 1661.

32. Sandivik, B.P.J. and Edmonds, D.V., Metall. Trans., 1979, **10A**, pp. 895-907.

33. Bhadeshia, H.K.D.H. and Edmonds, D.V., The Bainite Transformation in a Silicon Steel, Metall. Trans., 1979, **10A**, pp. 895-907.

34. Kang, M.K., Sun, J.L., and Yang, Q.M., High-Temperatures Transmission Electron Microscopy in situ Study of Lower Bainite Carbide Precipitation, Metall. Trans., 1990, **21A**, pp. 853-858.

35. Bhadeshia, H.K.D.H., The Lower Bainite Transformation and the Significance of Carbide Precipitation, Acta Metall., 1980, **28**, pp. 1103-1114.

36. Jack, K.J., Structural Transformation in the Tempering of High Carbon Martensitic Steels, J. Iron Steel Inst., 1951, **169**, pp. 26-36.

37. Kalish, D. and Cohen, M., Mater. Sci & Eng., 1970, **6**, pp. 156-166.

38. Irvine, K.J. and Pickering, F.B., J. Iron Steel Inst., 1958, **188**, pp. 101.

39. Speich, G.R., Growth Kinetics of Bainite in a Three Per Cent Chromium Steel, in: *DECOMPOSITION OF AUSTENITE BY DIFFUSIONAL PROCESSES*, Zackay, and Aaronson, eds. Interscience, New York, **1962**, pp. 353-396.

40. Ohmori, Y., The Precipitation of Iron Carbides in Lower Bainite and Tempered Martensite in Fe-C alloy, in: *PROCEEDINGS OF THE INTERNATIONAL CONFERENCE ON MARTENSITIC TRANSFORMATION*, The Japan Institute of Metals, **1986**, pp. 587-594.

41. Purdy, G.R. and Hillert, M., On the Nature of the Bainite Transformation in Steels, Acta Metall., 1984, **32**, pp. 823-828.

42. Kinsman, K.R. and Aaronson, H.I., in: *TRANSFORMATIONS AND HARDENABILITY IN STEELS*, Climax Molybdenum Company, Ann Arbor, MI, **1967**, pp. 39.

43. Leontyev, B.A. and Kovalevskaya, G.V., Phys. Met. Metallogr., 1974, **38**, pp. 139.

44. Kennon, N.F., Schematic Transformation Diagrams for Steels, Metall. Trans., 1978, **9A**, pp. 57-66.

45. Lieberman, D.S., Crystal Geometry and Mechanisms of Phase Transformations in Crystalline Solids, in: *PHASE TRANSFORMATIONS*, ASM, Metals Park, Ohio, **1970**, pp. 1-58.

46. Christian, J.W. and Edmonds, D.V., The Bainite Transformation, in: PROCEEDINGS OF AN INTERNATIONAL CONFERENCE ON PHASE TRANSFORMATIONS IN FERROUS ALLOYS, Marder, A.R. and Goldstein, J.I. eds. AIME, New York, **1984**, pp. 293-325.

47. Bhadeshia, H.K.D.H., Diffusional and Displacive Transformations, Scripta Metall., 1987, **21**, pp. 1017-1022.

48. Bowles, J.S. and Mackenzie, J.K., The Crystallography of Martensite Transformations, Acta Metall., 1954, **2**, pp. 129,138,22.

49. Wechsler, M.S., Lieberman, D.S., and Read, T.A., Trans. AIME, 1953, **194**, pp. 1503.

50. Christian, J.W., The Origin of Surface Relief Effects in Phase Transformations, in: *DECOMPOSITION OF AUSTENITE BY DIFFUSIONAL PROCESSES*, Zackay, V.F. and Aaronson, H.I. eds. Interscience, New York, **1962**, pp. 371-386.

51. Clark, H.M. and Wayman, C.M., Surface Relief Effects in Solid-State Phase Transformations, in: *PHASE TRANSFORMATIONS*, ASM, Metals Park, Ohio, **1970**, pp. 59-114.

52. Oblak, J.M., Goodenow, R.H., and Hehemann, R.F., Trans. AIME, 1964, **230**, pp. 258.

53. Eichen, E. and Aaronson, H.I., Acta Metall., 1966, **14**, pp. 1637.

54. Dahmen, U., Surface Relief and the Mechanism of a Phase Transformation, Scripta Metall., 1987, **21**, pp. 1029-1034.

55. Oblak, J.M. and Hehemann, R.F., in: *TRANSFORMATION AND HARDENABILITY IN STEEL*, Climax Molybdenum Company, Ann Arbor, MI, **1967**, pp. 15.

56. Bhadeshia, H.K.D.H., Solute-drag, Kinetics and the Mechanism of the Bainite Reaction in Steels, in: *PROCEEDINGS OF AN INTERNATIONAL CONFERENCE ON PHASE TRANSFORMATIONS IN FERROUS ALLOYS*,

Marder, A.R. and Goldstein, J.I. eds. The Metallurgical Society of AIME, Warrendale, Pennsylvania, **1984**, pp. 335-339.

57. Kaufman, L., Radcliffe, S.V., and Cohen, M., Thermodynamics of the Bainite Reaction, in: *DECOMPOSITION OF AUSTENITE BY DIFFUSIONAL PROCESSES*, Zackay, V.F. and Aaronson, H.I. eds. Interscience, New York, **1962**, pp. 313-352.

58. Pickering, F.B., *PHYSICAL METALLURGY AND THE DESIGN OF STEELS*, Applied Science Publishers, Essex, UK, 1978, pp. 104.

59. Irvine, K.J., Pickering, F.B., Heselwood, W.C., and Atkins, M., The Physical Metallurgy of Low-carbon, Low-alloy Steels Containing Boron, J. Iron Steel Inst., 1957, **186**, pp. 54-67.

60. Smith, D.W. and Hehemann, R.F., Influence of Structural Parameters on the Yield Strength of Tempered Martensite and Bainite, J. Iron Steel Inst., 1971, **209**, pp. 476-481.

61. Siriwardene, P.P.L.G., *PH.D. THESIS*, Cambridge University, Cambridge, UK, 1955,

62. Pickering, F.B., The Structure and Properties of Bainite in Steels, in: TRANSFORMATION AND HARDENABILITY IN STEELS, Climax Molybdenum Co., Ann Arbor, MI, **1967**, pp. 109-129.

63. Curry, D.A. and Knott, J.F., The Relationship between Fracture Toughness and Microstructure in the Cleavage Fracture of Mild Steel, Metal Sci., 1976, pp. 1-6.

64. Pickering, F.B., High-Strength, Low-alloy Steels - A Decade of Progress, in: MICRO ALLOYING 75, PROCEEDINGS OF AN INTERNATIONAL SYMPOSIUM ON HIGH-STRENGTH, LOW-ALLOY STEELS, Union Carbide Corporation, New York, **1975**, pp. 9-31.

65. Roberts, M.J., Effect of Transformation Substructure on the Strength and Toughness of Fe-Mn Alloys, Metall. Trans., 1970, **1**, pp. 3287-3294.

66. Langford, G. and Cohen, M., Strain Hardening of Iron by Severe Plastic Deformation, Trans. ASM, 1969, **62**, pp. 623-638.

67. Langford, G. and Cohen, M., Calculation of Cell-Size Strengthening of Wire-Drawn Iron, Metall. Trans., 1970, **1**, pp. 1478-1480.

68. Langford, G. and Cohen, M., Microstructural Analysis by High-Voltage Electron Diffraction of Severely Drawn Iron Wires, Metall. Trans., 1975, **6A**, pp. 901-910.

69. Naylor, J.P., The Influence of the Lath Morphology on the Yield Stress and Transition temperature of Martensitic-Bainitic Steels, Metall. Trans., 1979, **10A**, pp. 861-873.

70. Daigne, J., Guttmenn, M., and Naylor, J.P., Mater. Sci & Eng., 1982, **56**, pp. 1-10.

71. Brozzo, P., Buzzichelli, G., Mascanzoni, A., and Mirabile, M., Microstructure and Cleavage Resistance of Low-carbon Bainitic Steels, Metal Sci., 1977, **11**, pp. 123-129.

72. Marder, A.R., Structure-property Relationships in Ferrous Transformation Products, in: *PROCEEDINGS OF AN INTERNATIONAL CONFERENCE ON PHASE TRANSFORMATIONS IN FERROUS ALLOYS*, Marder, A.R. and Goldstein, J.I. eds. AIME, New York, **1984**, pp. 11-41.

73. Kinsmann, K.R. and Aaronson, H.I., Discussion of Reference xx, in: TRANSFORMATION AND HARDENABILITY IN STEELS, Climax Molybdenum, Ann Arbor, MI, **1964**, pp. 33-38.

74. Vasudevan, P., Craham, L.W., and Axon, H.J., J. Iron Steel Inst., 1958, **190**, pp. 386-391.

75. Edmonds, D.V. and Cochrane, R.C., Structure-Property Relationships in Bainitic Steels, Metall. Trans., 1990, **21A**, pp. 1527-1540.

76. McIvor, I.D., British Steel Research Rep., 1972, **Prod/PM/6498/-/72/A**,

77. Bush, M.E. and Kelly, P.M., Strengthening Mechanisms in Bainitic Steels, Acta Metall., 1971, **19**, pp. 1363-1371.

78. Yang, J.R., Cambridge, 1987,

79. Ritchie, R.O., On the Relationship Between Fracture Toughness and Charpy V-notch Energy in Ultrahigh Strength Steel, in: *WHAT DOES THE CHARPY TEST REALLY TELL US?* Rosenfield, A.R., Gegel, H.L., Hasson, D.F., Rath, B.B., and Stephens, J.R. eds. ASM, Metals Park, Ohio, **1978**, pp. 54-73.

80. Kim, C., Johnson, A.R., and Hosford, W.F., Fracture toughness of AISI M2 High-Speed Steel and Corresponding Matrix Tool Steel, Metall. Trans., 1982, **13A**, pp. 1595-1605.

81. Tomita, Y., Improved Lower Temperature Fracture Toughness of Ultrahigh Strength 4340 Steel through Modified Heat Treatment, Metall. Trans., 1987, **18A**, pp. 1495.

82. Sandvik, B.P.J. and Nevalrinen, H.P., Structure-Property Relationships in Commercial Low-Alloy Bainitic-Austenitic Steel with High Strength, Ductility, and Toughness, Metals Tech., 1981, **8**, pp. 213-220.

83. Aranzabal, J., Gutierrez, I., Rodriguez-Ibabe, J.M., and Urcola, J.J., Influence of Heat Treatments on Microstructure and Toughness of Austempered Ductile Iron, Materials Sci. and Tech., 1992, **8**, pp. 263-273.

84. Bhadeshia, H.K.D.H. and Edmonds, D.V., Bainite in Silicon Steels: New composition-Property Approach Part 1, Metal Sci., 1983, **17**, pp. 411-419.

85. Pacyna, J. and Witek, L., The Effect of Carbides on Fracture Toughness of Steels of Ferritic Matrix, Metals Tech., 1988, **59(2)**, pp. 68-74.

86. Bowen, P., Druce, S.G., and Knott, J.F., Effects of Microstructure on Cleavage Fracture in Pressure Vessel Steel, Acta Metall., 1986, **34 (6)**, pp. 1121-1131.

87. Miihkinen, V.T.T. and Edmonds, D.V., Fracture Toughness of Two Experimental High-Strength Bainitic Low-Alloy Steels Containing Silicon, Materials Sci. and Tech., 1987, **3**, pp. 441-449.

88. Bodnar, R.L., Taylor, K.A., Albano, K.S., and Heim, S.A., Improving the Toughness of 3-1/2NiCrMoV Steam Turbine Disk Forgings, J. of Eng. Mater. and Tech., 1989, **111**, pp. 61-70.

89. Irvine, K.J., Pickering, F.B., and Gladman, T., Grain-Refined C-Mn Steels, J. Iron Steel Inst., 1967, **205**, pp. 161-182.

90. Ohtani, H., Teerasaki, F., and Kunitake, T., The Microstructure and Toughness of High Tensile Strength Steels, Trans. ISIJ, 1972, **12**, pp. 118-127.

91. Grange, R.A., Strengthening Steel by Austenite Grain Refinement, Trans. ASM, 1966, **59**, pp. 26-48.

92. Birkbeck, G., Effect of Aluminum-Killing on the Yield and Fracture Behavior of 0.16-0.2C, 0.65-0.75Mn Steel, J. Iron Steel Inst., 1968, **206**, pp. 909-910.

93. Hardwick, D. and Pirt, K.R., The Toughness of Tempered Martensite, J. Iron Steel Inst., 1960, **196**, pp. 301-308.

94. Yokota, M.J. and Lai, G.Y., Toughness of Lath vs Plate Martensites, Metall. Trans., 1975, **6A**, pp. 1832-1835.

95. Lai, G.Y., Wood, W.E., Clark, R.A., Zackay, V.F., and Parker, E.R., The Effect of Austenitizing Temperature on the Microstructure and Mechanical Properties of As-Quenched 4340 Steel, Metall. Trans., 1974, **5**, pp. 1663-1670.

96. Youngblood, J.L. and Raghavan, M.R., Metall. Trans., 1977, **8A**, pp. 1439-1448.

97. Wood, W.E., Eng. Fract. Mech., 1975, **7**, pp. 219.

98. Ritchie, R.O., Francis, B., and Server, W.L., Metall. Trans., 1976, **7A**, pp. 831.

99. Ritchie, R.O., Francis, B., and Server, W.L., Metall. Trans., 1977, **8A**, pp. 1197.

100. Ritchie, R.O. and Horn, R.M., Further Considerations on the Inconsistency in Toughness Evaluation of AISI 4340 Steel Austenitized at Increasing Temperatures, Metall. Trans., 1978, **9A**, pp. 331-341.

101. Dulieu, D., in: *PROCEEDINGS: THIRD INTERNATIONAL CONFERENCE ON THE STRENGTH OF METALS AND ALLOYS*, **1973**, pp. 383.

102. Carlson, M.F., Rao, B.V.N., Ritchie, R.O., and Thomas, G., in: *PROCEEDINGS: FOURTH INTERNATIONAL CONFERENCE ON THE STRENGTH OF METALS AND ALLOYS*, **1976**, pp. 509.

103. Ferguson, W.G., Clark, N.E., and Watson, B.R., Metals Tech., 1976, **3**, pp. 208.

104. Zackay, V.F. and Parker, E.R., Fracture Toughness, in: *ALLOY AND MICROSTRUCTURAL DESIGN*, Tien, J.K. and Ansell, G.S. eds. Acdemic Press, New York, **1976**, pp. 213-250.

105. Clark, R.A. and Thomas, G., Design of Strong Tough Fe/Mo/C Martensitic Steels and the Effects of Cobalt, Metall. Trans., 1975, **6A**, pp. 969-979.

106. Wilshaw, T.R., Rau, C.A., and Tetelman, A.S., A General Model to Predict the Elastics-Plastic Stress Distribution and Fracture Strength of Notched Bars in Plane Strain Bending, Eng. Fract. Mech., 1968, **1**, pp. 191-211.

107. Naylor, J.P. and Krahe, P.R., The Effect of the Bainite Packet Size on Toughness, Metall. Trans., 1974, **5**, pp. 1699-1701.

108. Tomita, Y. and Okabayashi, K., Improvement of Lower Temperature Mechanical Properties of 0.4 Pct C-Ni-Cr-Mo Ultrahigh Strength Steel with the Second Phase Lower Bainite, Metall. Trans., 1983, **14A**, pp. 485-492.

109. Tomita, Y., Effect of Microstructure on Plane-Strain Fracture Toughness of AISI 4340 Steel, Metall. Trans., 1988, **19A**, pp. 2513-2521.

110. Matsuda, S., Inoue, T., and Mimura, H., Toughness and Effective Grain Size in Heat-Treated Low-Alloy High Strength Steels, Trans. ISIJ, 1972, **12**, pp. 325-333.

111. Naylor, J.P. and Blondeau, R., The Respective Roles of the Packet Size and the Lath Width on Toughness, Metall. Trans., 1976, **7A**, pp. 891-894.

112. Gerberich, W.W., Hemmings, P.L., and Zackay, V.F., Fracture and Fractography of Metastable Austenites, Metall. Trans., 1971, **2**, pp. 2243-2253.

113. Bhadeshia, H.K.D.H. and Edmonds, D.V., Tempered Martensite Embrittlement: Role of Retained Austenite and Cementite, Metal Sci., 1979, **13**, pp. 325-334.

114. Heitmann, W.E. and Babu, P.B., Influence of Bainite in the Microstructure on Tensile and Toughness Properties of Microalloyed Steel Bars and Forgings, in: FUNDAMENTALS OF MICROALLOY FORGING STEELS, Golden, Colorado, **1986**, pp. 55-72.

115. Liu, Y.H., Correlation of Microstructures with Toughness in HP 9-4-45 Lower Bainite and Tempered Martensite, Trans. ASM, 1969, **62**, pp. 55-63.

116. Liu, Y.H., Effect of Carbides on Fracture Path in Lower Bainite and Tempered Martensite, Trans. ASM, 1969, **62**, pp. 544-547.

117. Shelton, P.W. and Wronski, A.S., Cracking in M2 High Speed Steel, Metal Sci., 1983, **17**, pp. 533-539.

118. Carlson, M.F., Rao, B.V.N., and Thomas, G., The Effect of Austenitizing Temperature Upon the Microstructure and Mechanical Properties of Experimental Fe/Cr/C Steels, Metall. Trans., 1979, **10A**, pp. 1273-1284.

119. Sarikaya, M., Steinberg, B.G., and Thomas, G., Optimization of Fe/Cr/C Base Structural Steels for Improved Strength and Toughness, Metall. Trans., 1982, **13A**, pp. 2227-2237.

120. Zackay, V.F., Parker, E.R., and Wood, W.E., Influence of Some Microstructural Features on the Fracture Toughness of High Strength Steels, in: *THE MICROSTRUCTURE AND DESIGN OF ALLOYS*, **1973**, pp. 175-179.

121. Syn, C.K., Fultz, B., and Morris, J.W.,Jr., Mechanical Stability of Retained Austenite in Tempered 9Ni Steel, Metall. Trans., 1978, **9A**, pp. 1635-1640.

122. Webster, D., Optimization of Strength and Toughness in Two High-Strength Stainless Steels, Metall. Trans., 1971, **2**, pp. 1857-1862.

123. Webster, D., Development of a High Strength Stainless Steel with Improved Toughness and Ductility, Metall. Trans., 1971, **2**, pp. 2097-2104.

124. Marschall, C.W., Hehemann, R.F., and Troiano, A.R., The Characteristics of 9% Nickel Low Carbon Steel, Trans. ASM, 1962, **55**, pp. 135-148.

125. Rao, B.V.N. and Thomas, G., Structure-Property Relations and the Design of Fe-4Cr-C Base Structural Steels for High Strength and Toughness, Metall. Trans., 1980, **11A**, pp. 441-456.

126. Antolovich, S.D. and Singh, B., On the Toughness Increment Associated with the Austenite to Martensite Phase Transformation in TRIP Steels, Metall. Trans., 1971, **2**, pp. 2135-2141.

127. Leslie, W.C. and Miller, R.L., The Stabilization of Austenite by Closely-Spaced Boundaries, Trans. ASM, 1964, **57**, pp. 972-979.

128. Sandvik, B.P.J., the Bainite Reaction in Fe-Si-C Alloys: The Primary Stage, Metall. Trans., 1982, **13A**, pp. 777-787.

129. Mcmahon, J.A. and Thomas, G., Development of Economical, Tough, Ultra-High-Strength Fe-Cr-C Steels, in: *THE MICROSTRUCTURE AND DESIGN OF ALLOYS*, **1973**, pp. 180-184.

130. Parker, E.R. and Zackay, V.F., Microstructural Features Affecting Fracture Toughness of High Strength Steels, Eng. Fract. Mech., 1975, **7**, pp. 371-375.

131. Webster, D., Increasing the Toughness of the Martensitic Stainless Steel AFC 77 by Control of Retained Austenite Content, Ausforming and Strain Aging, Trans. ASM, 1968, **61**, pp. 816-828.

132. Ohtani, H., Okaguchi, C., Fujishiro, Y., and Ohmori, Y., Morphology and Properties of Low-carbon Bainite, Metall. Trans., 1990, **21A**, pp. 877-888.

133. Rolfe, S.T. and Barsom, J.M., Effect of Temperature, Loading Rate, and Plate Thickness on Fracture Toughness, in: *FRACTURE AND FATIGUE CONTROL IN STRUCTURES - APPLICATIONS OF FRACTURE MECHANICS*, Prentice-Hall, Inc., Englewood Cliffs, New Jersey, **1977**, pp. 92-139.

134. Broek, D., *ELEMENTARY ENGINEERING FRACTURE MECHANICS*, Martinus Nijhoff Publishers, Boston, 1986,

135. Anderson, T.L., *FRACTURE MECHANICS - FUNDAMENTALS AND APPLICATIONS*, CRC Press, Boca Raton, 1991,

136. Broek, D., The Role of Inclusions in Ductile Fracture and Fracture Toughness, Eng. Fract. Mech., 1973, **5**, pp. 55-66.

137. Briant, C.L. and Messmer, R.P., Electronic Effect of Sulphur in Nickel - A Model for Grain Boundary Embrittlement, Phi. Mag., 1980, **42**, pp. 569-576.

138. Wood, W.A., Recent Observations on Fatigue Fracture in Metals, in: *ASTM STP 237*, ASTM, **1958**, pp. 110-121.

139. Mughrabi, H., Wang, R., Differt, K., and Essmann, U., Fatigue Crack Initiation by Cyclic Slip Irreversibilities in High-Cycle Fatigue, in: *FATIGUE MECHANISMS: ADVANCES IN QUANTITATIVE MEASUREMENT OF PHYSICAL DAMAGE ASTM STP 811*, Lankford, J., Davidson, D.L., Morris, W.L., and Wei, R.P. eds. ASTM, Philadelphia, PA, **1983**, pp. 1-45.

140. Bowles, C.Q. and Broek, D., On the Formation of Fatigue Striations, Int. J. Fracture Mechanics, 1972, pp. 75-85.

141. James, M.R. and Morris, W.L., The Role of Microplastic Deformation in Fatigue Crack Initiation, in: *ASTM STP 811*, Lankford, J., Davidson, D.L., Morris, W.L., and Wei, R.P. eds. ASTM, Philadelphia, PA, **1983**, pp. 46-70.

142. Brown, W.F. and Srawley, J.E., *PLANE STRAIN CRACK TOUGHNESS TESTING OF HIGH STRENGTH METALLIC MATERIALS ASTM STP 410*, ASTM, Rahway, NJ, 1969,

143. Samuels, L.E., Tempering of Martensite, in: *OPTICAL MICROSCOPY OF CARBON STEELS*, ASM, **1980**, pp. 373-409.

144. Standard Test Methods for Determining Average Grain Size, ASTM E112-88, in: *ANNUAL BOOK OF ASTM STANDARDS, VOL. 03.01*, ASTM, **1989**,

145. Johnson, W.A. and Mehl, R.F., Reaction Kinetics in Processes of Nucleation and Growth, Trans. AIME, 1939, **135**, pp. 416-458.

146. Avrami, M., Kinetics of Phase Change. I, J. Chem. Phys., 1939, **7**, pp. 1103-1112.

147. Christian, J.W., *THE THEORY OF TRANSFORMATIONS IN METALS AND ALLOYS*, Pergamon Press, 1975,

148. The ASTM Committee on Fracture Testing of High-Strength Sheet Materials, Fracture Testing of High-Strength Sheet Materials: A Report of a special ASTM Committee, ASTM Bull., 1960, pp. 29-40.

149. Standard Method of Sharp-Notch Tension Testing of High-Strength Sheet Materials, ASTM E338-81, in: *ANNUAL BOOK OF ASTM STANDARDS, VOL. 03.01*, ASTM, **1989**, pp. 445-449.

150. McClintock, F.A. and Irwin, G.R., Plasticity Aspects of Fracture Mechanics, in: *FRACTURE TOUGHNESS TESTING AND ITS APPLICATIONS, ASTM STP 381*, ASTM, Philadelphia, PA, **1965**, pp. 84-110.

151. Squirrell, S.J., Pisarski, H.G., and Dawes, M.G., Welding Inst. Res. Bull., 1986,

152. LePera, F.S., Improved Etching Technique to Emphasize Martensite and Bainite in High Strength Dual-phase Steel, Journal of Metals, 1980, pp. 38-39.

153. Meyer, S.L., *DATA ANALYSIS FOR SCIENTISTS AND ENGINEERS*, Jonh Wiley and Sons, Inc., New York, 1975,

154. Oka, M. and Okamoto, H., Isothermal Transformation in Hypereutectoid Steels, in: *PROCEEDINGS OF THE INTERNATIONAL CONFERENCE ON MARTENSITIC TRANSFORMATIONS*, The Japan Institute of Metals, **1986**, pp. 271-275.

155. Schaaber, O., Some Observations on Isothermal Austenite Transformation Near the Ms Temperature, Journal of Metals, 1955, **7**, pp. 559-560.

156. Wood, W.E., *MECHANISM OF ENHANCED TOUGHNESS IN MARTENSITIC ALLOYS, FINAL REPORT FOR THE PERIOD OCT. 1, 1975 - SEPT. 30, 1976 TO THE NAVY, NAVAL AIR SYSTEMS COMMAND, CONTRACT NO. N00019-76-C-0149*, 1976, pp. 1-75.

157. Avrami, M., Kinetics of Phase change. II, J. Chem. Phys., 1940, **8**, pp. 212-224.

158. Avrami, M., Kinetics of Phase Change. III, J. Chem. Phys., 1941, **9**, pp. 177-184.

159. Bhadeshia, H.K.D.H., Kinetics of the Bainite Transformation, in: MARTENSITIC TRANSFORMATIONS, PROCEEDINGS OF THE 6TH INTERNATIONAL CONFERENCE ON MARTENSITIC TRANSFORMATIONS, Sydney, Australia, **1989**, pp. 263-274.

160. Radcliffe, S.V. and Rollason, E.C., The Kinetics of the Formation of Bainite in High-purity Iron-carbon Alloys, J. Iron Steel Inst., 1959, **191**, pp. 56-65.

161. Umemoto, M., Horiuchi, K., and Tamura, I., Transformation Kinetics of Bainite during Isothermal Holding and Continuous Cooling, Trans. ISIJ, 1982, **22**, pp. 854-861.

162. Okamoto, H. and Oka, M., Lower Bainite with Midrib in Hypereutectoid Steels, Metall. Trans., 1986, **17A**, pp. 1113-1120.

163. Hawkins, M.J. and Barford, J., Experimental Kinetics of Bainite Formation, J. Iron Steel Inst., 1972, **210**, pp. 97-105.

164. Aaronson, H.I. and Wells, C., Trans. AIME, 1956, **206**, pp. 1216-1223.

165. Speich, G.R. and Cohen, M., The Growth Rate of Bainite, Trans. AIME, 1960, **218**, pp. 1050-1059.

166. Goodenow, R.H., Matas, S.J., and Hehemann, R.F., Growth Kinetics and the Mechanism of the Bainite Transformation, Trans. AIME, 1963, **227**, pp. 651-658.

167. Zhang, S., Alloying Elements in Steel, in: *ALLOY STEEL*, Metallurgical Industry Publishing House, Beijing, **1980**, pp. 1-42.

168. Steven, W. and Haynes, A.G., The Temperature of Formation of Martensite and Bainite in Low-alloy Steels, JISI, 1956, **183**, pp. 349-359.

169. Kirkaldy, J.S., Thomson, B.A., and Baganis, E.A., Prediction of Multicomponent Equilibrium and Transformation Diagrams for Low Alloy Steels, in: *HARDENABILITY CONCEPTS WITH APPLICATIONS TO STEEL*, AIME, Chicago, **1977**, pp. 82-125.

170. Prohaszka, J., On the Incubation Time of Isothermal TTT diagram, in: *FIFTH INTERNATIONAL CONGRESS ON HEAT TREATMENT OF MATERIALS*, Budapest, Hungary, **1986**, pp. 17-22.

171. Barford, J., Kinetic Aspects of the Bainite Reaction, J. Iron Steel Inst., 1966, **204**, pp. 609-614.

172. Kang, M.K., Chen, D.M., Yang, S.P., and Hu, G.L., The Time-Temperature-Transformation Diagram within the Medium Temperature Range in some Alloy Steels, Metall. Trans., 1992, **23A**, pp. 785-795.

173. Russell, K.C., Grain Boundary Nucleation Kinetics, Acta Metall., 1969, **17**, pp. 1123-1131.

174. Tetelman, A.S. and McEvily, A.J.,Jr., *FRACTURE OF STRUCTURAL MATERIALS*, John Wiley & Sons, Inc., New York, 1967,

175. Irwin, G.R. and Kies, J.A., Welding Research Sup., 1954, **19**, pp. 193-198.

176. Creager, M. and Liu, A.F., The Effect of Reinforcements on the Slow Stable Tear and Catastrophic Failure of Thin Metal Sheet, in: *AMERICAN INSTITUTE OF AERONAUTICS AND ASTRONAUTICS*, **1971**, pp. 71-113.

177. McCabe, D.E., Introduction (to ASTM STP 527), in: *FRACTURE TOUGHNESS EVALUATION BY R-CURVE METHODS*, ASTM, Philadelphia, PA, **1973**, pp. 1-2.

178. Griffith, A.A., The Phenomena of Rupture and Flow in Solids (1920), in: FRACTURE MECHANICS RETROSPECTIVE, Barsom, J.M. ed. ASTM, Philadelphia, PA, **1987**, pp. 31-68.

179. McCabe, D.E. and Heyer, R.H., R-Curve Determination Using a Crack-Line-Wedge-Loaded (CLWL) Specimen, in: *FRACTURE TOUGHNESS EVALUATION BY R-CURVE METHODS*, ASTM, Philadelphia, **1973**, pp. 17-35.

180. Irwin, G.R., Fracture Dynamics, in: *FRACTURING OF METALS*, ASM, Cleveland, **1948**, pp. 147-166.

181. Orowan, E., Energy Criteria of Fracture, Welding Journal, 1955, **34**, pp. 157s-160s.

182. Ritchie, R.O., Knott, J.F., and Rice, J.R., On the Relationship between Critical Tensile Stress and Fracture Toughness in Mild Steel, J. Mech. Phys. Solids, 1973, **21**, pp. 395-410.

183. Dolby, R.E. and Knott, J.F., Toughness of Martensitic and Martensitic-Bainitic Microstructures with Particular Reference to Heat-Affected Zones in Welded Low-Alloy Steels, J. Iron Steel Inst., 1972, **210**, pp. 857-865.

184. Hahn, G.T. and Rosenfield, A.R., Experimental Determination of Plastic Constraint ahead of a Sharp Crack under Plane-Strain Conditions, Trans. ASM, 1966, **59**, pp. 909-919.

185. Hill, R., *MATHEMATICAL THEORY OF PLASTICITY*, Oxford, London, 1950,

VITA

The author was born on March 9, 1958, in Beijing, China. He survived the cultural revolution which destroyed millions of other children's dreams. He enrolled at the Beijing Institute of Technology in 1978 and received his B.E. degree in Materials Science and Engineering in 1982. Then he worked as a heat treating engineer in Red Flag factory, a subsidiary of the Ministry of Weapon Industry.

The author joined the Central Iron & Steel Research Institute in 1984 to pursue a M.S. degree in Materials Science. Sensing a reverse to the 'open door' policy which would hinder his future career, he left China in 1986 for the United States and attended the Western Michigan University for a Master degree in Computer Science. He equated his experience of leaving the field of materials science as that of losing home and welcomed, with all his heart, the opportunity offered by the Oregon Graduate Institute in 1988 leading to a Ph.D. degree in Materials Science & Engineering. He completed the requirements for the Doctor of Philosophy degree in January 1994.

Based on his experience, the author believes that the critical ingredients to a successful career are opportunity, persistence, luck, and intelligence.